# Titanium epoxidation catalysts : zeolite and silsesquioxane based materials

*DOI:*

[10.6100/IR516268](10.6100/IR516268)

*Document status and date:*
Published: 01/01/1998

*Document Version:*
Publisher's PDF, also known as Version of Record (includes final page, issue and volume numbers)

*Please check the document version of this publication:*

• A submitted manuscript is the version of the article upon submission and before peer-review. There can be important differences between the submitted version and the official published version of record. People interested in the research are advised to contact the author for the final version of the publication, or visit the DOI to the publisher's website.
• The final author version and the galley proof are versions of the publication after peer review.
• The final published version features the final layout of the paper including the volume, issue and page numbers.

[Link to publication](Link to publication)

# Titanium Epoxidation Catalysts:

## Zeolite and Silsesquioxane based Materials

Simon Krijnen

Stellingen

behorende bij het proefschrift

# Titanium Epoxidation Catalysts:
## Zeolite and Silsesquioxane based Materials

van

## Simon Krijnen

1.  IJzer gesubstitueerde aluminofosfaten zijn beslist ongeschikt als
    katalysatoren voor vloeistoffase oxidatie reacties.

2.  Het introduceren van namen voor 'nieuwe technieken' (zoals de
    zogenaamde 'Atom-Planting Method' door Yashima *et al.*) is, wanneer
    deze technieken bepaald niet nieuw zijn, niet wenselijk.

    T. Yashima, K. Yamagishi, S. Namba, *Stud. Surf. Sci. Catal.*, 60, 1991, p. 171.
    P. Wu, T. Komatzu, T. Yashima, *J. Phys. Chem., 99,* 1995, p. 10923.
    Dit proefschrift.

3.  Het getuigt niet van een brede kijk wanneer bij het zoeken naar sporen
    titaandioxide in zeoliet samples met behulp van de titaan $2p_{3/2}$ band in een
    XPS spectrum niet wordt vermeld dat de zuurstof 1s band een veel
    duidelijkere indicator kan zijn.

    M. Stöcker, *Microporous Mater.*, 1996, p. 235.
    S. Kaliaguine, *Stud. Surf. Sci. Catal.*, 1996, p. 191.
    Dit proefschrift.

4.  Het vergelijken van katalysatoren waarvan de belading met het actieve
    centrum onbekend is, mag geen katalytisch onderzoek heten. Dergelijke
    'katalysatoren' kunnen slechts worden beschouwd als een vervuiling die
    aanwezig is tijdens de (blanco-)reactie.

    P.T. Tanev, M. Chibwe, T.J. Pinnavaia, *Nature, 368,* 1994, p. 321.

5.  Het vergelijken van het uitvoeren van een quantum-chemische berekening
    door een theoretisch chemicus met het doen van een chemisch experiment
    in een laboratorium, doet afbreuk aan de kwaliteiten die van een goed
    experimenteel chemicus verwacht mogen worden.

6.  Het vasthouden aan het gebruik van zuiver empirische karakteriserings-
    methoden, zoals de potlood-hardheidstest en de nageltest, door de coatings-
    industrie vertraagt een wetenschappelijke benadering van de karakterisering
    van coatings.

    Standard test method for Film Hardness by Pencil Test, American Society for Testing
    and Materials, Philadelphia, *ASTM Standards Designation D 3363 -92a,* 1993.
    P. Fink-Jensen, *Pure Appl. Chem., 10,* 1965, p. 241.

7.  Het gezegde dat een echte chemicus gaten in z'n kleren behoort te hebben,
    zegt meer over de praktische vaardigheden van deze chemicus dan over zijn
    echtheid.

8.  Het feit dat een staande ovatie na een (toneel)voorstelling een gewoonte
    lijkt te worden, doet afbreuk aan de mogelijkheid om je waardering te uiten
    voor de spelers.

9.  Moderne architecten zijn vaak weinig genuanceerde denkers: zij drukken
    zich het liefst uit in termen van staal, glas en gewapend beton.

10. Het inkleuren van de eerste geluidsfilms (van Stan Laurel en Oliver Hardy
    in het bijzonder) getuigt van weinig respect voor de makers en is enkel
    bedoeld voor een verwend publiek.

11. Het gebruik van de term 'houtje-touwtje' aanpak onderschat de degelijkheid
    van de dito jassen.

12. De beste stellingen zijn van bamboe.

    J.J.A. Janssen, *Natuur en Techniek, 6,* 1995, p. 412.
    J.J.A. Janssen, *Gate, 1,* 1998, p. 26.

# Titanium Epoxidation Catalysts:

## Zeolite and Silsesquioxane based Materials

Proefschrift

ter verkrijging van de graad van doctor aan de
Technische Universiteit Eindhoven, op gezag van de
Rector Magnificus, prof.dr. M. Rem, voor een
commissie aangewezen door het College voor
Promoties in het openbaar te verdedigen
op woensdag 11 november 1998 om 16.00 uur

door

**Simon Krijnen**

geboren te Son en Breugel

Dit proefschrift is goedgekeurd door de promotoren:

prof.dr.ir. J.H.C. van Hooff
en
prof.dr. R.A. van Santen

Copromotor: dr. H.C.L. Abbenhuis

*"Zie, hoe alles naar het geheel toe streeft,*
*hoe het ene in het andere werkt en leeft."*

J.W. Goethe

*Aan mijn ouders*

*Voor Suzanne*

# Contents

# Abbreviations and definitions

AAS         Atomic Adsorption Spectroscopy
AlPO        Aluminophosphate
BE          Binding Energy [eV]
Bea         Zeolite beta
BET         Brunauer Emmett and Teller method
CVD         Chemical Vapor Deposition
DRUV-Vis    Diffuse Reflectance UV-Visible Spectroscopy
FT-IR       Fourier Transformed Infra-Red Spectroscopy
IR          Infra-Red Spectroscopy
MAS         Magic Angle Spinning
MCM-41      Mobil Composition of Matter 41
MeAPO       Metal Substituted Aluminophosphate
Mor         Zeolite mordenite
NMR         Nuclear Magnetic Resonance
PDMS        Poly Dimethyl Siloxane
PV          Pore Volume [ml/g]
SEM         Scanning Electron Microscopy
TBHP        *tert.*-Butyl Hydroperoxide
TEM         Tunneling Electron Microscopy
TS-1        Titanium Silicalite-1
TS-2        Titanium Silicalite-2
uc          unit cell (of a zeolite)
UV-Vis      UV-Visible Spectroscopy
XPS         X-ray Photoelectron Spectroscopy
XRD         X-Ray Diffraction
ZSM-5       Zeolite Secony Mobil 5
TOF         Turn Over Frequency [mol mol$^{-1}$ h$^{-1}$]


In a hypothetical reaction scheme:     $A \ + \ B \ \xrightarrow{\ cat\ } \ C \ + \ D$

in which:   A is the substrate,
            B is the oxidizing agent,
            C is the product wanted,
            D is the (unwanted) side product and
            *cat* is the catalyst used,

the following definitions were applied:     $Conversion \ of \ A = \dfrac{[A]_{t=0} - [A]_{t=t}}{[A]_{t=0}} * 100 \ \%$

$$Selectivity \ of \ A \ towards \ C = \dfrac{[C]_{t=t}}{[A]_{t=0} - [A]_{t=t}} * 100 \ \%$$

$$TOF = \dfrac{[A]_{t=0} - [A]_{t=t}}{[cat] * t} \quad \left[ \dfrac{mol}{mol \ h} \right]$$

# 1

# Introduction

In this Chapter a brief introduction is given on heterogeneous titanium catalysts for liquid phase oxidation reactions. Also zeolites in general and various titanium catalysts are discussed. A justification is presented for our approach to synthesize large pore titanium zeolites. In addition, various heterogenization methodologies are discussed from a broad perspective as an introduction for a new heterogenization method to be reported. In the end, the general scope of this thesis is presented.

## 1.1 Oxidation catalysis

The selective, partial oxidation of hydrocarbons is a field for both academic and industrial relevance and challenge. The controlled transformation of hydrocarbon feedstocks into more sophisticated oxygenated products is one of the most important steps in the production of intermediates for the fine chemical industry. In recent years, the use of traditional stoichiometric processes is being subjected to increasing environmental pressure.
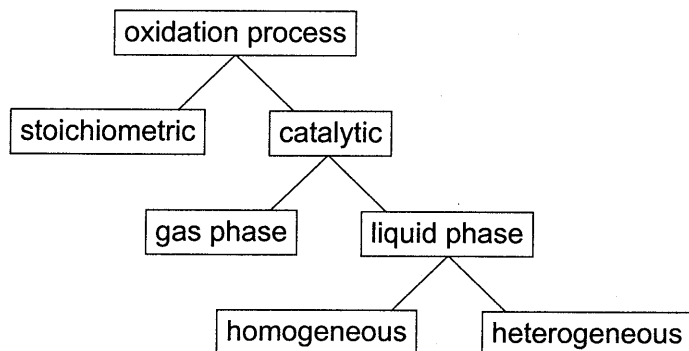


*Figure 1.1 Process options for (industrial) oxidation processes.*

In the fine chemicals industry classical oxidants like potassium dichromate or permanganate were used in stoichiometric amounts, resulting in 5 to 50 times kilogram of waste (mostly inorganic salts) per kilogram of product[1]. In other words, most of the atoms offered at the start of the reaction are not part of the wanted product, so the atom-selectivity (or atom utilization) is very low. Currently, there is considerable pressure to replace these outdated methods by cleaner catalytical technologies.

When the choice is made for a catalytic alternative, there are still some options to consider (see figure 1.1). First of all: is a gas phase or liquid phase oxidation preferred? This will depend largely on the boiling point and thermal stability of the reactants, especially of a desired fine chemical intermediate. Such compounds are often unstable at elevated temperatures, ruling out gas phase application. Although catalytic gas phase oxidation reactions are important[2], in this thesis emphasis is put on the liquid phase applications of oxidation catalysts. Another important choice to consider, is whether the oxidation catalysis should be performed homogeneously, in which the catalyst is in the same phase as the reactants, or heterogeneously, in which the catalyst is in another phase (see also section 1.6). The main advantage of homogeneous catalysts is the ease of accessibility of the active site, resulting in a high activity and no mass transfer limitations. Their main disadvantages are their low thermal stability and the difficulty of recovery and regeneration. These problems can be solved with heterogeneous catalysts, which are easy to recover by filtration which allows recycling of the catalyst. The solid, heterogeneous phase, however, can introduce mass transfer limitations, presumably resulting in a lower activity or selectivity.

## 1.2  Titanium oxidation catalysts

Among the homogeneous titanium oxidation catalysts, the Sharpless type catalyst is the best known example[3]. This is a highly active and selective asymmetric epoxidation catalyst, using *tert.*-butyl hydroperoxide (TBHP) as the oxidizing agent, together with a chiral bidentate ligand, *e.g.* diethyl tartrate. The homogeneous catalyst is made *in-situ* from the tartrate and a tetra-alkoxy titanium(IV) species. In the asymmetric epoxidation of allylic alcohols enantiomeric excesses of over 95% are reached. Other homogeneous titanium catalysts, like titanyl acetyl acetonate, are also reported to be selective catalysts in the oxidation of allylic alcohols to their corresponding ketones or aldehydes as well as in epoxidation reactions[4]. A major drawback of these homogeneous titanium complexes is that none of them are stable in the presence of water; all catalysis should be performed in water-free, aprotic solvents. For instance in the case of Sharpless catalysis, usually molecular sieves (or 'molsieves') are added to the reaction mixture to adsorb even trace amounts of water present (see section 1.3).

The first heterogeneous titanium oxidation catalyst was patented in 1971 by Shell Oil[5]. This titanium(IV) silicon dioxide catalyst is prepared by impregnating silica with $TiCl_4$ or an

organo-titanium compound, followed by calcination. The obtained titanium catalyst is highly active but becomes only truly heterogeneous after a certain time on stream[6]. The combination of titanium(IV) with silicon dioxide seems to provide the right stereochemical and electronic environment for an active titanium oxidation catalyst. The structure of the active site has been suggested to be an isolated, siloxy bonded titanyl species[4]. Later investigations, however, also concerning zeolitic systems, suggest that the truly active site is closer to a titanium site which is tripodally or tetrapodally attached by siloxy units[7,8]. An example of such a four coordinated titanium species is present in Titanium Silicalite 1 (abbreviated as TS-1), which was first patented by Enichem in 1983[9]. When the titanium content does not exceed 1 - 2 wt%, isolated titanium sites are incorporated as part of the zeolite structure, capable of catalyzing a variety of liquid phase oxidation reactions. In contrast to the Shell catalyst, the structure of TS-1 is an ordered, crystalline microporous structure, allowing to enforce shape selective catalysis (see section 1.3). It is generally accepted that the active site in TS-1 is the four coordinated titanium species, from which one siloxy unit has reacted with the peroxide resulting in a titanium hydroperoxo species[7,8,10-13]. In figure 1.2 this is schematically shown with an epoxidation reaction as example.
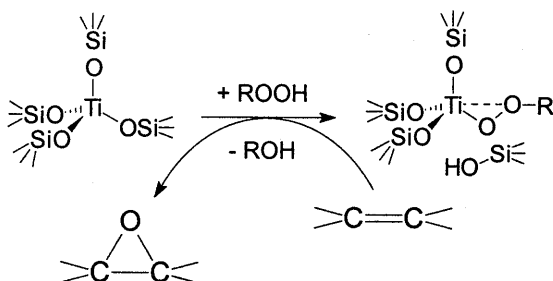


*Figure 1.2  Representation of the titanium(IV) site incorporated in a silicate structure, acting as an epoxidation catalyst with a peroxide as oxidizing agent.*

## 1.3 Molecular Sieves

Molecular sieves, or zeolites, are microporous, crystalline aluminosilicates, built from $SiO_4$ and $AlO_4$ tetrahedra. These tetrahedra are connected to one another by shared oxygen atoms to form a three dimensional network, containing regular formed pores. The name *zeolite* was first used in 1756 by the mineralogist Cronstedt to describe Stilbite, the first mineral zeolite identified[14]. Nowadays, 98 different zeolite structures are known, all with their own type of pores, pore structure, density, aluminum content and crystal structure[15]. Facts of the zeolites, which are referred to in this thesis, are summarized in table 1.1.

*Table 1.1 Physical properties of some zeolites*

| zeolite name | structure type code | range Si/Al | pore size in number of T-atoms | pore opening [Å] | pore structure[a] |
|---|---|---|---|---|---|
| **ZSM-5** (silicalite 1)[b] | MFI | 12 - ∞ | 10-ring | 5.6 × 5.3 | 3 D |
| | | | 10-ring | 5.5 × 5.1 | |
| **ZSM-11** (silicalite 2)[b] | MEL | 12 - ∞ | 10-ring | 5.4 × 5.3 | 2 D |
| **mordenite** | MOR | 5 - 10 | 12-ring | 7.0 × 6.5 | 1 D |
| | | | 8-ring | 5.7 × 2.6 | |
| **beta** | BEA | 8 - ∞[c] | 12-ring | 7.6 × 6.4 | 3 D |
| | | | 12-ring | 5.5 × 5.5 | |
| **faujasite** | FAU | 2.3 | 12-ring | 7.4 × 7.4 | 3 D |

*[a] The dimensionality of the zeolite pore structure is only based upon the pores, which are accessible for catalytically interesting substrate molecules, like linear alkenes, [b] the term 'silicalite' is used for the same structure when no aluminum is present, [c] Only very recently all-silica beta syntheses are reported[16,17].*

As can be seen from table 1.1, the dimensions of the zeolite pores are of a molecular scale. That is the reason why these structures are often referred to as 'molecular sieves'. When choosing the right zeolite catalyst for a certain reaction one can discriminate between substrate (reactant) molecules having different sizes; some can enter the pore structure, while others cannot. This is called *reactant selectivity*. Other types of selectivity, that can be used in zeolite catalysis, are *product selectivity*, only molecules small enough to leave the pore structure are found in the product, and *transition state selectivity*, only transition states which can fit in the pore structure can be passed.



**MFI** viewed along [010]    **MOR** viewed along [001]    **BEA** viewed along [100]

*Figure 1.3   Cross section views of different zeolite structures, viewed along their main channel. Each line represents a Si-O-Si bond.*

The different structures of some zeolites are shown in figure 1.3. In this figure the structures are presented in zeolite short hand notation; all Si-O-Si bonds are plot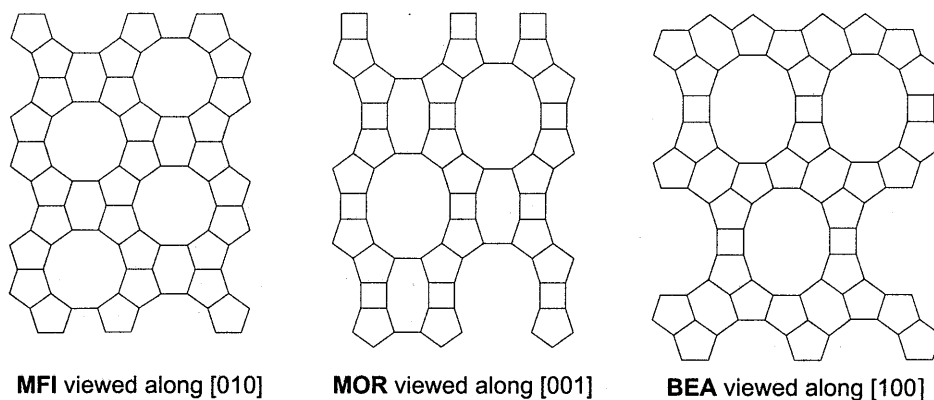ted as a line, resulting in the location of silicon on the intersection of lines and the oxygen located in the middle of the line. When a silicon ($Si^{4+}$) in the zeolite framework is replaced by a trivalent ion such as aluminum ($Al^{3+}$), the negative loading of the framework has to be compensated and a cation will be introduced. Such cations can be $H^+$, $Na^+$, $K^+$, $Ca^{2+}$, etc. Metals, like silicon or aluminum but also guest metals like titanium, incorporated in the zeolite framework are called T-atoms and can be found on their T-atom positions; at the intersection of lines in figure 1.3.

Zeolite structures display different characteristics, such as:
• their ability to adsorb molecules. Especially their strong affinity towards water is used in the application of zeolites as drying agents. But also hydrocarbons or other molecules can be strongly adsorbed.
• their ion exchange properties. The cation that is needed for charge compensation when a trivalent ion is incorporated in the zeolite lattice (usually aluminum for silicon), can be ion exchanged for other cations. This property is used in the application of zeolites as water softener in detergents, in which the $Ca^{2+}$ and $Mg^{2+}$ are removed from the washing water.
• acid catalysis. When the charge compensation cation is a proton, a very strong Brønsted acid site is present in the micropores of the zeolite. This acidic site is capable of catalyzing selectively several organic reactions, such as cracking, isomerisation, etc.
• their ability to incorporate small amounts of guest metals, such as Fe, Ga, Ti, on T-atom sites of the framework, so-called isomorphous substitution. These catalytically interesting metals can be present at a T-atom site of the zeolite framework, isolated from the other guest metals and rigidly, four coordinated attached to the zeolite lattice (discussed further in section 1.4).

The formation of a crystalline material which contains nano-scale pores is not restricted to Si and Al oxides, also other metal oxides, of P, B, Ga, Zn etc., can form zeolite-like structures. The most important example of these zeolite related materials are the aluminophosphates (AlPO's) consisting of $AlO_4$ and $PO_4$ tetrahedra, built in the AlPO framework alternately 1:1. Their names are numbered, yet the most important are AlPO-5 (AFI structure) and AlPO-11 (AEL structure)[15].

## 1.4 Metal substituted molecular sieves as oxidation catalysts

As mentioned above, Titanium silicalite 1 (TS-1), is an active and selective catalyst in liquid phase oxidation reactions using hydrogen peroxide as the oxidizing agent[18,19]. In these catalysts titanium is incorporated at T-atom sites of the MFI structure (see figure 1.3).

Various oxidation reactions can be catalyzed by TS-1, such as; olefin epoxidation, oxidation of primary alcohols to aldehydes, aromatic hydroxylation and ammoxidation of cyclohexanone to cylcohexanone oxim (see figure 1.4).
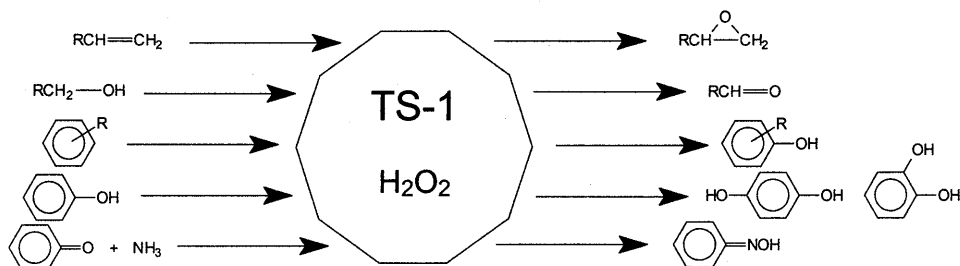


*Figure 1.4  Oxidation reactions catalyzed by titanium silicalite 1 (TS-1).*

Because of the success of the TS-1 catalyst in the 1980s, many research groups tried to incorporate titanium or other metals in all kinds of zeolite structures. The most well known examples are the MeAPO's, metal substituted aluminophosphates. Because of the acidic synthesis conditions for these AlPO's (in contrast to the in general basic synthesis conditions for zeolites), it is easy to introduce other (guest) metals in the synthesis mixture without an immediate precipitation of the metal (hydr)oxide. During the 80s and 90s the synthesis and application of several MeAPO's were reported, for example: VAPO, CoAPO, CrAPO, MnAPO. At that time the term 'redox molecular sieves' was introduced, since these type of metals will change their oxidation state in oxidation catalysis. Later, however, this term is applied for all transition metal containing microporous structures, including TS-1. Yet, this is somewhat misleading since titanium catalyzes oxidation reactions without a change in oxidation state. Of course, the oxidation catalysis concerned are redox type reactions in terms of oxidant and substrate.

Initially, it was believed that all those metal containing molecular sieves were stable catalysts. The microporous lattice of the zeolite offers protection towards solvolysis of the active metal center which could be followed by leaching of the catalyst. Nevertheless, in the last years, more and more metal substituted molecular sieves are proven to leach small percentages of their active metal during catalysis. Already in 1994 it was reported that CoAPO-5 looses a significant amount of cobalt under strongly alkaline conditions[20,21]. The first report concerning the stability of MeAPO's in neutral conditions deals with the application of VAPO-5 in alcohol oxidation reactions with TBHP[22]. It was proven, by a removal of the heterogeneous catalyst from the reaction mixture by filtration and studying the proceeding reaction in the filtrate, that the VAPO-5 looses small amounts of vanadium (about 0.9 - 12.5 % of the total amount of vanadium). Initiated by these results, it is reported that also Cr-silicalite-1, CrAPO-5 and CrAPO-11 appeared to be unstable during oxidation catalysis[23].

This is ascribed to the leaching of active chromium species, probably initiated by the formation of the alkylperoxo metal complex.

Another major drawback of the aluminophosphate structures is the fact that they consist of $Al^{3+}$ and $P^{5+}$ tetrahedra, built alternately into the AlPO framework. The differences in loading introduced by alternating 3+ and 5+ tetrahedra result in a relatively hydrophilic framework, in contrast with the hydrophobic silicalite framework of TS-1. Applying a hydrophilic molecular sieve in liquid phase oxidation catalysis, will always end in pore blocking by the polar organics involved, resulting in major diffusion limitations. We may, therefore, conclude that these type of structures are far from ideal to apply in liquid phase oxidation catalysis. Where TS-1, on the other hand, has a perfect hydrophobicity for liquid phase oxidation reactions. The concentration of the polar hydrogen peroxide at the active site is kept low and at the same time polar oxygenated products are removed quickly from the hydrophobic zeolite micropores.

## 1.5 Post synthesis modification

As can be seen from table 1.1, the pore opening of Titanium Silicalite-1 (MFI structure) is only $5.6 \times 5.3$ Å. In fact, the MFI structure is only accessible for linear alkenes or alkanes and para-substituted bezenes, while, for instance, aliphatic cyclic compounds, such as cyclohexane or cyclooctane can hardly enter the MFI pore system (kinetic diameter of cyclohexane is approximately 6.0 Å)[24]. This is confirmed with catalytic experiments in which cyclohexene could not be epoxidized over TS-1[8]. When we succeed in the incorporation of titanium in large pore zeolite structures, such as mordenite and beta (see figure 1.3), we might be able to oxidize larger substrates, like cyclic compounds.

Large pore titanium zeolites would certainly widen the application of titanium zeolites in oxidation catalysis. The difficulty is that most precursor gels need strong basic conditions to form the right zeolite, especially with the large pore zeolites, like mordenite. Those basic conditions are often achieved by the addition of NaOH or KOH. The silicalite structure is one of the rare examples that can be made easily in the absence of these alkali ions. A high alkali content of the precursor gel will result in the formation of titanium oxide species, most probably outside the zeolite framework. Even the presence of very small amounts of alkali, like trace impurities in the template source in the silicalite-1 synthesis gel[25], can result in not incorporated titanium species. In line with this, most large pore zeolites, as mordenite or faujasite, cannot be synthesized without aluminum in the precursor gel[26], which, as explained in section 1.4, results in a relatively hydrophilic framework, not useful for an active heterogeneous oxidation catalyst.

These problems can be overcome with a post synthesis procedure: First the desired (large pore) zeolite is synthesized, containing aluminum sites. Then this zeolite is *dealuminated*; the aluminum sites are removed from the zeolite lattice, for instance by an acid extraction, resulting in defect sites (so-called hydroxyl nests) in the zeolite lattice. In a second step, titanium is introduced in the zeolite framework, via a reaction of the hydroxyls of the defect site with a titanium precursor, like TiCl$_4$. This route is visualized in Figure 1.5.
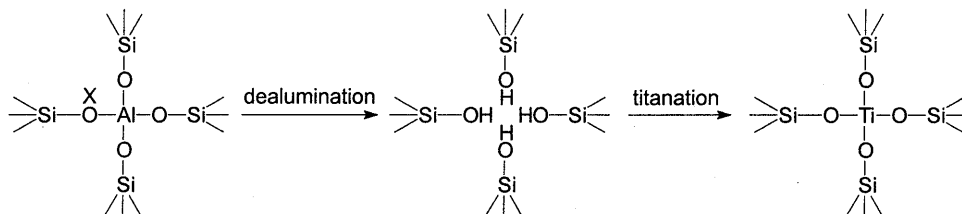


*Figure 1.5 A schematic two-dimensional representation of a titanium zeolite made via post synthesis modification. In the first step aluminum is removed by an acid treatment (dealumination), in a second step titanium is introduced by a reaction of the resulting vacant site with a titanium precursor, like TiCl$_4$ (titanation). The charge compensation cation present at the aluminum site in the parent zeolite is represented by* X.*.*

Obviously, the advantage of this approach compared to the direct synthesis is that it should be applicable for all zeolites as long as they contain aluminum. Moreover, the titanium content can be tuned within the titanation experiment while in case of the direct synthesis a maximum is reached at about 2 wt% for isolated, tetrahedral incorporated titanium[27]. The disadvantage of the post synthesis procedure can be the number of steps needed for this synthesis.

## 1.6 Heterogenization of homogeneous catalysts

Besides the heterogenization of titanium catalysts *via* an incorporation of the titanium site in a zeolite structure, we can consider the heterogenization of a well defined and stable homogeneous oxidation complex. Such heterogenized homogeneous metal complexes have the advantage that the catalytic center, for instance the titanium site, is well defined and has a known activity in homogeneous catalysis. The best explored examples of heterogenization techniques in (oxidation) catalysis are schematically represented in figure 1.6, followed by a short description for each of these techniques.
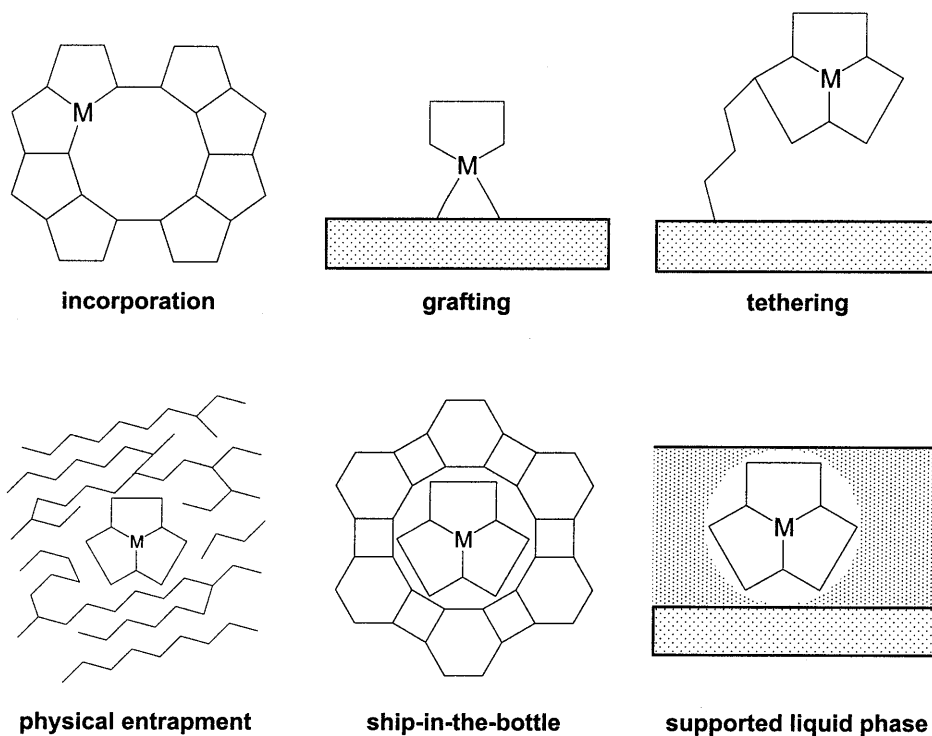
*Figure 1.6 Schematic representation of the various ways for heterogenization of an arbitrary metal (M) complex.*

- Grafting or Tethering. Usually, the term 'grafting' is used for the reaction of metals with the surface groups (like SiOH groups), resulting in the host material acting as a ligand for the active metal complex[28,29]. Whereas 'tethering' refers to the reaction of (one of) the metal ligand(s) with surface groups[30,31]. In the latter case the surrounding of the active metal complex is equal to the homogeneous case, while in the case of grafting the host becomes one of the metal ligands.

- Physical entrapment. Several mesoporous hosts, like sol-gel silica[32] or polymer structures, like PDMS membranes[33], can be used to physically 'entrap' a homogeneous complex by synthesizing the host around the complex. These materials have large pores, which is beneficial for the diffusion of organics through the host material. On the other hand, a very tenuous, mesoporous structure will have less 'control' over the entrapped homogeneous complex, which can result in leaching of the complex out of the host material.

- Ship-in-the-bottle catalysts, which is a special kind of the above mentioned 'physical entrapment'[34]. The homogeneous complex is made inside its host material, usually a cage

like zeolite structure like X or Y, from its starting parts: the metal center and the ligands. After complexation with the metal center, the complex should be too large to leave the zeolite pores. The resulting complexes are entrapped sterically or electrostatically inside the host and not chemically bound to the host.

- Supported liquid phase immobilization. With this method a metal complex is heterogenized by dissolving it in a very thin solvent layer, supported on a mesoporous host. The reactants are present in another liquid phase, which is immiscible with the first, supported liquid phase. The catalysis takes place at the interface between these phases[35].

## 1.7 Scope of this thesis

In this thesis emphasis is put on the development of heterogeneous titanium oxidation catalysts for liquid phase applications. Additionally, attention will be paid to a homogeneous titanium complex in oxidation catalysis and its heterogenization. Different large pore titanium zeolites, all synthesized according to the above described post synthesis modification, will be investigated. This research, as a part of the NIOK[§] project EZ BC-1, "Redox Molecular Sieves; Solid, Stable and Recyclable catalysts for Liquid Phase Oxidation Reactions", is approached from a catalyst development point of view. The oxidation reactions chosen are adapted from known reactions in the field of homogeneous and heterogeneous oxidation chemistry. The choice for titanium based oxidation catalysts is validated with the already known successful homogeneous as well as heterogeneous titanium oxidation catalysts. The main objective of this research is to develop well-defined heterogeneous titanium based oxidation catalysts.

In Chapter 2 and 3 respectively the dealumination and titanation of large pore zeolites is described. For both treatments an optimized procedure will be discussed. Special attention is paid to the stability of the defected zeolites in the dealumination procedure and the avoidance of the formation of catalytically inactive titanium oxide species in the titanation procedure. The application of the obtained titanium zeolites in liquid phase epoxidation catalysis is described in Chapter 4, in which the stability of the obtained materials plays an important role. We change to other titanium based systems in Chapter 5; complexes known as titanium silsesquioxanes will be discussed and find their application in highly defined homogeneous titanium oxidation catalysts. Moreover, we obtained evidence for the proposed mechanism of the activation of the active titanium site by a peroxide attack. Finally, in Chapter 6, the successful heterogenization of an active and stable homogeneous titanium complex in MCM-41 type structures is reported. The obtained, self-assembled materials, are highly stable and recyclable oxidation catalysts.

---

§ NIOK means (in Dutch) 'Nederlands Instituut voor Onderzoek in Katalyse', which is translated into: 'Netherlands Institute for Catalysis Research'. This research project is done in close collaboration with drs. H.E.B. Lempers and prof. dr. R.A. Sheldon, from the Delft University of Technology.

# References

1.  R.A. Sheldon, *Catal. Today., 19*, (**1994**), p. 215.
2.  K. Weissermel, H.-J. Arpe, *Industrial Organic Chemistry*, VCH, Weinheim, 2nd edition, (**1993**).
3.  T. Katsuki, K. B. Sharpless, *J. Am. Chem. Soc., 102*, (**1980**), p. 5974.
4.  R.A. Sheldon, *Stud. Surf. Sci. Catal., 55*, (**1990**), p. 1.
5.  Shell Oil, British Patent 1 249 079, (**1971**).
6.  R.A. Sheldon, *J. Mol. Catal., 7*, (**1980**), p. 107.
7.  M.G. Clerici, *Appl. Catal., 68*, (**1991**), p. 249.
8.  M.G. Clerici, P. Ingallina, *J. Catal., 140*, (**1993**), p. 71.
9.  M. Taramasso, G. Perego, B. Notari, US Pat., 4 410 501, (**1983**).
10. A. Zecchina, S. Bordiga, C. Lamberti *et al.*, *Catal. Today, 32*, (**1996**), p. 97.
11. W. Adam, A. Corma, T. Indrasena Reddy, M. Renz, *J. Org. Chem., 62*, (**1997**), p. 3631.
12  C. B. Khouw, C. B. Dartt, J. A. Labinger, M. E. Davis, *J. Catal., 149*, (**1994**), p. 195.
13  E. Karlsen, K, Schöffel, *Catal. Today, 32*, (**1996**), p. 107.
14. A. F. Cronstedt, Rön och beskrifning om en obekant bärg art, som kallas Zeolites, Svenska 15 Vetenskaps Akademiens Handlingar Stockholm, 17, (**1756**), p. 120 (translated by J. L. Schlenker and G. H. Kühl in *Proc. 9th Int. Zeolite Conf.*, Montreal (Ed. R von Ballmoos, J.B. Higgins, M.M.J. Treacy) Butterworth-Heinemann, (**1992**), p. 3).
15. W.M. Meier, D.H. Olson, Ch. Baerlocher, *Atlas of Zeolite Structures Types, Zeolites, 17*, (**1996**).
16. J. C. van der Waal, M. S. Rigutto, H. van Bekkum, *J. Chem. Soc. Chem. Commun.*, (**1994**), p. 1241.
17. T. Blasco, M.A. Camblor, A. Corma *et al.*, *J. Phys. Chem. B., 102*, (**1998**), p. 75.
18. U. Romano, A. Esposito, F. Maspero, C. Neri, M.G. Clerici, *La Chimici & L'Industria, 72*, (**1990**), p. 610.
19. E. Höft, H. Kosslick, R. Fricke, H.-J. Hamann, *J. Prakt. Chem., 388*, (**1996**), p. 1.
20. M. Peeters, *Pd.D. Thesis*, Eindhoven University of Technology, (**1993**).
21. B. Krauhaar-Czarnetzki, W.G.M. Hoogervorst, W.H.J. Stork, *Stud. Surf. Sci. Catal., 84*, (**1994**), p. 1869.
22. M.J. Haanepen, A.M. Elemans-Mehring, J.H.C. van Hooff, *Appl. Catal. A., 152*, (**1997**), p. 203.
23. H.E.B. Lempers, R.A. Sheldon, *Stud. Surf. Sci. Catal., 105*, (**1997**), p. 1061.
24. J.H.C. van Hooff, J. W. Roelofsen, *Stud. Surf. Sci. Catal., 58*, (**1991**), p. 241.
25. A.J.H.P. van der Pol, J.H.C. van Hooff, *Appl. Catal. A., 92*, (**1992**), p. 93
26. D.W. Breck, *Zeolite Molecular Sieves*, John Wiley & Sons Inc., (**1974**).
27. G. Bellussi, M.S. Rigutto, *Stud. Surf. Sci. Catal., 85*, (**1994**), p. 177.
28. T. Maschmeyer, F. Rey, G. Sanker, J.M. Thomas, *Nature, 378*, (**1995**), p. 159.
29. R. Anwander, R. Roesky, *J. Chem. Soc., Dalton. Trans*, (**1997**), p. 137.
30. Although their definition differs from ours, using the term 'grafting', a few examples of what we call tethering are: a) A. Corma, A. Fuerte, M. Iglesias, Sánchez, *J. Mol. Cat. A., 107*, (**1996**), p. 225; b) J.F. Díaz, K.J. Balkus, F. Bedioui, V. Kurshev, L. Kevan, *Chem. Mater., 9*, (**1997**), p. 61.
31. D. Brunel, A. Cauvel, F. Fajula, F. DiRenzo, *Stud. Surf. Sci. Catal., 97*, (**1995**), p. 173.
32. a) D. Avnir, *Acc. Chem. Res. 28*, (**1995**), p. 328; b) Y. Shvo, Y. Becker, M. Gal, *J. Chem. Soc. Chem. Commun.*, (**1994**), p. 2719; c) D. Avnir, S. Braun, O. Lev, M. Ottolenghi, *Chem. Mater., 6*, (**1994**), p. 1605.
33. a) P.E.F. Neys, I.F.J., Vankelecom, R.F. Parton, W. Dehean, G.L'Abbé, P.A. Jacobs, *J. Mol. Cat. A., 126*, (**1997**), p. L9; b) R.F. Parton, I.F.J. Vankelcom, D. Tas, K.M.B. Janssen, P.-P. Knops-Gerrits, P.A. Jacobs, *J. Mol. Cat. A., 113*, (**1996**), p. 283.
34. a) K.J. Balkus Jr, A.K. Khanmamedova, K.M. Dixon, F. Bedioui, *Appl. Catal. A, 143*, (**1996**), p. 159; b) for a recent review see: D.E. de Vos, F. Thibault-Starzyk, P.-P. Knops-Gerrits, R.F. Parton, P.A. Jacobs, *Macromol. Symp., 80*, (**1994**), p. 157.

35.   a) J.P. Arhancet, M.E. Davis, J.S. Merola, B.E. Hanson, *Nature, 339*, (**1989**), p. 454; b) J.P. Arhancet, M.E. Davis, J.S. Merola, B.E. Hanson, *J. Catal., 121*, (**1990**), p. 327; c) K.T. Wan, M.E. Davis, *Nature, 370*, (**1994**), p. 449; d) M.J. Naughton, R.S. Drago, *J. Catal., 155*, (**1995**), p. 383.

# 2

# Dealumination of zeolites

In this Chapter different ways to dealuminate a zeolite are described. This, with the aim to obtain highly defected and, at the same time, relatively stable zeolites suitable to use as starting materials for titanation purposes (see Chapter 3). For both zeolites used, Mordenite and Beta, an oxalic acid and nitric acid dealumination procedure is applied. In addition, a thermal treatment is used in combination with these acid extraction methods, to optimize the dealumination procedure. The dealuminated zeolites are characterized with FT-IR, $^{29}$Si MAS NMR, XRD and pore volume measurements. The differences found in degrees of dealumination using different zeolites and dealumination procedures is primarily explained with the possibility of silicon migration. Using a nitric acid dealumination in combination with an intermediate thermal treatment, we succeeded in obtaining a dealumination degree of 93 % for Mordenite, while the crystallinity as well as the stability of the aluminum deficient Mordenite is maintained. Using silsesquioxanes as model compounds to mimic particular defect sites in zeolites, we were able to assign the two most commonly reported hydroxyl bands for dealuminated zeolites at 3500 cm$^{-1}$ and 3700 cm$^{-1}$, to hydroxyl nests and hydroxyl pairs, respectively.

## 2.1 Introduction

Dealumination refers to the process in which aluminum is removed from the framework of a zeolite. Upon the removal of the aluminum site also a cation will be removed since charge compensation is no longer required. When this cation is a proton, the number of Brønsted acid sites in the zeolite is decreased. In this way it is possible to tune the overall acidity of the zeolite by a controlled dealumination. Obviously, this is one of the major applications of dealumination in zeolite catalysis. Our goal, however, is to create vacant sites by the removal of aluminum, which can be filled in a later step with titanium. Besides this, dealumination will lead to a less hydrophilic framework, necessary for obtaining good liquid phase oxidation catalysts.

Dealumination can be done in different ways: (1) acid leaching with moderate to strong acids in aqueous solutions[1,2], (2) using chelating compounds, such as ethylene diamine tetraacidic

acid (H$_4$EDTA)[3] or acetyl acetone (acac)[4], (3) with thermal or hydrothermal treatment[5], (4) using silicon halides (e.g. SiCl$_4$) in vapor phase applications at elevated temperatures[6] or in liquid phase applications (e.g. (NH$_4$)$_2$SiF$_6$)[7] or (5) using reactive compounds, like fluorine gas or phosgene[8].

These different methods for the extraction of aluminum leave behind different sites in the zeolite framework. Such a site can be a vacant site which is a cluster of four silanol groups (often referred to as a hydroxyl nest). In general, the use of acids or chelating compounds results in the formation of such hydroxyl nests, as depicted in figure 2.1. The formation of such nests upon acid leaching was first reported by Barrer and Makki already in 1964 in a dealumination study of the zeolite clinoptilolite with HCl[1]. Throughout this work the term 'hydroxyl nest' (or vacant site) is used for the site as present right in figure 2.1, whereas the term 'defect site' is more generally used for all kinds of defects in zeolite structures.
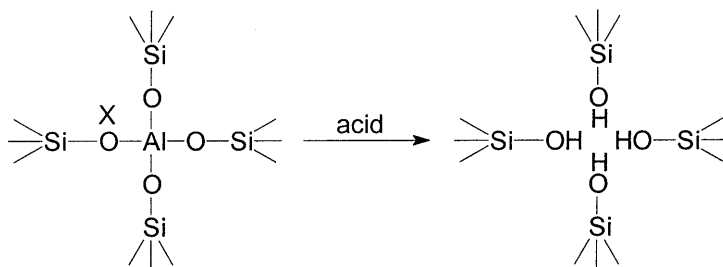


*Figure 2.1  A two-dimensional representation of the formation of a hydroxyl nest (  X represents a cation).*

Thermal or hydro thermal treatment, however, requires such high temperatures for aluminum to be extracted from the framework that vacant sites are no longer stable and dehydroxylation starts to occur, visualized in figure 2.2. The resulting highly deformed structures have been reported earlier in IR studies on dealuminated Mordenites[2,9].
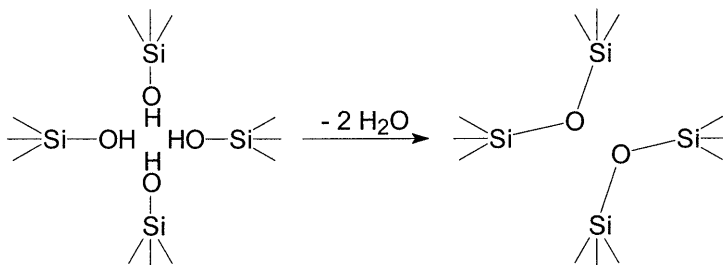


*Figure 2.2  A two-dimensional representation of the dehydroxylation of a hydroxyl nest.*

Another way to stabilize the zeolite framework is by applying relatively elevated temperatures in a heat treatment, causing T-atom migration. The aluminum species extracted from the framework cannot be removed from the sample and will cluster into extra framework aluminum species, most probably aluminum oxide. At the same time the vacant sites formed are filled by migrating silicon species, inducing a higher mesoporousity[10]. Finally, the consecutive combination of different procedures can combine their separate advantages. Moreover, this will increase the total degree of dealumination, while at the same time the amount of aluminum removed per treatment can be limited which is beneficial for maintaining the framework crystallinity[11].

## 2.2 Spectroscopic characterization and stability of silanol groups

There are many spectroscopic studies on silanol groups or silanol nests in dealuminated zeolites. In all studies the zeolite sample has to be dried first so that all physisorbed water is removed and the only hydroxyl frequencies left are arising from hydroxyl groups attached to the zeolite framework. These drying conditions are seldom subject of discussion, that is, if they are mentioned at all. The drying treatments, summarized in table 2.1, are done *in-situ* under vacuum at temperatures varying from 300°C to 600°C for 30 minutes to several hours.

*Table 2.1 Spectroscopic characterization of hydroxyl groups at defect sites in dealuminated zeolites.*

| Zeolite | drying conditions | frequency OH vibration bands | | assignment hydroxyl bands[d] ~ 3500 cm$^{-1}$ | ~ 3700 cm$^{-1}$ | reference |
|---------|-------------------|---------------|------|------------------|------------------|-----------|
| MOR | 500°C, 1.5h | 3500 | 3700 | nests | nests | [9] |
| MOR | 400°C, 14h | 3500 | 3700 | -[c] | vicinal | [15] |
| MOR | 420°C, 8h. | 3510 | 3675 | 'defects' | 'defects' | [16] |
| FAU | -[a] | - | 3710 | - | nests | [7,17] |
| FAU | 450°C, -[b] | 3565 | 3738 | -[c] | 'defects' | [18] |
| FAU | 400°C, 15h[e] | 3530 | 3700 | -[c] | 'defects' | [19] |
| BEA | 400°C, 0.5h | 3560 | - | nests | - | [20] |
| BEA | 450°C, 14h. | - | 3670 | - | 'defects' | [21] |
| MFI | 500°C, 3h | 3500 | 3728 | nests | 'defects' | [22] |
| MFI | -[b] | 3515 | 3680 | nests | vicinal | [23] |
| MFI | 400°C, -[b] | 3500 | 3680 | 'defects' | 'defects' | [24] |
| MFI | 500°C, -[b] | 3500 | 3700 | 'defects' | 'defects' | [25] |
| MFI | 600°C, -[b] | 3500 | 3725 | nests | 'defects' | [26] |

*[a] IR samples were not dried but measured in pressed KBr pellets. [b] Further experimental details were not mentioned. [c] This band was not assigned by the authors. [d] The general term 'defects' is used when the author(s) assignment is not clear. [e] Zeolite samples were reported to be dried 'overnight'.*

We have to keep in mind that the aim of our study is, first of all, the creation of hydroxyl nests. These nests are relatively unstable (defect!) sites, which can degrade upon high temperature treatments, used with drying. So, the question that arises is: Which drying temperature should be applied to be sure that all the water is removed and at the same time no significant decrease of the number of hydroxyl nests is caused? Possible reactions that can occur upon a too severe thermal treatment are: dehydroxylation (depicted in figure 2.2) as reported for ZSM-5[12] and Mordenite[2,13], as well as migration of defects to the outer surface[14] or eventually, a collapse of the zeolite framework[5].

It can be seen from table 2.1 that even after severe drying conditions, the two most common hydroxyl bands arising from defect sites are still clearly observed. We studied the stability of the hydroxyl groups with *in-situ* Fourier Transform Infra-Red spectroscopy (FT-IR). The FT-IR spectra of a dealuminated Mordenite treated at different temperatures and different times are shown in figure 2.3. A drying period for 1 hour at 450°C already removes all the physisorbed water as was indicated by the complete disappearance of the typical IR bending mode of water at 1680 cm$^{-1}$. In other words: All the intensity shown in figure 2.3 is due to hydroxyls that are part of the zeolite framework. Clearly can be seen that temperatures of 500°C and higher are destructive to the hydroxyl groups, which is confirmed by a recent study of Mishin *et al.*[27]. It is concluded that a drying period for 1 hour at 450°C is sufficient to remove the water without being too destructive for the hydroxyl groups.



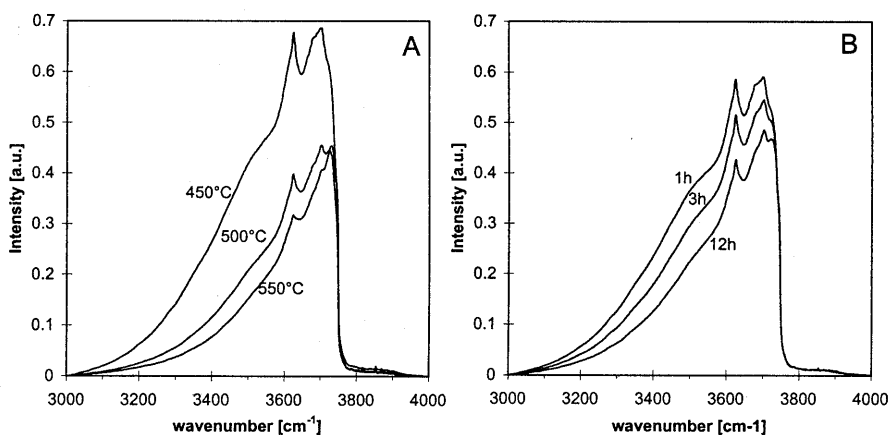*Figure 2.3 FT-IR spectroscopy on dealuminated Mordenite treated in-situ at different temperatures for 1 hour (A) and at 450°C for different times (B).*

Considering the different hydroxyl bands in IR studies on dealuminated zeolites, in general we can distinguish between 6 most commonly observed bands in the hydroxyl region, i.e. 3000 cm$^{-1}$ - 4000 cm$^{-1}$ [9,26,28].

Two of these bands (the so-called 3500 cm$^{-1}$ and 3700 cm$^{-1}$ band, marked in bold) are related to the defect sites in zeolites and have our special attention, as indicated by the assignment study in table 2.1.

**3500 cm$^{-1}$** :   hydroxyls in a defect site, highly hydrogen bridged
3610 cm$^{-1}$ :   hydroxyls from the Brønsted acid site
3660 cm$^{-1}$ :   hydroxyls of extra framework aluminum species
**3700 cm$^{-1}$** :   hydroxyls in a defect site, weakly hydrogen bridged
3730 cm$^{-1}$ :   hydroxyls of isolated silanol groups (disturbed)
3745 cm$^{-1}$ :   hydroxyls of isolated silanols

The discussion about the (different) assignment of the 3500 cm$^{-1}$ and the 3700 cm$^{-1}$ band is continued in section 2.5. Important to note already at this point is the conclusion that the band at 3500 cm$^{-1}$ can be ascribed positively to hydroxyl nests in zeolites, as depicted in figure 2.1. The generally sharp band at 3610 (- 3620) cm$^{-1}$ is the Brønsted acid band, which is probably one of the most studied bands in zeolite spectroscopy[29]. Upon (thermal) dealumination this acid site can be extracted from the zeolite framework, resulting in extra framework aluminum species. Such species can give rise to a band around 3660 cm$^{-1}$, generally accepted as the hydroxyls attached to 'Al(O)OH' species. A fifth band that can be recognized (see also the nitric acid dealuminated Mordenites, section 2.4) is a signal at 3730 cm$^{-1}$. This is only present in dealuminated zeolites and tends to grow with the Si/Al ratio. This band is almost as sharp as the 3745 cm$^{-1}$ band, arising from isolated silanols, located at the outer surface. The little shift (about 15 cm$^{-1}$) can be explained with a reasonably weak interaction with a neighboring oxygen, probably, but certainly not with hydrogen bridging with another hydroxyl group. Therefore, we suggest these isolated silanols to be present inside the Mordenite channels or mesopores, at lattice imperfections arising from dealumination. This is confirmed with the FT-IR spectra obtained for zeolite Beta (see section 2.4), well known for its internal defects[30], in which this band is clearly visible. Also other Infra-Red studies on zeolite Beta and on dealuminated ZSM-5 agree with this assignment [26,28].

## 2.3 Dealumination with oxalic acid

Considering the different techniques to dealuminate a zeolite framework, oxalic acid combines two important features; it provides both acid and chelating properties, which should be ideal for dealumination under mild conditions. The weak acid can extract the aluminum from the zeolite framework and the chelating function keeps the aluminum species dissolved. Water soluble aluminum oxalate complexes as in figure 2.4 are reported in a study on the dealumination of Beta zeolites[20]. In the same report the creation of silanol nests upon oxalic acid treatment is confirmed. The dimensions of the aluminum-oxalic acid complex are close to the pore diameter of both Mordenite and Beta, yet it should just fit in both (maximum

dimension of the aluminum trioxalate complex: 0.64 nm; pore size of the Mordenite 12-ring channel: 0.65 x 0.70 nm, pore size of the Beta 12-ring channels: 0.64 x 0.76 nm and 0.55 x 0.55 nm). In table 2.2 different oxalic acid dealuminated zeolites are summarized.

*Table 2.2  Oxalic acid dealuminated Mordenite.*

| sample[a] | acid-to-aluminum molar ratio | Si/Al (bulk)[b] | Si/Al (NMR) | degree of dealumination[c] |
|---|---|---|---|---|
| Mor/I | - | 6.7 | 6.4 | - |
| Mor/I-8.2a | 0.28 | 8.2 | 8.9 | 16 % |
| Mor/I-8.2b | 0.56 | 8.2 | 10.3 | 16 % |
| Mor/I-14 | 1.4 | 14 | 14.3 | 48 % |
| Mor/I-33 | 1.4 | 33 | 16 | 77 % |

*[a] Sample names consist of the type of zeolite (Mor) followed by the zeolite batch (I or II) and the Si/Al ratio (see also Section 2.7). In all cases ca. 0.25 M oxalic acid was used at 50°C, except for sample Mor/I-33 reflux conditions were used. [b] Determined with Chemical Analysis (AAS). [c] Calculated from the bulk Si/Al ratio.*
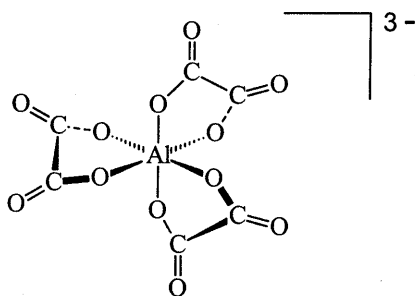


*Figure 2.4  Aluminum trioxalate complex*

As can be seen from these data more aluminum is extracted by applying higher oxalic acid over aluminum ratios. The framework Si/Al ratios calculated from the $^{29}$Si MAS NMR with the equation proposed by Engelhardt *et al.*[31] (equation 2.1) are in good agreement with the Si/Al ratios measured by elemental analysis.

$$\frac{Si}{Al} = \frac{\sum_{n=0}^{4} I_n}{\frac{1}{4} \cdot \sum_{n=0}^{4} n \cdot I_n} \qquad (2.1)$$

This equation is based upon the assumption that no Al-O-Al linkages are present in the zeolite framework and that the contribution of the Si(OH) band to the intensity of the Si(1Al) band is negligible. The former assumption is known as the Löwenstein rule, who stated already in

1954 that it was impossible for aluminum to have an aluminum neighbor[32]. Probably due to the latter assumption this equation loses its predictive value with increasing degree of dealumination, as can be seen with the last sample in table 2.2, Mor/I-33. In that case the contribution of the Si(OH) band to the Si(1Al) band becomes significant, resulting in a higher discrepancy. This is in good agreement with the results of Bodart et al.[33] who showed the same trend for nitric acid and hydrochloric acid dealuminated Mordenites. A slightly higher Si/Al ratio determined with $^{29}$Si MAS NMR can be explained by the formation of extra framework aluminum species. Such extra framework aluminum species are most probably aluminum oxide like structures, in which the environment of the aluminum is changed into an octahedral coordination. This is confirmed by $^{27}$Al MAS NMR measurements where the band at around 0 ppm, which has been assigned to octahedral aluminum species[11,33], is increasing with higher Si/Al ratios of the dealuminated zeolites. Also in Infra-Red analysis the formation of aluminum oxide species is confirmed by the formation of the band at around 3670 cm$^{-1}$, assigned to hydroxyl groups arising from extra framework aluminum species (see figure 2.5). It is generally accepted that a band at around 3660 cm$^{-1}$ is arising from hydroxyl species on aluminum oxide[2].

FT-IR is also used for studying the formation of defect sites. In the hydroxyl region different bands can be recognized and assigned to different hydroxyl groups (see section 2.2). In figure 2.5 the FT-IR spectra of oxalic acid dealuminated Mordenites are shown. Both the 3500 cm$^{-1}$ and the 3700 cm$^{-1}$ band increase in intensity by applying higher oxalic acid concentrations. Thus, a decrease of the aluminum content leads to an increase in hydroxyl bands corresponding to defect sites.
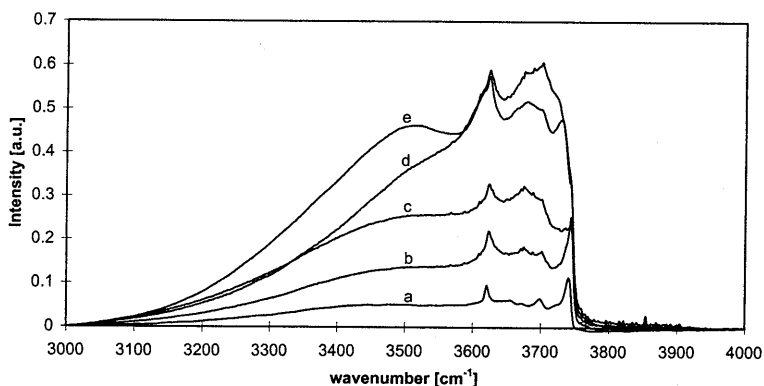


*Figure 2.5 FT-IR spectra of oxalic acid dealuminated Mordenite: [a] parent Mor/I, [b] Mor/I-8.2a, [c] Mor/I-8.2b, [d] Mor/I-14, [e] Mor/I-33.*

The sample dealuminated at reflux conditions shows a much higher intensity of the 3500 cm$^{-1}$ band. This is in line with the much higher Si/Al ratio obtained, Si/Al = 33. The band at

around 3620 cm$^{-1}$, arising from bridging hydroxyl groups, or Brønsted acid sites, is also enlarged by the dealumination treatment. This is due to the ion exchange of the sodium cation in the starting Mordenite with the acidic protons from the oxalic acid. The intensity of this band is dependent on the degree of ion exchange and on the aluminum content of the zeolite. Above a certain level of dealumination this band should decrease in intensity, as will be discussed in section 2.4.

The crystallinity of the acid leached Mordenites was investigated with X-Ray Diffraction techniques. The XRD diffraction pattern of a modified zeolite shows a small change upon aluminum extraction (see figure 2.6). First, a loss in intensity is observed for the majority of peaks positioned at $2\theta > 15°$. These decreasing intensities can be explained by a small loss in crystallinity due to some structural rearrangements. A second phenomenon is the increase of the first three peaks in the XRD diffraction pattern, at $2\theta = 6.5°$ (110), $2\theta = 8.6°$ (020) and $2\theta = 9.8°$ (200), upon acid treatment. This is a generally observed feature in acid leached zeolites in this study (see also XRD diffraction patterns of dealuminated Mordenites in section 2.4) and is also noticed in some other dealumination reports, although not explained by their authors[5,8]. We believe that this behavior relates to the water adsorption in the zeolite lattice. Since the cation in the neighborhood of the aluminum site is a hydrophilic site, water molecules will be strongly adsorbed there [34], possibly even in an clustered way [35,36]. When this water is removed by the removal of the cation in a dealuminated zeolite, we see a significant increase in these diffraction bands. The same trend is observed for the removal of the water out of the parent zeolite. With temperature dependent XRD diffraction measurements, the water was removed *in-situ* by heating up the sample. In these diffraction patterns was the same strong increase of the first three diffraction peaks observed when the sample was heated up to 200°C. According to TGA measurements about 80-90 % of the physisorbed water is removed at that temperature.



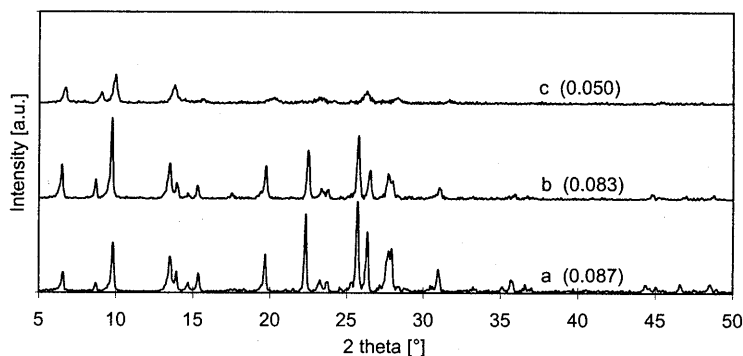*Figure 2.6   XRD diffraction patterns of (dealuminated) Mordenite: [a] parent Mor/I, [b] Mor/I-14, [c] Mor/I-14 treated at 400°C for 2 hours. The numbers in between brackets represent the micropore volume in [ml/g].*

Apparently, the adsorption of water around the cation site in a hydrated zeolite, causes a less ordered framework resulting in less intensity in the diffraction bands at low 2θ. This effect is neutralized when the cation (or only the water) is removed in a dealuminated zeolite. Furthermore, the intensities in the resulting diffraction pattern for dealuminated Mordenite show much better resemblance with the calculated (theoretical) powder diffraction patterns for Mordenite [37].

Besides the already mentioned stability of the silanol groups towards drying treatments for characterization purposes (see section 2.2), the (highly) defected zeolites also have to survive the titanation treatment, executed at elevated temperatures (typically 500°C) to activate the titanium precursor (see Chapter 3). Concerning this thermal stability of the oxalic acid dealuminated Mordenites, a completely different behavior at elevated temperatures was found for the oxalic acid dealuminated Mordenite treated at reflux conditions in comparison with the Mordenites dealuminated at 50°C. The former sample showed no loss in XRD crystallinity when treated at 400°C while the 50°C dealuminated samples, for example the sample Mor/I-14 (see figure 2.6) almost totally collapsed at 400°C. This difference in thermal stability can be explained by silicon migration. Such migration of silicon atoms into defect sites of the zeolite will heal the zeolite structure. This healing, therefore, will be more pronounced at higher temperatures or longer times, as reported by Apelian and co-workers,[20] and therefore a higher extent of stabilization is reached with higher dealumination temperatures.

*Table 2.3  Oxalic acid dealuminated Beta.*

| sample | calcined | oxalic acid | Si/Al | degree of dealumination |
|--------|----------|-------------|-------|-------------------------|
| Bea | - | - | 37.5 | - |
| Bea-141 | - | 0.25 M | 141 | 74 % |
| Bea-160 | 550°C, 5h | 0.25 M | 160 | 77 % |
| Bea-267 | - | 1.5 M | 267 | 86 % |
| Bea-321 | 550°C, 5h | 1.5 M | 321 | 88 % |

*Sample names consist of the type of zeolite (Bea) followed by the Si/Al ratio (see also Section 2.7).*

Because of these results a series of Beta dealuminated samples is prepared using oxalic acid at reflux conditions (see table 2.3). Since in this case the parent zeolite was in the ammonium form, we performed also a thermal dealumination beforehand in which the zeolite is heated at 550°C, for 5 hours. Afterwards, an acid extraction will remove the (non) framework aluminum species. This effect is expressed in the higher Si/Al ratios obtained with the samples which were thermally treated before the acid dealumination. After acid extraction all samples were free from extra framework aluminum indicated by the absence of the 3660 cm$^{-1}$ band in their IR spectra. All oxalic acid dealuminated Beta zeolites did survive a thermal treatment at 500°C. Note that the much higher Si/Al ratios obtained for dealuminated Beta are

due to the higher starting Si/Al ratio (Si/Al = 37.5). This is also expressed in the total disappearance of the Brønsted acid 3610 cm$^{-1}$ band in their IR spectra. The degree of dealumination of the Na-Mordenite (Mor/I-33 , table 2.2), treated under the same conditions, has the same order of magnitude (77 %) as its Beta analogue (74 %). However, in the case of Beta, the higher starting Si/Al ratio made it possible to obtain high dealuminated and at the same time high temperature stable zeolites, since less defect sites were created.

In conclusion, the oxalic acid treatment is capable of extracting a sufficient amount of aluminum out of the zeolite without a collapse of the framework structure. In the case of dealuminated Mordenite, however, we believe that a more sophisticated dealumination procedure is necessary when we want to reach an extraction level over 90 - 95 % removed aluminum. Such a level is essential for obtaining high silica zeolites with a highly hydrophobic framework. This hydrophobicity is necessary to obtain, after titanium incorporation, an active and selective liquid phase oxidation catalyst.

## 2.4 Dealumination with nitric acid

In earlier reports nitric acid was proven to be a powerful extracting acid, capable of removing the majority of the aluminum atoms from the zeolite lattice, without destroying the zeolite framework or its (XRD) crystallinity [9,11]. We varied the molarity of the nitric acid and also performed multi-step treatments, in which in between the zeolite was thermally treated to remove the aluminum atoms from their framework positions.

From table 2.4 it can be seen that applying a higher molarity of nitric acid leads, obviously, to higher Si/Al ratios and a higher hydroxyl nest concentration, which is confirmed by IR analysis on these dealuminated Mordenites (figure 2.7). Also we see that a thermal treatment of the parent sodium Mordenite has a negligible influence on the final degree of dealumination after the acid extraction. This is in agreement with the findings of Beyer *et al.*[38], who reported that a sodium Mordenite was stable up to 800°C and Bodart *et al.*[33], who showed that a sodium Mordenite is hardly dealuminated at 600°C even in the presence of steam. This in contrast to the NH₄Beta parent material where during a heat treatment in an inert atmosphere ammonia is removed and Brønsted acid sites are created, which are not stable and sensitive for thermal dealumination (see Table 2.3).

Regarding the dealuminated Mordenites, the Brønsted acid site, created by ion exchange with the strong acid, can be clearly seen at around 3620 cm$^{-1}$ (figure 2.7). Applying higher molarities of the nitric acid, more aluminum is removed and the Brønsted acid band is diminished, while both the 3500 cm$^{-1}$ and the 3700 cm$^{-1}$ band gradually grow with increasing Si/Al ratio.

*Table 2.4  Nitric acid dealuminated Na-Mordenite.*

| sample | thermal treatment | acid treatment | Si/Al ratio | total degree of dealumination |
|---|---|---|---|---|
| Mor/I | - | - | 6.7 | - |
| Mor/I-35 | - | 7 M | 35 | 82 % |
| Mor/I 39 | 700°C, 1h | 7 M | 39 | 83 % |
| Mor/I-48 | 700°C, 1h | 9 M | 48 | 86 % |
| Mor/I-79 | 700°C, 1h | 10 M | 79 | 92 % |
| Mor/I-150 | 700°C, 1h | 14 M | 150 | 96 % |
| Mor/I-53[a] | - | 7 M | 52 | 87 % (11 %)[d] |
| Mor/I-75[a] | 500°C ,1h | 7 M | 75 | 90 % (32 %)[d] |
| Mor/I-00[a, b] | 700°C ,1h | 7 M | [b] | [b] |
| Mor/II | - | - | 6.1 | - |
| Mor/II-33a | - | 7 M | 33 | 78 % |
| Mor/II-33b[c] | 700°C, 1h | - | 33 | 78 % |
| Mor/II-116[c] | 700°C ,1h | 7 M | 116 | 93 % (70 %)[d] |

*Sample names consist of the type of zeolite (Mor) followed by the zeolite batch (I or II) and the Si/Al ratio (see also Section 2.7). [a] With sample Mor/I-35 as parent sample. [b] XRD Crystallinity < 10 % : zeolite structure totally collapsed. [c] with sample Mor/II-33a as parent sample. [d] Percentage between brackets is the calculated degree of dealumination for the last step only.*

Both trends are also nicely shown in figure 2.11, where the intensity of the band arising from a hydroxyl nest smoothly increases, whereas the 3610 cm$^{-1}$ Brønsted acid band finds its optimum around 80-85 % dealumination, corresponding to approximately Si/Al = 40.
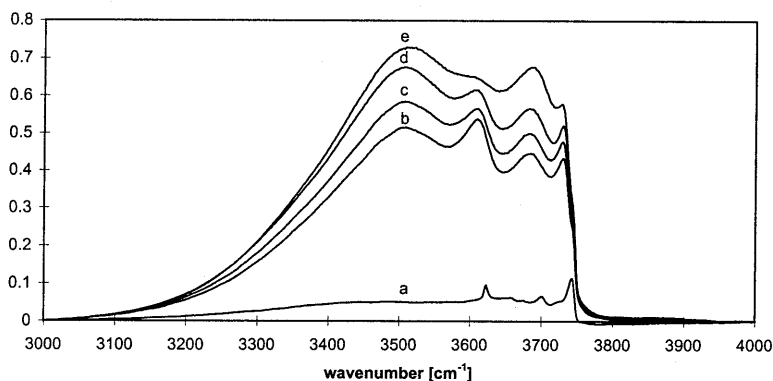


*Figure 2.7  FT-IR spectroscopy on nitric acid dealuminated Mordenite (series I): [a] parent Mor/I, [b] Mor/I-39, [c] Mor/I-48, [d] Mor/I-79, [e] Mor/I-150.*

To be able to reach higher Si/Al ratios, without losing the zeolite stability necessary for the titanation step, we performed a multi-step dealumination, in which the zeolite is stabilized in

between by a thermal treatment. Thus, in the first step about 80 % of the aluminum is extracted, leaving defect sites behind. Then, by the thermal treatment, these defect sites are (partially) healed by silicon migration or by dehydration and at the same time the last aluminum sites left will be extracted and extra framework aluminum species will be formed (see 3660 cm$^{-1}$ band in Mor/II-33b). The second acid treatment will leach the framework aluminum atoms and the non-framework aluminum species. In table 2.3 it is shown that such calcination can be successfully performed at 500°C. Nevertheless, the second acid treatment is not as effective as the first, respectively 32 % versus 82 %, although more effective with the in between heat treatment (without heat treatment we found 11 % dealumination in the second step). A treatment at 700°C appeared to be too destructive for the dealuminated Mordenite (Mor/I), although this was exactly the same multi-step dealumination treatment as reported by Wu et al.[9] An explanation for this could be the fact that Wu and co-workers started with an H-Mordenite, which will be thermally dealuminated to a great extent during the first thermal treatment, resulting also in a higher stability of the dealuminated zeolite due to silicon migration. Another influencing parameter in this respect could be the crystal size of the starting material. Our Na-Mordenite-I has very small crystals (0.01 - 0.1 μm), which could affect the stability in a negative way. To test this hypothesis we applied the same dealumination treatment on another sodium-Mordenite ( Mor/II, Si/Al = 6.5) with a significant larger particle size of about 0.1 - 2 μm (see Table 2.4). This Mordenite with larger crystallites was stable with regard to the 700°C treatment, which was demonstrated by an unchanged micropore volume as well as a hardly changed XRD intensity of the main diffraction bands (see figure 2.8). We obtained, within a three step procedure, a dealumination degree of 93 % without any loss in crystallinity or stability.
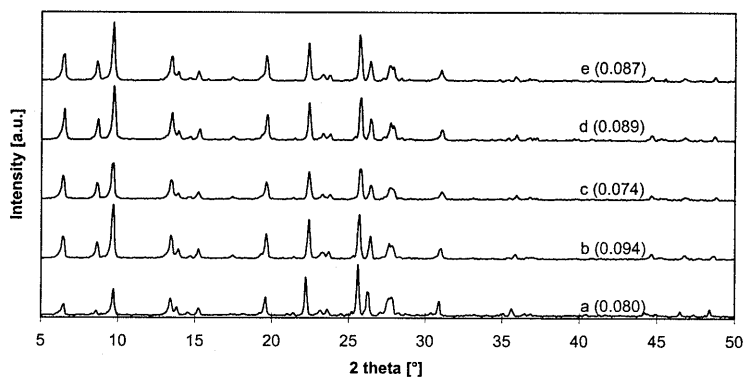


*Figure 2.8   XRD diffraction patterns of (dealuminated) Mordenite: [a] parent Mor/II, [b] Mor/II-33a, [c] Mor/II-33b, [d] Mor/II-116, [e] Mor/II-116 treated at 500°C for 1.5 hours in a titanation experiment. The numbers in between brackets represent the micropore volume in [ml/g].*

Obviously, the higher temperature applied (700°C) is much more effective than the 500°C in the case of Mor/I, resulting in a 70 % degree of dealumination for the second step. With FT-IR analysis the formation of hydroxyl nests was confirmed (see figure 2.9). When

comparing sample mor/I35 with mor/II33, it is noticeable that their Si/Al ratios after the first nitric acid treatment are as good as the same (respectively a Si/Al ratio of 35 and 33). Furthermore, the shape of their IR spectra in the hydroxyl region are almost overlapping, demonstrating that these samples behave the same in the acid dealumination treatment and that their thermal stability is a more macroscopic feature. In summary, the influence of crystal size on a (thermal) dealumination treatment is shown by the comparison of the Mor/I and Mor/II series in dealumination behavior. A too small crystal size of the parent mordenite (Mor/I) results in thermally unstable dealuminated mordenite samples.
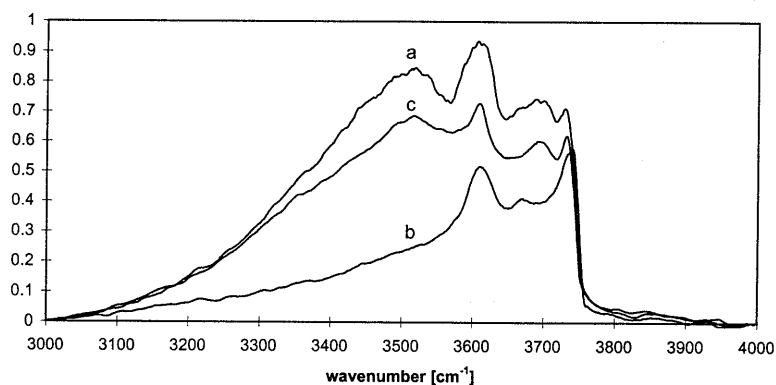


*Figure 2.9 FT-IR spectroscopy on nitric acid dealuminated Mordenite (series II): [a] Mor/II-33a, [b] Mor/II-33b, [c] Mor/II-116.*

Subjecting the relatively high silica parent Beta zeolite to the nitric acid dealumination, very high Si/Al ratio's were obtained (as far as Si/Al = 450, see table 2.5). We can conclude that it is easier to dealuminate zeolite Beta than Mordenite with nitric acid (applying 7 M nitric acid results in 82 % dealumination for Mordenite and 93 % dealumination for Beta). This difference will be discussed in section 2.5.

*Table 2.5 Nitric acid dealuminated Beta.*

| sample | molarity nitric acid | Si/Al ratio | degree of dealumination |
|---|---|---|---|
| Bea | - | 37.5 | - |
| Bea-72 | 1 M | 72 | 49 % |
| Bea-170 | 4 M | 170 | 78 % |
| Bea-450 | 7 M | 450 | 92 % |

*Sample names consist of the type of zeolite (Bea) followed by the Si/Al ratio (see also Section 2.7).*

The FT-IR spectra of the nitric acid dealuminated Beta samples are plotted in figure 2.10. Again a nice trend can be observed as a function of Si/Al ratio, and at the same time the gradual disappearance of the Brønsted acid band with the degree of dealumination, as was

already mentioned in the case of nitric acid dealuminated Mordenites (see above). The position of the, so-called, 3500 cm$^{-1}$ band for dealuminated Mordenite is in the case of dealuminated Beta somewhat shifted to higher wavelengths: around 3540 cm$^{-1}$ for all samples.
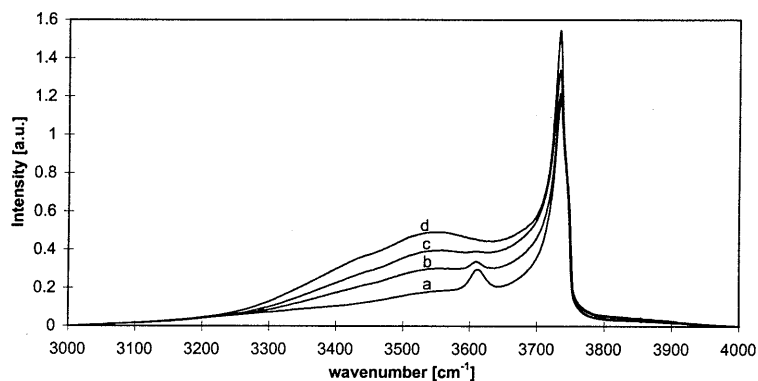


*Figure 2.10   FT-IR spectroscopy on nitric acid dealuminated Beta: [a] parent Beta, [b] Bea-72, [c] Bea-170, [d] Bea-450.*

The gradual increase of the 3500 cm$^{-1}$ band as a function of Si/Al ratio, becomes even more pronounced when we plot its intensity *versus* the degree of dealumination (see figure 2.11). For both Mordenite (3500 cm$^{-1}$) and Beta (3540 cm$^{-1}$) clear trends are observed, which are roughly overlapping. This can indicate that the amount of hydroxyls formed is not related to the absolute amount of aluminum removed, since the same *degree* of dealumination is reached with a completely different absolute amount of aluminum leached. This again is an indication for migration of T-atoms through the zeolite framework.
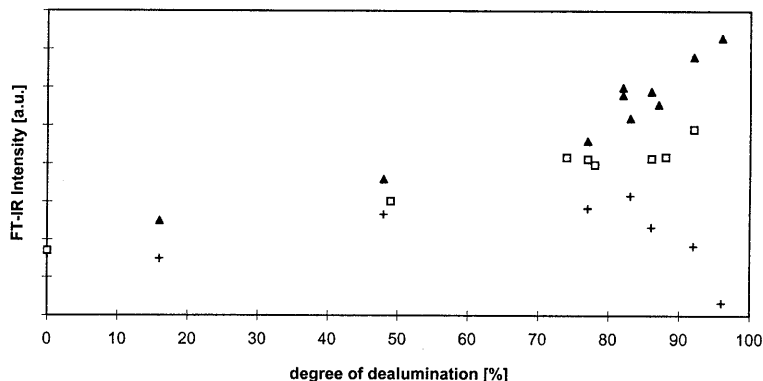


*Figure 2.11  The intensity of the 3500 cm$^{-1}$ band (▲) and of the 3610 cm$^{-1}$ band (+) for dealuminated Mordenites (series I) and of the 3540 cm$^{-1}$ band for dealuminated Betas (□) as a function of dealumination degree.*

## 2.5 Model compounds for zeolite defect sites

Concerning the assignment of the two most commonly observed hydroxyl bands in dealuminated zeolites, the bands around 3500 cm$^{-1}$ and 3700 cm$^{-1}$, it is stated by Wu and co-workers that both bands should arise from hydroxyl groups in defect sites of a dealuminated Mordenite[9]. Their statement is based on the fact that both hydroxyl groups exhibit the same behavior upon acid dealumination. As can be seen from the several references in table 2.1, however, the assignment of these bands is not unambiguous. Moreover, our study concerning the behavior of these two bands with varying dealuminating acid and dealumination temperature showed totally different behavior of these two bands. Therefore, it seems evident that these two bands should arise from different hydroxyl species.

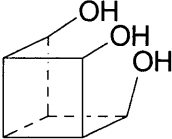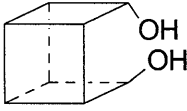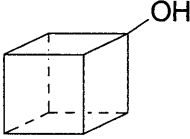Since the 3500 cm$^{-1}$ band is shifted about 240 cm$^{-1}$ to lower frequency compared to the isolated silanols at 3745 cm$^{-1}$, we assume that these OH bonds are highly weakened due to their internal hydrogen bonding. Moreover, the broad appearance of this band is indicative for strong delocalization caused by the hydrogen bridges. The shift of the 3700 cm$^{-1}$ band is only about 40 cm$^{-1}$ away from the isolated silanol band and is considerably less broad compared to the 3500 cm$^{-1}$ band. This very different appearance of the 3700 cm$^{-1}$ band implies again that this band arises from a different, but still moderately disturbed, OH species. The different nature of those two bands is confirmed by titanation reactions of these silanol groups showing a totally different behavior of these bands upon the reaction with different titanium precursors (see section 3.3). Also in a study of Moreno *et al.* the plotted spectra show a significantly different response of the 3500 cm$^{-1}$ and the 3700 cm$^{-1}$ band as a function of temperature, again indicating their different origin [15].

The controversy concerning the contradictory assignments of the 3500 cm$^{-1}$ and 3700 cm$^{-1}$ bands in respect to the various possible defect sites in zeolites might be resolved by the use of model compounds. These models must fulfill several conditions, like the ability for the OH groups to form hydrogen bridges as well as the silica environment of these OH species and the actual formation of a T-atom vacancy. These demands can be realized satisfactory by the use of silsesquioxane complexes. Silsesquioxane is the general name for a family of molecules with the formula [RSiO$_{3/2}$]$_n$, where 'R' is an inorganic or organic group and 'n' can be between 4 and about 30, but typically 6, 8, 10 or 12. These cage compounds are perfect candidates to mimic silica surfaces [39] (for a further introduction into silsesquioxane complexes, see Chapter 5). Incompletely condensed complexes contain OH groups and, as such, can be used for modeling the defect sites in zeolites. Some of these complexes, which can be considered as possible models for defect sites in zeolites, are plotted in table 2.6. Clearly, a zeolite-like T-atom vacancy can be recognized in complex I, whereas complex III represents the isolated, non hydrogen bridging OH groups at the outer surface of the zeolite, and complex II can be considered as a hydrated Si-O-Si bridge. The geometry of these complexes was fully optimized with a density functional method[40,41] in the Dgauss

program[42]. The vibrational spectra can also be calculated and the results for the OH stretching vibrations are summarized in table 2.6. The difference between the calculated frequencies in this table is of more importance than the absolute value. Starting from complex III, as a model for the isolated OH groups, its OH stretching vibration has the highest calculated frequency. A shift of about 300 cm$^{-1}$ is obtained for the main bands of complex I, the silsesquioxane model for a zeolite T-atom vacancy, *i.e.* the actual hydroxyl nest. This shift is in good agreement with the 250 cm$^{-1}$ shift found experimentally for the 3500 cm$^{-1}$ band in the FT-IR spectra of dealuminated zeolites (see table 2.1). The comparable shift is an indication for the fact that the three membered OH nest is a reliable model, also for a four membered hydroxyl nest. Important to mention is the significant increase of the average OH bond distance upon hydrogen bridging, while the hydrogen bridge distance clearly decreases. Considering complex II, only a small shift is obtained, indicative for weakly hydrogen bonded OH groups, which is confirmed by the hardly changed OH distance and the rather large OH bridging distance for this complex. This shift is in good correspondence with the measured shift of the 3700 cm$^{-1}$ band for dealuminated zeolites. Moreover, the weaker hydrogen bridges for this type of defect site should result in a less broad signal, which is indeed obtained for all dealuminated Mordenites (see figure 2.5, 2.7 and 2.9).

*Table 2.6  Incompletely condensed silsesquioxane complexes and their calculated O-H stretching vibrations and O-H distances$^a$.*

| | ( I ) | ( II ) | ( III ) |
|---|---|---|---|
| | OH OH OH (silsesquioxane cube structure) | OH OH (silsesquioxane cube structure) | OH (silsesquioxane cube structure) |
| Calculated OH stretching vibrations$^b$ [cm$^{-1}$] | 3403 ($\Delta$ = **294**) 3396 ($\Delta$ = **301**) 3331 ($\Delta$ = **366**) | 3698 ($\Delta$ = **-1**) 3675 ($\Delta$ = **22**) | 3697 ($\Delta$ = **0**) |
| average O—H **bond** distance | 0.996 Å | 0.980 Å | 0.978 Å |
| average O - - H **bridge** distance | 1.89 Å | 2.62 Å | - |

*[a] Lines in figures represent Si-O-Si units which are terminated by hydrogen atoms at each corner.*
*[b] $\Delta$ represents the difference of the calculated vibration with the 3697 cm$^{-1}$ vibration for the isolated OH group in complex III.*

From our dealumination study as well as the results obtained with the titanation of zeolites (see Chapter 3), it is concluded that the two FT-IR bands at 3500 cm$^{-1}$ and 3700 cm$^{-1}$ cannot be ascribed to the same (kind of) defect site. Both the effect on the acid treatment and the difference in behavior using different titanium precursors leads to this conclusion. Moreover,

the shift difference in the FT-IR spectra of around 200 cm$^{-1}$ implies a completely dissimilar nature of these bands. The new approach to this controversy, using models for defect sites in zeolites, gives a new tool to solve this issue. Based on its FT-IR shift and the OH distances of the model compound III, the band at 3500 cm$^{-1}$ must indisputably be assigned to hydroxyl nests (*i.e.* T-atom vacancies, as depicted in figure 2.1). Simultaneously, the band at 3700 cm$^{-1}$ cannot be assigned to the same kind of hydroxyl cluster and evidence is found in our approach using silsesquioxane model compounds for the assignment of this band to a hydroxyl pair, featuring less hydrogen bonding.

The possibility of the 3730 cm$^{-1}$ band, observed in FT-IR spectra of dealuminated Mordenites, to be assigned to a type of structural defect site can be excluded. This band exhibits a shift of hardly 15 cm$^{-1}$ and its appearance and band shape is much more like an isolated, non bridging OH group. The increase of the 3730 cm$^{-1}$ band as a function of dealumination degree can easily be explained by the formation of 'extra' (mesoporous) surface area, as was determined by BET analysis. The weak interaction of an isolated OH group with a possible neighboring or opposite oxygen atom on this defected (mesoporous) surface is likely and can explain the marginal shift in relation to the 3745 cm$^{-1}$ band.

## 2.6 Discussion and conclusions

The stability study on the oxalic acid dealuminated Mordenites reveals a different behavior when the acid dealumination takes place at reflux conditions in comparison with a treatment at 50°C. Only the former seems to result in truly stable zeolites. This difference in thermal stability can be explained by silicon migration, which will be more pronounced at higher temperatures or longer times, and therefore a higher extent of stabilization is reached with higher dealumination temperatures[20]. Another fact supporting this interpretation is the theoretically impossible degree of dealumination that is reached when the amount of accessible aluminum sites is kept in mind. According to a preferential aluminum siting in the side-pockets of the Mordenite framework, this accessible amount of aluminum is estimated to be 30 - 50 % §. Because the aluminum atoms sited in these side pockets are hardy accessible for the leaching acid it should be possible to dealuminate Mordenite only up to 50 - 70 % with one acid treatment. Since we reached significantly higher percentages of 77 % in the first oxalic acid treatment step and up to 82 % with nitric acid dealuminated Mordenites, we propose the migration to be possible at the used reflux conditions. Furthermore, this explains the lesser degree of dealumination obtained from oxalic acid dealumination performed at

---

§ On the basis of NMR spectroscopy Bodart *et al.* reported that about 50 % of the aluminum sites are inaccessible because these are sited in the 8-rings or the so-called side pockets[33]. Later, this percentage changed to about 30 % in a sorption study of Zholobenko *et al.*[43] but a few years later 50 % was again published by Datka *et al.* based up on pyridine adsorption studies[44]. Finally, Bonn confirmed both statements by his FT-IR investigation and estimated the amount of inaccessible aluminum at 30 - 50 %[45].

lower temperatures (50°C, table 2.2), as was also shown in a temperature dependent dealumination study on Mordenite of Bodart *et al.*[33]

Another point concerning the oxalic acid dealumination is the formation of the aluminum oxalic acid complex. Because of the tight fit in both Mordenite and Beta we expect serious diffusion limitations in dealuminating these zeolites. Since Beta has a higher dimensionality and Mordenite-I and Beta have about the same crystal size, Beta might be expected to be dealuminated easier. Comparing, however, the degrees of dealumination for Beta and Mordenite-I, respectively 74 and 77 %, no such effect can be recognized. Conclusively, although the formation of the aluminum-oxalic acid complex cannot be ruled out in solution, we hardly doubt the formation of these complexes in the zeolite channels and, consequently, their active role in leaching aluminum from the zeolite framework.

When the nitric acid treatment on Mordenite is compared with the results obtained with Beta, we have to conclude that it seems more easy to dealuminate the Beta than the Mordenite samples (table 2.4 and table 2.5, comparing the 7 M nitric acid dealumination, resulting in a dealumination degree of 82 %, 78 % and 92 %, for respectively Mor/I, Mor/II and Beta). An explanation in terms of different crystal sizes seems evident for the two Mordenite samples. With decreasing crystal size the zeolite becomes easier to dealuminate. For zeolite Beta all the aluminum is accessible, in contrast to the Mordenite structure (see above), resulting in the highest degree of 92 % dealumination.

The assignment of the 3500 cm$^{-1}$ and the 3700 cm$^{-1}$ band, previously attributed to defect sites in zeolites, is clarified. Using calculations on model silsesquioxane clusters we have to conclude that the 3500 cm$^{-1}$ band arises from actual hydroxyl nests (or T-atom vacancies), whereas the 3700 cm$^{-1}$ band originates from hydroxyl pairs, exhibiting less hydrogen bonding. As a result, the 3500 cm$^{-1}$ band is the only O-H stretch vibration to be assigned to a hydroxyl nest, resulting from the removal of aluminum out the zeolite framework. This is in line with the nice trend observed for this band as a function of dealumination degree (see figure 2.11). Conclusively, all the bands that intensify with increasing dealumination degree, *i.e.* 3500 cm$^{-1}$, 3700 cm$^{-1}$ and at 3730 cm$^{-1}$, are attributed to defect sites arising from the dealumination treatment. More specific, these bands are assigned to hydroxyl nests, hydroxyl pairs and isolated hydroxyls, respectively.

## 2.7 Experimental

Two different parent Mordenites were used: (1) Na-Mordenite from PQ-Zeolites (kindly delivered by Shell Research and Technology Center Amsterdam, The Netherlands) with a Si/Al ratio of 6.7 and a crystal size between 0.01 - 0.1 μm (agglomerates 0.5 - 50 μm), referred to as Mor/I, and (2) Na-Mordenite (kindly delivered by Akzo-Nobel, The Netherlands) with a starting Si/Al of 6.5 and a crystal size 0.1 - 2 μm (agglomerates 10 - 30 μm), referred to as Mor/II. The parent NH$_4$-Beta material was from PQ-Zeolites, and had a Si/Al of 37.5 and crystal size between 0.01 - 0.1 μm (agglomerates 100 - 1000 μm). Sample names for the

different zeolites consist of their zeolite structure (Mor or Bea), the different parent batches in the case of Mordenite (I or II) followed by the Si/Al bulk ratio of that sample. In the case of two dealuminated samples with the same Si/Al ratio, they are numbered a, b, c, etc.

Dealumination with aqueous oxalic acid (p.a., Acros) was performed with 0.25 M oxalic acid in the case of Mordenite. In the case of Beta 0.25 or 1.5 M oxalic acid was used. All treatments were performed in a 100 ml glass reactor equipped with a condensor at 50°C or reflux conditions for 5 hours under vigorously stirring. Afterwards the sample was filtered, washed and dried at 80°C.

Dealumination with aqueous nitric acid (65%, Merck) was performed with a known molarity of nitric acid (10 ml per g zeolite) in a 100 ml glass reactor equipped with a condensor at reflux conditions for 5 hours under vigorously stirring. Afterwards the sample was filtered, washed and dried at 80°C.

All calcination treatments were performed in a flow of dry nitrogen/oxygen mixture or air at the temperature reported during the time reported, except for a calcination performed in between two acid dealumination treatments, in those cases a flow of dry nitrogen was used.

The weight percentages of aluminum were determined by atomic absorption spectrometry (AAS) using a Perkin Elmer 3030 Atomic Absorption Spectrophotometer. For this purpose the samples were wetted with a few drops of distilled water and sulfuric acid (p.a., Merck) and then dissolved in concentrated hydrofluoric acid (p.a., Merck). The volatile siliconfluoride formed, was evaporated and to the residue $K_2S_2O_7$ (p.a., Merck) was added and melted. The cooled melt was dissolved in 2.5 molar sulfuric acid. The standard addition method was used to determine the aluminum concentration. Later, a faster procedure was used, in which the samples were dissolved in a 1:1:1 mixture of distilled water, concentrated nitric acid (p.a., Merck) and concentrated hydrofluoric acid (p.a., Merck). The aluminum concentration was determined by direct comparison with reference solutions.

Water contents of the zeolite samples, were determined with a Shimadzu TGA-50 thermogravimetric analyzer. About 10-15 mg of sample was heated under static conditions in air to 700°C with a rate of 5°C per minute.

Micro pore volumes were determined by adsorption of n-butane from a dry helium flow at room temperature. Before this, samples were dehydrated at 350°C for 15 minutes. The pore volume was determined by the relative increase of mass due to the adsorbed n-butane, which was measured using a Cahn 2000 electrobalance.

MAS NMR spectra were recorded on a Bruker MSL 400 NMR spectrometer, operating at a field of 9.4 T. Samples were analyzed as-synthesized and the obtained spectra were normalized on the highest peak.. $^{27}$Al MAS NMR spectra were obtained at 104.2 MHz using 1 μs pulses and 1 s delay. A 4 mm probe was used and the magic angle spinning rate was 10 kHz. Chemical shifts were measured with $Al(H_2O)_6^{3+}$ as external reference. Number of scans varied between 2000 and 7000. $^{29}$Si MAS NMR spectra were obtained at 79.49 MHz using 5.5 μs pulses and 10 s delay. A 7 mm probe was used and the magic angle spinning rate was 3.5 kHz. Chemical shifts were measured with tetrametylsilane as external reference. Number of scans varied between 300 and 2000. $^1$H-$^{29}$Si Cross Polarization (CP) MAS NMR spectra were obtained with the same probe and spinning rate and using 4 μs pulses and 5 s delay. Number of scans varied between 2000 and 12000.

Fourier Transformed Infrared (FT-IR) spectra were taken at room temperature on a Bruker IFS 113V spectrophotometer equipped with a vacuum cell. Before this, the samples were pressed into 10 mg of self-supporting wafers and dried at 450°C for 1 hour in vacuum, unless otherwise reported. The obtained spectra were baseline corrected linearly from 3000 cm$^{-1}$ to 4000 cm$^{-1}$. The absolute intensities of the different vibration bands are determined from the height of the band maximum.

X-Ray Diffraction (XRD) data were obtained with a Philips PW 7200 X-ray powder diffractometer, using Cu-Kα radiation. Diffractograms were taken between 5° and 50° 2θ, using a scan speed of 1° per minute. The obtained diffraction patterns were corrected for baseline, background, and Kα2 elimination. Temperature dependent XRD data were collected with a Siemens Diffractometer D 5000 using Cu-Kα radiation. The diffractometer was equipped with a secondary monochromator, a variable diaphragm V 20 and a nickel filter, the angular velocity was 1.2°C/min. *In-situ* measurements at elevated temperatures were done using a heating system built in the diffractometer and developed by Behruzi and Scherberich at the Institute of Crystallography of the University of the Technology Aachen.

Computational details: Calculations are based on the density functional theory (DFT)[40,41] as implemented in the Dgauss program (version 4.0) produced by Oxford Molecular Ltd.[42] A generalized gradient approximation to the exchange (Becke)[46] and correlation (Lee, Yang and Parr)[47] was used, and applied self-consistently. The Gaussian basis sets used are of double-zeta quality and include polarization functions for all atoms (DZVP2)[48]. They were optimized for the use in density functional calculations in order to minimize the basis set superposition error (BSSE)[49]. A second set of basis functions, the fitting basis set, is used to expand the electron density in a set of single-particle Gaussian-type functions. All geometry optimizations were carried out fully relaxed, so as to avoid introducing unnatural strain in the molecules. The second derivatives are calculated analytically in the harmonic approximation. This gives a good approximation to compute vibrational spectra. The silsesquioxanes were approximated by substituting the large organic groups on the silicon atoms by hydrogen atoms. This approximation seems reasonable as these group are located relatively far from the hydroxyl groups of interest to this study.

# References

1.  R.M. Barrer, M.B.Makki, *Can. J. Chem., 42*, (**1964**), p. 1481.
2.  F. Goovaerts, E.F. Vansant, P. de Hulsters, J. Gelan, *J. Chem. Soc., Faraday Trans. 1, 85*, (**1989**), p. 3675.
3.  G.T. Kerr, *J. Phys. Chem., 72*, (**1968**), p. 2594.
4.  L.P. Shirinskaya, V.S. Komarov, N.P. Pryakhina, Russ. *J. Phys. Chem., 49*, (**1975**), p. 580.
5.  Y. Hong, J.J. Fripiat, *Microporous Mater., 4,* (**1995**), p. 323.
6.  J. Klinowski, J.M. Thomas, M.W. Anderson, C.A. Fyfe, G.C. Gobby, *Zeolites, 3*, (**1983**), p. 5.
7.  G.W. Skeels, D.W. Breck, in: *Proceedings of the Sixth International Zeolite Conference* (Ed. D. Olson, A. Bisio), Butterworth Ltd, UK, (**1984**), p. 87.
8.  P. Fejes, I. Kiricsi, I. Hannus, Á. Kiss, Gy. Schöbel, *React. Kinet. Catal. Lett., 14*, (**1980**), p. 481.
9.  P. Wu, T. Komatsu, T. Yashima, *J. Phys. Chem., 99*, (**1995**), p. 10923.
10. M.M. Olken, J.M. Garces, *Catal. Lett., 2*, (**1989**), p. 243.
11. L. Bertea, H.W. Kouwenhoven, R. Prins, *Appl. Catal. A: Gen., 129*, (**1995**) p. 229.
12. K. Yamagishi, S. Namba, T. Yashima, *J. Phys. Chem., 95*, (**1991**), p. 872.
13. M.J. van Niekerk, J.C.Q. Fletcher, C.T. O'Conner, *J. Catal., 138*, (**1992**), p. 150.
14. B. Kraushaar, L.J.M. van de Ven, J.W. de Haan, *Stud. Surf. Sci. Catal. 37*, (**1988**), p. 167.
15. S. Moreno, G. Poncelet, *Microporous Mater., 12*, (**1997**), p. 197.
16. M. Jiang, H.G. Karge, *J. Chem. Soc. Faraday. Trans., 92*, (**1996**), p. 2641.
17. Z. Zhang, X. Liu, Y. Xu, R. Xu, *Zeolites, 11*, (**1991**), p. 232.
18. T. Chevreau *et al.*, *Zeolites, 10*, (**1990**), p. 226.
19. A. Corma, V. Fornés, F. Rey, *Appl. Catal., 59*, (**1990**), p. 267.
20. M.R. Apelian, A.S. Fung, G.J. Kennedy, T.F. Degnan, *J. Phys. Chem., 100*, (**1996**), p. 16577.
21. M. Maache, A. Janin, J.C. Lavalley, J.F. Joly, E. Benazzu, *Zeolites, 13*, (**1993**), p. 419.
22. K. Yamagishi, S. Namba, T. Yashima, *J. Phys. Chem., 95*, (**1991**), p. 872.
23. W.F. Hölderich, J. Röseler, G. Heitmann, A.T. Liebens, *Catal. Today, 37*, (**1997**), p. 353.
24. G.L. Woolery, L.B. Alemany, R.M. Dessau, A.W. Chester, *Zeolites, 6*, (**1986**), p. 14.
25. A. Zecchina, S. Bordiga, G. Spoto, L. Marchese, G. Petrini, G. Leofanti, M. Padovan, *J. Phys. Chem., 96*, (**1992**), p. 4991.
26. A. Jentys, G. Rumplmayr, J.A. Lercher, *Appl. Catal., 53*, (**1989**), p. 299.
27. I.V. Mishin, G. Pál-Borbély, H.G. Karge, *Stud. Surf. Sci. Catal. 94*, (**1995**), p. 294.
28. I. Kiricsi, C. Flego, G. Pazzuconi, W.O. Parker Jr., R. Millini, C. Perego, G. Bellussi, *J. Phys. Chem., 98*, (**1994**), p. 4627.
29. for a review see: D. Barthomeuf, *in* Zeolite Microporous Solids: Synthesis, Structure and Reactivity (Eds. E.G. Derouane, *et al.* ), Kluwer Academic Publishers, The Netherlands, (**1992**),      p. 193.
30. M. M. J. Treacy, J. M. Newsam, *Nature, 332*, (**1988**), p. 249.
31. G. Engelhardt, U. Lohse, E. Lippmaa, M. Tarmak, M. Mägi, *Z. Anorg. Allg. Chem., 482,* (**1981**), p. 49.
32. W. Löwenstein, *Am. Mineral., 39*, (**1954**), p. 92.
33. P. Bodart, J. B. Nagy, G. Debras, Z. Gabeliza, P.A. Jacobs., *J. Phys. Chem. 90*, (**1986**), p. 5183.
34. D.W. Breck, *Zeolite Molecular Sieves*, John Wiley & Sons, New York (**1974**), p. 412.
35. J. Sauer, *Science, 271*, (**1996**), p. 774.
36. D.H. Olson, S.A. Zygmunt, M.K. Erhardt, L.A. Curtiss, L.E. Iton, *Zeolites, 18*, (**1997**), p. 347.
37. M.M.J. Treacy, J.B. Higgens, R. von Ballmoos, *Zeolites, 16*, (**1996**).
38. H.K. Beyer, I.M. Belenykaja, I.W. Mishin, G. Borbely, *Stud. Surf. Sci. Catal.,* 18, (**1984**), p. 133.
39. F.J. Feher, D.A. Newman, J.F. Walzer, *J. Am. Chem. Soc., 111*, (**1989**), p. 1741.
40. P. Hohenberg, W. Kohn, *Phys. Rev. B, 136,* (**1964**), p. 864.
41. W. Kohn, L. J. Sham, *Phys. Rev. B, 140*, (**1965**), p. 1133.
42. J. Andzelm, E. Wimmer, *J.Chem. Phys., 96*, (**1992**), p. 1280.

43. V. Zholobenko, M.A. Makarova, J. Dwyer, *J.Phys.Chem. 97,* (**1993**), p. 5962.

44. J. Datka, B. Gil, A. Kubacka, *Zeolites 17*, (**1996**), p. 428.

45. M. Bonn, *Ph.D. Thesis*, Eindhoven University of Technology, (**1996**).

46. A. D. Becke, *J. Chem. Phys, 84,* (**1986**), p. 4524.

47. C. Lee, R. G. Parr and W. Yang, *Phys. Rev. B, 37*, (**1988**), p. 785.

48. N. Godbout, D. R. Salahub, J. Andzelm and E. Wimmer, *Can. J. Chem., 70*, (**1992**), p. 560.

49. J. Sauer, *Chem. Rev., 89,* (**1989**), p. 199.

# 3

# Titanation of zeolites

The synthesis of titanium zeolites *via* a gas phase titanation using Chemical Vapor Deposition (CVD) of $TiCl_4$ is described in this Chapter. The results of the titanation using CVD techniques are compared to the results obtained with an aqueous phase titanation. The latter procedure shows a significant formation of titanium oxide species, whereas the CVD titanation can provide $TiO_2$ free titanium zeolites. FT-IR analysis demonstrated the actual reaction of the hydroxyl nests of the dealuminated zeolite with the titanium precursor. The resulting incorporated titanium sites are thoroughly investigated, using combined XPS, Raman and DRUV-Vis spectroscopy. Our results show that, in order to prevent the formation of $TiO_2$ and to reach a high titanium distribution, small zeolite crystals should be used, in a fluid bed application. In the case of the one dimensional Mordenite structure, in general, a preferential titanation of the outer regions was found. Especially in combination with a large crystal size, this results in the formation of $TiO_2$ particles. Combining the different spectroscopic techniques, we can conclude that the O 1s band for $TiO_2$, the binding energy of the Ti $2p_{3/2}$ band, the Ti2p/Ti3p ratio, and the DRUV-Vis onset are good indicators when the formation of titanium oxide is investigated. With respect to the presence of very low titanium oxide contents, however, Raman spectroscopy can give the decisive evidence, since this technique is extremely sensitive for titanium oxide species.

## 3.1 Introduction

Titanation is the process in which titanium is introduced in the framework T-atom sites of the zeolite. Usually, the term refers to a post-synthesis modification, in which the incorporation of titanium is carried out after the zeolite has been made. For a successful titanation, first defect sites should be created in the zeolite, which are potentially active sites for titanium precursors to react with. Such defect sites could be created *via* the removal of aluminum atoms from the zeolite framework (see Chapter 2). A possible reaction of a defect site with a titanium precursor, like titanium tetrachloride, is depicted in figure 3.1.
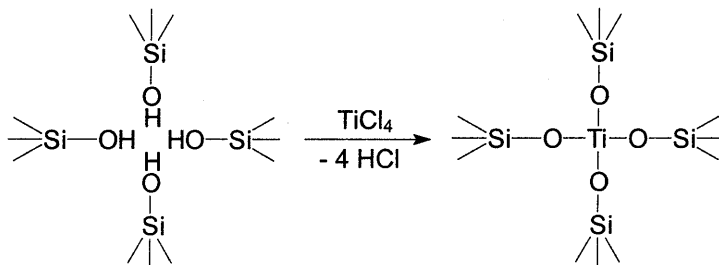
*Figure 3.1  A two-dimensional representation of the incorporation of a titanium site into a defect site of a zeolite using titanium(IV) tetrachloride.*

The literature, different titanium precursors and techniques are reported in attempts to fulfill the desired introduction of titanium into a zeolite framework or onto a silica surface (see also Figure 3.2): (1) Titanium halides, usually $TiCl_4$, can be used at elevated temperatures to incorporate titanium into a zeolite framework[1,2,3,4], or graft titanium onto a silica surface[5,6], (2) An aqueous solution of ammonium titanyl oxalate is used in the synthesis of titanium Beta catalysts[7,8], (3) Titanium alkoxides can be used in the modification of a silica surface, for instance titanium isopropoxide[9], (4) Aqueous ammonium hexafluorotitanate is used in the post-synthesis formation of different titanium zeolites[10,11].
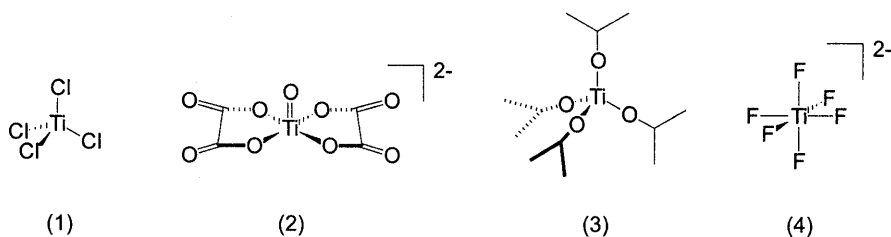


*Figure 3.2  Different titanium precursors used in titanation (numbers refer to the examples described above).*

Our aim is to incorporate titanium into the zeolite structure *via* a reaction with a hydroxyl nest inside the zeolite channel. Ferrini and Kouwenhoven already showed that a reaction of an aluminum containing zeolite with a $TiCl_4$ precursor, did not decrease the aluminum content of the zeolite[2]. The majority of the titanium was deposited on the outer surface of their zeolites. Therefore, the use of zeolites containing vacant sites seems necessary. Incorporation of titanium into such hydroxyl nest should result in a tetrahedral titanium site, active and stable in liquid phase oxidation catalysis. At the same time, the deposition of titanium onto the outer surface of the zeolite crystals, resulting in a less defined titanium site, should be avoided. Such a site will be weakly bounded to the zeolite framework and will be more accessible to coordinating species, which opens the possibility of leaching. The stability of titanium species

anchored to a silica framework with less than three siloxy units is at least questionable (see Chapter 5). To avoid this, incorporation of the titanium into a T-atom site of the zeolite framework is necessary. To facilitate the incorporation reaction of titanium at defect sites, which are present inside the zeolite micropores, small titanium precursors are preferable. In this respect large, ionic and hydrated precursors from aqueous solutions should be avoided. A clear advantage of gas phase *versus* liquid phase incorporation is the opportunity to use more elevated temperatures in a gas phase application. Higher temperatures facilitate the diffusion of the titanium precursor through the zeolite micropores. Besides these effects, the well known clustering of small titanium alkoxides, like titanium ethoxide, $Ti(OC_2H_5)_4$, encountered in liquid phase applications should be avoided [12], since these clusters are too large to enter the micropores. Such structures can be considered as precursors for titanium oxide species, which are unwanted products in the preparation of selective titanium catalysts. In conclusion, the preference for small, monomeric and non hydrated titanium precursors in gas phase applications leads to the choice for gaseous $TiCl_4$ as the titanium precursor. The gas phase  process of preparing titanium zeolites will be referred to as Chemical Vapor Deposition, CVD, since the titanium precursor is in the vapor phase and will be deposited on (or preferably *in*) the solid, zeolite substrate.

Concerning the type of gas phase application, we can distinguish between a static, closed system or an open system with flowing gas. The incorporation of titanium from 1 mole of $TiCl_4$ will lead to 4 moles of HCl (see figure 3.1). This byproduct should be removed quickly, which leads to the preference for a flowing system. A second choice considers the type of zeolite bed applied in a flowing system: a fixed (or static) bed *versus* a fluid bed. A fluid bed will exclude possible temperature or concentration gradients over the zeolite bed [13]. With the high flows applied, the gaseous HCl is removed quickly from the zeolite bed. Moreover, the high mass flow of carrier gas guarantees a very low $TiCl_4$ concentration, which will be beneficial in preventing the formation of $TiO_2$ species. In practice, however, the very small zeolite particles, having a broad particle size distribution (from zeolite crystals to agglomerates: ca. 0.01 μm - 1000 μm) will be hard to fluidize. In most applications this will lead to spouted (or entrained) bed types of fluidization. In this study both fluid beds and fixed zeolite beds are investigated together with an aqueous phase titanation which was performed for reasons of comparison.

## 3.2  Titanium incorporation

Various aluminum deficient zeolites were titanated according to the fluid bed or fixed bed conditions as described in section 3.1. For a schematic representation of the experimental set-up, see figure 3.17 in the experimental section 3.6. With this procedure it is possible to introduce titanium into a dealuminated zeolite, as shown in figure 3.3. Dependent on the amount of titanium offered, different titanium loadings were obtained.
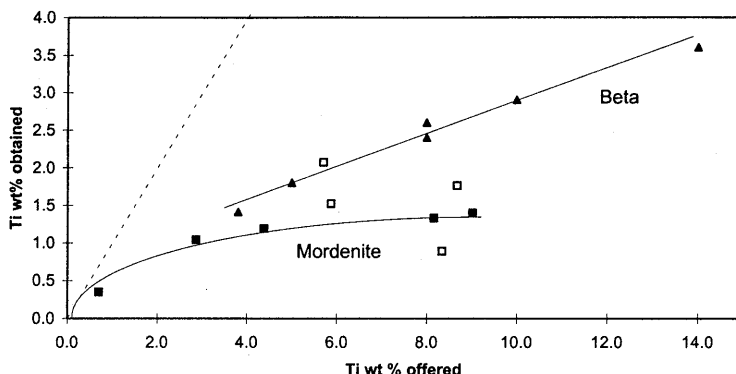
*Figure 3.3  The obtained titanium content of fluid bed titanated Beta (▲) and fluid bed titanated Mordenite (□) as well as fixed bed titanated Mordenite (■), versus the offered amount of titanium per gram zeolite (wt% Ti offered).*

For zeolite Beta a linear correlation can be recognized whereas for Mordenite a declining slope can be seen with increasing amount of titanium offered. Considering the two different bed types used for titanated Mordenites, the fluid bed titanation shows a less clear trend in comparison with the fixed bed. The obtained titanium contents, however, are comparable with the results of the fixed bed titanated Mordenite as well as with the fluidized titanated Betas. This indicates the minor influence the type of zeolite bed has on the amount of titanium introduced during titanation. The fluidized Beta shows a much better trend than the fluidized Mordenite, in agreement with the experimental difficulties to obtain a good fluidized bed for the Mordenite samples. During fluidization the zeolite particles tends to agglomerate to larger particles of about 1 mm, dependent on type of zeolite used. This agglomeration appeared to be hard to control in the case of Mordenite. Though, it prevents the zeolite particles to leave the zeolite bed in the CVD titanation reactor, since the not agglomerated, very small zeolite particles are blown out the CVD reactor. As reported, millimeter size particles with the density of a zeolite should form a bubbly type of fluidized bed[14,15], which is in good agreement with our experiments.

In table 3.1 the elemental analysis of the titanium Mordenites, series I is summarized. The discussion considering the Ti $2p_{3/2}$ binding energies is postponed to section 3.3 and 3.4. A CVD titanation of a higher dealuminated Mordenite (higher Si/Al), thus having a higher defect site concentration, leads to an increased titanium content (*ergo* a lower Si/Ti ratio: compare sample Ti51Mor/I-79 and Ti63Mor/I-39, table 3.1). This result confirms the proposed incorporation of titanium into defect sites of the dealuminated zeolite. Furthermore, applying a higher concentration of the titanium precursor in CVD titanation results in a higher titanium content (sample Ti51Mor/I-39) and also in a lower defect site concentration, as is indicated by the hydroxyl nest band at 3500 cm$^{-1}$  (see figure 3.4). This is again indicative for the actual reaction of TiCl$_4$ with the hydroxyl nests.

*Table 3.1  Titanium Mordenites series I.*

| sample[a] | Si/Ti (bulk) | Si/Ti (XPS)[b] | Ti 2p$_{3/2}$ BE [eV] | Ti offered [mmol] |
|---|---|---|---|---|
| Ti63Mor/I-39 | 63 | 40 | 458.8 | 0.7 |
| Ti51Mor/I-39 | 51 | 26 | 459.0 | 1.4 (2 x C)[c] |
| Ti44Mor/I-39 | 44 | 23 | 459.0 | 1.4 (2 x t)[d] |
| Ti51Mor/I-79 | 51 | 38 | 458.6 | 0.7 |

*[a] Sample names consist of the Si/Ti ratio, followed by type of zeolite, and the Si/Al ratio (see also Section 3.6). Titanation carried out at 400°C. [b] Si/Ti XPS ratio is based on Si2p/Ti2p ratio. [c] Amount of titanium offered is doubled by applying a double concentration (2 x C) of TiCl$_4$ in the gas flow, [d] Amount of titanium offered is doubled by applying a double time (2 x t) for titanation.*
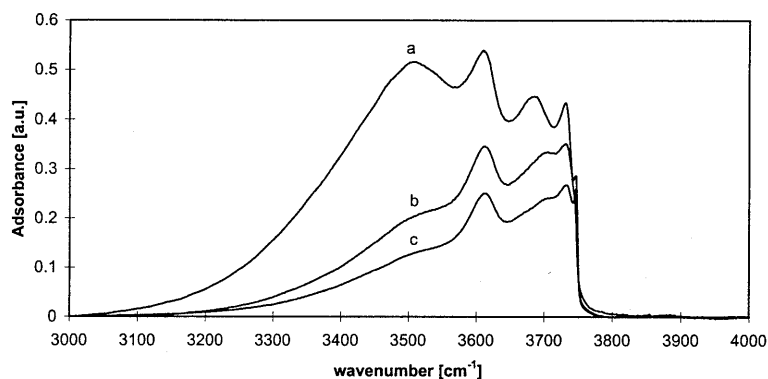


*Figure 3.4  FT-IR spectroscopy on dealuminated and titanated Mordenites: [a] Mor/I-39, [b] Ti63Mor/I-39 and [c] Ti51Mor/I-39.*

According to the postulated low thermal stability of the hydroxyl nests, as extensively described in Chapter 2, the decrease in intensity in the hydroxyl region in FT-IR analysis should arise primarily from the titanium incorporation. To verify this, a highly dealuminated Mordenite (Mor/II-116), was titanated with different loadings and compared to an untitanated but identical thermally treated sample (in table 3.2 the titanated samples with Mor/II-116 as a parent material are summarized). With this blank experiment, the effects of the reaction temperature on the decrease in hydroxyl nest concentration can be visualized. In figure 3.5 their FT-IR spectra are plotted, which are somewhat more noisy than the previous spectra of Mor/I samples, since the particle size of Mor/II is about 20 times higher, resulting in a high background spectrum for these samples.

*Table 3.2  CVD titanated zeolites.[a]*

| sample | CVD bed | wt%Ti offered | Si/Ti (bulk) | Si/Ti (XPS)[b] |
|---|---|---|---|---|
| Ti0Mor/II-116 | fixed | 0 | ∞ | ∞ |
| Ti226Mor/II-116 | fixed | 0.70 | 226 | 126 |
| Ti75Mor/II-116 | fixed | 2.85 | 75 | 45 |
| Ti65Mor/II-116 | fixed | 4.38 | 65 | 36 |
| Ti58Mor/II-116 | fixed | 8.16 | 58 | 26 |
| Ti33Mor/II-6.1 | fluid | 5.70 | 33 | 6 |
| Ti51Mor/II-116 | fluid | 5.88 | 51 | 7 |
| Ti43Mor/II-116 | fluid | 8.68 | 43 | 11 |

*[a] Sample names consist of the Si/Ti ratio, followed by type of zeolite, and the Si/Al ratio (see also Section 3.6). Titanation carried out at 500°C. Except for sample Ti33Mor/II-6.1, all have Mor/II-116 as a parent material (Ti33Mor/II-6.1 has the non dealuminated Mor/II-6.1 as parent). [c] Si/Ti XPS ratio is based on Si2p/Ti2p ratio.*
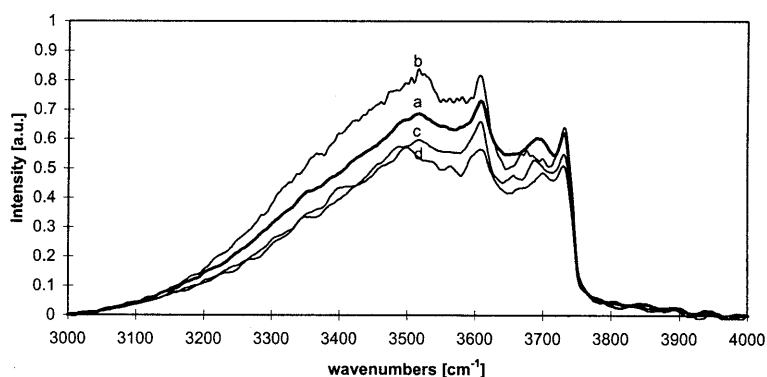


*Figure 3.5   FT-IR spectroscopy on dealuminated and titanated Mordenites: [a] Mor/II-116, [b] Ti0Mor/II-116, [c] Ti65Mor/II-116 and [d] Ti51Mor/II-116.*

Surprisingly, a somewhat higher level of the hydroxyl nest band at 3500 cm⁻¹ for the thermal treated but *non titanated* Mordenite was found (Ti0Mor/II-116). This could possibly be due to a thermal extraction of the last framework aluminum atoms left after dealumination. Unfortunately, the aluminum content of this sample is already so low that the resulting aluminum oxide band at 3660 cm⁻¹ is hardly recognizable. Nevertheless, the difference with the three titanated Mordenite samples is clear: in all cases their intensity is significantly lower than that of the non titanated sample, indicating that the measured decrease of amount of hydroxyl nests in FT-IR is due to their reaction with the titanium precursor.

The titanium site obtained is investigated using various techniques, as Diffuse Reflectance UV-Vis spectroscopy (DRUV-Vis), RAMAN spectroscopy and X-ray Photoelectron Spectroscopy (XPS)[16,17]. For an extensive analysis concerning the latter two, see section 3.3

and 3.4. With UV-Vis spectroscopy information can be derived concerning the coordination of the titanium site. This technique is performed in the diffuse reflectance mode since solid samples are investigated. DRUV-Vis spectroscopy shows the ligand to metal charge transfer band for titanium (2p oxygen to 3d titanium). For octahedrally coordinated titanium oxide species (like in $TiO_2$) the maximum of this band lies around 340 nm (onset around 420 nm). Whereas for a tetrahedrally coordinated titanium in a siliceous host (like for instance in pure TS-1 or TS-2) this band is shifted to 210 - 230 nm, with an onset of around 250 nm (see figure 3.6). The titanium Mordenites, as summarized in table 3.1, all have the same maximum intensity between 210 - 230 nm as found for TS-1 and TS-2 [18,19]. This demonstrates the actual creation of tetrahedral titanium sites into defect sites of dealuminated zeolites as depicted in figure 3.1. Besides this maximum, however, in all cases a shoulder at around 250 nm can be observed. This can be explained in two ways: (1) by the formation of octahedral but *isolated* titanium sites, which are reported to have their maximum intensity at 240 - 260 nm [18,20]. Such higher coordinated species could arise, for instance, from hydrated, but still isolated titanium sites, (2) by the formation of very small titanium oxide species. When the size of a titanium oxide particle reaches molecular dimensions, like 10 - 20 Å, size quantization (q-size) effects start to play a role [21,22]. The environment of the titanium sites in such cluster is significantly different from the bulk situation resulting in a so-called blue shift. Titanium oxide particles occluded inside the Mordenite micropores are reported to have their maximum adsorption in the UV-visible spectra at 260 nm[23].
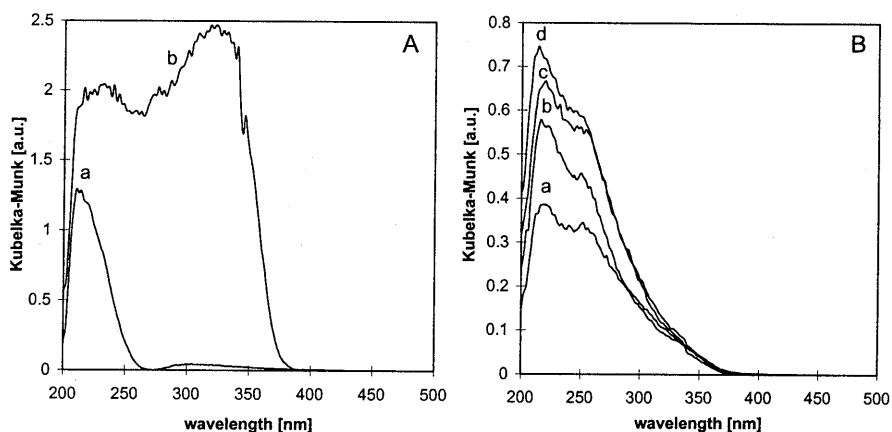


*figure 3.6 Diffuse reflectance UV/Vis spectroscopy on (A): [a] TS-1 and [b] titanium oxide and (B): different titanium Mordenites, in which [a] Ti63Mor/I-39, [b] Ti51Mor/I-39, [c] Ti44Mor/I-39 and [d] Ti51Mor/I-79.*

Considering the possibility of titanium oxide species which are occluded inside the zeolite micropores, this would certainly result in severe diffusion limitations. Especially, in the case of a one dimensional zeolite structure, like Mordenite, such limitations should be avoided. Moreover, in oxidation catalysis, titanium oxide would possibly decompose hydrogen

peroxide unselectively, which is an unwanted side reaction. Fortunately, from pore volume measurements we can conclude that all titanium zeolites prepared *via* the post-synthesis modification have an essentially unaltered micro pore volume. As such, formation of titanium oxide particles *inside* the zeolite micro pores is unlikely, which of course does not rule out the formation of titanium oxide species outside the zeolite crystals.

The distribution of the titanium sites over the zeolite crystals was investigated using XPS spectroscopy. Because the photoelectrons exited can travel only a few atomic distances through the solid, the information obtained originates from the outer shells of the zeolite crystal. A rule of thumb for the depth of the surface layer investigated by XPS is around 5 nm[16]. Therefore, this technique can provide surface sensitive information concerning, for instance, an elemental analysis. When the Si/Ti XPS ratios obtained for the Mor/I and the Mor/II series are compared with their Si/Ti bulk ratios, a higher discrepancy can be found for the Mor/II based titanium zeolites (see table 3.1and 3.2). The larger crystals of the Mor/II series seem to have a higher titanium enrichment of the outer regions than the smaller crystals of the Mor/I series. We have to keep in mind, however, that with increasing crystal size the volume probed by XPS becomes relatively smaller. Hence, a larger crystal size for the Mor/II series causes a lower part of the zeolite sample to be visible with XPS. This difference is visualized in figure 3.7.



Mor/I, Beta                      Mor/II
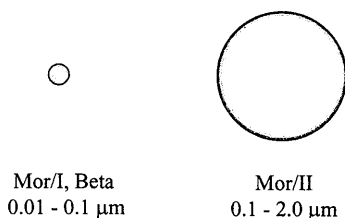0.01 - 0.1 µm                0.1 - 2.0 µm

*Figure 3.7 Schematic representation of the XPS probe depth for the different types of zeolites used, dependent on their average crystal size (black and gray indicates XPS visible and white corresponds to XPS invisible).*

Therefore, a comparison between the Mor/I and the Beta based titanated zeolites, having approximately the same crystal size, is more objective. The discussion with respect to the variation in probe depth is continued in section 3.3. In figure 3.8 the Si/Ti ratio determined by XPS is compared with the Si/Ti bulk ratio of all three types of titanated zeolites. A comparison between the Mor/I based samples and the Beta samples (having about the same crystal sizes), shows a better correspondence of the Si/Ti bulk and the Si/Ti XPS ratios between those two series than in comparison with the Mor/II based samples. This can be partly explained by the fact that with these small crystal sizes more bulk material is visible for XPS. The small but significant difference, however, between the Si/Ti XPS ratios for the Mor/I and Beta series, indicates that these small crystals (0.01 - 0.1 µm) are still not totally visible for XPS. In other words, even for crystal sizes of 0.01 - 0.1 µm, XPS can be regarded

as a surface sensitive technique. This means that the explanation of this difference, with regard to the distribution of titanium over the zeolite crystal, still holds. In summary, the titanium enrichment of the outer surface is the most pronounced for the Mor/II series, whereas the Mor/I series have a somewhat better distribution and the Beta samples have an almost perfect distribution of titanium over the zeolite crystal.
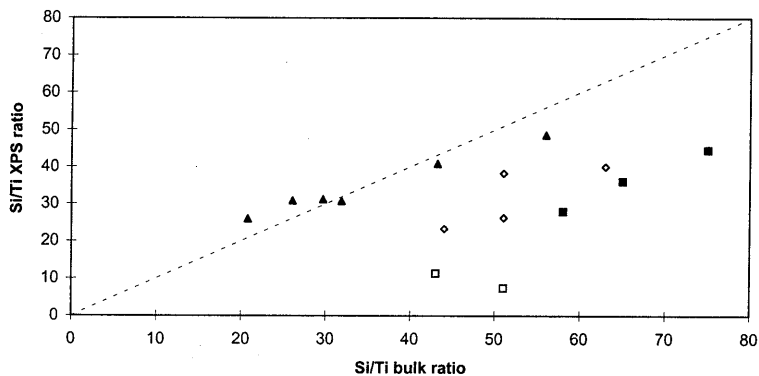


*Figure 3.8  The Si/Ti bulk versus the Si/Ti determined with XPS for different CVD titanated zeolites: titanated Beta (▲) and titanated Mordenite/I (◇), Mordenite/II, fluid bed (□) and fixed bed (■).*

The titanium substituted Betas clearly show a nice trend for the obtained Si/Ti ratios in line with the offered amount of titanium (table 3.3, figure 3.8). An almost optimal distribution of the offered amount of titanium over the zeolite crystal is in accordance with the linear correlation for the wt % Ti obtained versus the wt % Ti offered, as was shown in figure 3.3. This interpretation is explained with the higher dimensionality of the micropore system in comparison with the one dimensional Mordenite. This facilitates the diffusion of the titanium precursor during titanation and, therefore, results in a more homogeneous distribution of titanium over the zeolite crystals.

*Table 3.3  Titanated Beta zeolites prepared by fluid bed CVD titanation.*

| sample[a] | wt% Ti offered | Si/Ti (bulk) | Si/Ti (XPS)[b] |
|---|---|---|---|
| Ti56Bea-450 | 3.8 | 56 | 49 |
| Ti43Bea-160 | 5 | 43 | 41 |
| Ti32Bea-267 | 8 | 32 | 31 |
| Ti30Bea-321 | 8 | 30 | 31 |
| Ti27Bea-71 | 10 | 27 | 31 |
| Ti21Bea-170 | 14 | 21 | 26 |

*[a] Sample names consist of the Si/Ti ratio, followed by type of zeolite, and the Si/Al ratio (see also Section 3.6). Titanation carried out at 500°C. [b] Si/Ti XPS ratio is based on Si2p/Ti2p ratio.*

## 3.3 Comparison with aqueous phase titanation

Liquid phase titanation, using an aqueous solution of ammonium hexafluorotitanate, $(NH_4)_2TiF_6$, was studied as an alternative method for introducing titanium into a defected zeolite. In liquid phase applications a possible low thermal stability of a high dealuminated zeolite is not a point of concern (see also Chapter 2). Therefore, Mor/I-150 is considered as being an interesting candidate for liquid phase titanation. The procedure used according to the general outlines from Skeels and Flanigen[10] was recently reported to afford titanium substituted Y which was used as a catalyst in oxidative cleavage reactions [11]. The obtained Ti-Y catalyst has its maximum in the DRUV-Vis spectrum at around 260 - 270 nm. The authors assigned this to small titanium oxide particles, probably located inside the zeolite Y cages.

Applying this procedure to Mor/I-150 we obtained a Si/Ti bulk ratio of 19, whereas the Si/Ti ratio measured by XPS is only 4! The difference between these two ratios is more pronounced than the differences in the ratios of the CVD titanated samples. A much higher surface enrichment of titanium is measured for this aqueous phase titanated sample, Ti19Mor/I-150. Regarding the resulting titanium sites in this sample, studied by DRUV-Vis and plotted in figure 3.9 with sample Ti51Mor/I-79 for comparison, we see the main band at 260 nm, with a small shoulder at about 300 nm. Intensities at these wavelengths cannot be described any more with a shift of octahedral isolated titanium sites, but have to be assigned to small titanium oxide species. Interestingly, the microporous volume is unchanged after the aqueous phase titanation. The result with regard to the interpretation of the DRUV-Vis spectra is in agreement with the conclusions of Schlindler et al., concerning the formation of $TiO_2$ species [11]. In relation to their location, however, we have to conclude that $TiO_2$ is present outside the zeolite micropores, since its presence inside these micropores would undoubtedly result in a decrease in micropore volume. Moreover, this is in accordance with the relatively high titanium content measured with XPS (low Si/Ti).
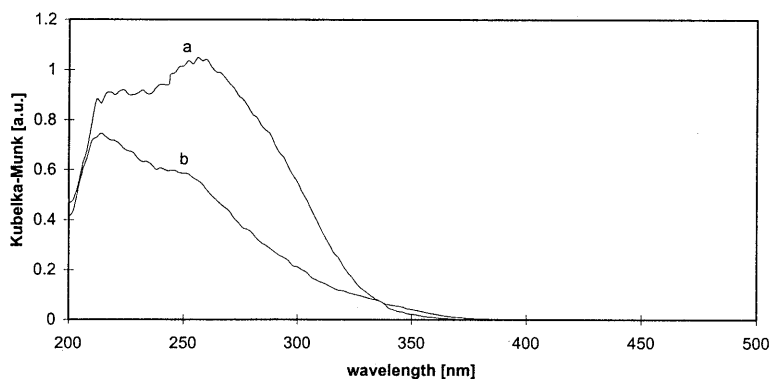


*Figure 3.9 Diffuse Reflectance UV-Vis spectroscopy on [a] Ti19Mor/I-150 and [b] Ti51Mor/I-79.*

The presence of titanium oxide species in the liquid phase titanated sample is further investigated using XPS spectroscopy. Besides being quantitatively, this technique also gives information concerning the coordination sphere or valence state of atoms. We used two bands, the Ti 2p and the O 1s, to obtain qualitative information about the titanium zeolites. The position of the Ti 2p band (divided in the electron levels Ti $2p_{1/2}$ and Ti $2p_{3/2}$) is reported to depend on the environment of the titanium site [16,17]. The Ti $2p_{3/2}$ signal has its maximum around 458 eV for octahedral and around 460 eV for tetrahedral coordinated titanium in a silica host, having -O-Si ligands [24,25]. For some natural octahedral $TiO_6$ species, however, also a maximum at 460 eV was found [26]. This implies that the Ti $2p_{3/2}$ band at 260 eV is not decisive in the determination of the titanium coordination. Considering the O 1s signal, it should be possible to differentiate between oxygen atoms in a silica environment, like $SiO_2$, or oxygen atoms in a titania environment, like $TiO_2$. The reported binding energies for these two different oxygen atoms are, respectively, 532.5 eV and 530.0 eV [27,28]. Figure 3.10 depicts the XP spectra of the O 1s region and Ti 2p region for the titanium Mordenites and for TS-1 as a reference material. Clearly, a well resolved shoulder, present at 530.2 eV, can be recognized for the aqueous phase titanated sample, which is absent for the other titanium Mordenites and for TS-1. This result obviously demonstrates the presence of a significant amount of titanium oxide in this aqueous phase titanated sample. The Ti $2p_{3/2}$ band is shifted to lower binding energies for the $TiO_2$ containing Ti19Mor/I-150 sample. Also this band is sharper than the Ti $2p_{3/2}$ signals for the gas phase titanated Mordenites, whose binding energies for this band are just in between the TS-1 sample and the titanium oxide containing aqueous phase titanated sample.
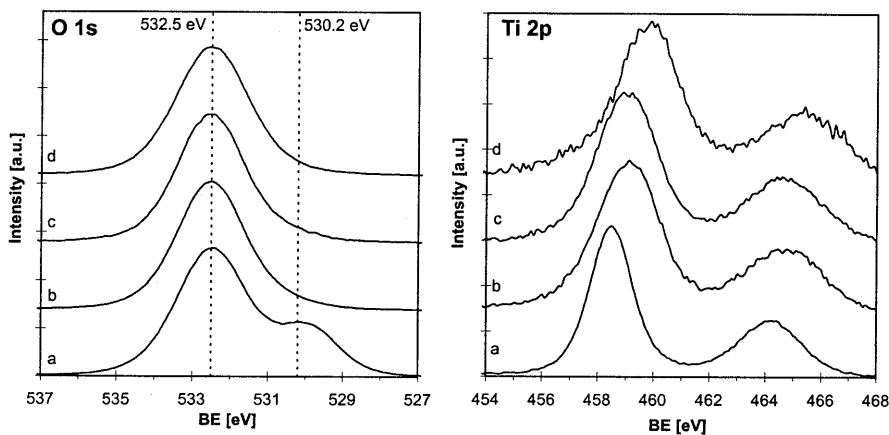


*Figure 3.10  XP spectra of the O 1s region (left) and the Ti 2p region (right) of: [a] Ti19Mor/I-150, [b] Ti51Mor/I-39, [c] Ti44Mor/I-39 and [d] TS-1.*

For none of the titanium Mordenites and titanium Betas reported in this thesis, a splitting of the Ti 2p bands was ever observed, as was published for $TiO_2$ containing titanium zeolites[16].

Although the Ti $2p_{3/2}$ band is somewhat broader for these titanium Mordenites and Betas (Ti $2p_{3/2}$ FWHM = 2.7 - 3.0 eV), it could nicely be fitted in all cases with only one Gaussian/Lorentz peak. Moreover, the Ti $2p_{3/2}$ bands are in all cases too *narrow* to be deconvoluted with two different titanium bands. The known distance between the Ti $2p_{3/2}$ in tetrahedral and octahedral environment equals about 2 eV (*vide supra*), which is clearly too large to use in deconvoluating the Ti 2p bands (see figure 3.10).

Considering the FT-IR hydroxyl region of the aqueous phase titanated sample, a different effect upon titanation can be recognized for the two different bands, that were previously assigned to defected sites in dealuminated zeolites (see section 2.5). In figure 3.11 the spectra are plotted for the titanated zeolite and its dealuminated parent sample. Regarding the decrease of the two different bands due to the incorporation of titanium, a strikingly different behavior is obtained for this aqueous phase titanation in comparison with the CVD titanation (see figure 3.11). In the latter case the main decrease upon titanation was found for the 3500 cm$^{-1}$ band, whereas in the aqueous phase application the dominant effect concerns the decrease of the 3700 cm$^{-1}$ band.

This new evidence for the entire dissimilar behavior of the 3500 cm$^{-1}$ band and the 3700 cm$^{-1}$ band further demonstrates the different origin of these two bands, in conformity with the assignment of these bands, stated in Chapter 2. On the basis of model compounds, it was concluded that the 3500 cm$^{-1}$ band arises from hydroxyl nests and the 3700 cm$^{-1}$ band arises from hydroxyl pairs in defected zeolites. Thus, using TiCl$_4$ as titanium precursor preferentially the hydroxyl *nests* are attacked, while (NH$_4$)$_2$TiF$_6$ reacts preferentially with the hydroxyl *pairs*.



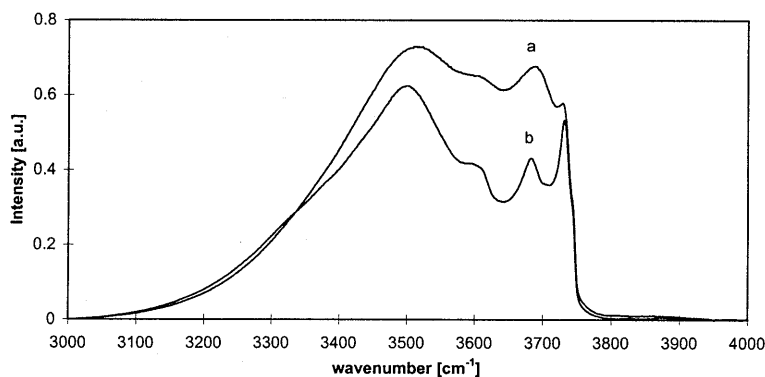*Figure 3.11 FT-IR spectroscopy on aqueous phase titanated Mordenite and its dealuminated parent material: [a] Mor/I-150 and [b] Ti19Mor/I-150.*

The different behavior of the different defect sites as a function of titanium precursor can be explained by their accessibility. The hexafluorotitanate ion, especially when hydrated, is much larger than the titanium chloride molecule. There is reported that its siliceous analogue,

$(NH_4)_2SiF_6$, can hardly enter the Mordenite 12-ring [29,30]. Therefore, it is supposed that these hydroxyl pairs, corresponding to the 3700 cm$^{-1}$ band, are present *outside* the zeolite micropores. It has to be concluded, however, that it is not impossible to create tetrahedral titanium sites with aqueous phase titanation, using $(NH_4)_2TiF_6$. The small decrease of the 3500 cm$^{-1}$ band can probably correspond to the shoulder at 220 nm in the DRUV-Vis spectrum of the aqueous phase titanated sample. This band was assigned to isolated, tetrahedral coordinated titanium sites in a zeolite (*vide infra*), and therefore, implies the incorporation of a small amount of titanium into T-atom vacancies of the Mordenite.

## 3.4 Further spectroscopic investigation

The various different titanium zeolites obtained by the CVD titanation procedure are further investigated using combined XPS, Raman and Diffuse Reflectance UV-Vis spectroscopy. This, to get a better understanding for the kind of titanium sites created, as well as their distribution over the zeolite crystal and the possible presence of traces of titanium oxide species. Raman spectroscopy has proven itself as a very powerful characterization method to detect titanium oxide species [31,32]. The only problem that can arise is the possibility of fluorescence: an unwanted high and broad background of the Raman spectrum, caused by the presence of strongly luminescent species, like organic aromatics or, for instance, traces of iron present in the zeolite. In figure 3.12 the Raman spectra of the most common titanium oxide structures (anatase and rutile) and the aqueous phase titanated Mordenite (Ti19Mor/I-150) are plotted. The effect fluorescence can have on the Raman spectrum is clearly visualized by the spectrum of Ti19Mor/I-150, although the presence of titanium oxide species with the anatase structure is still unmistakable.
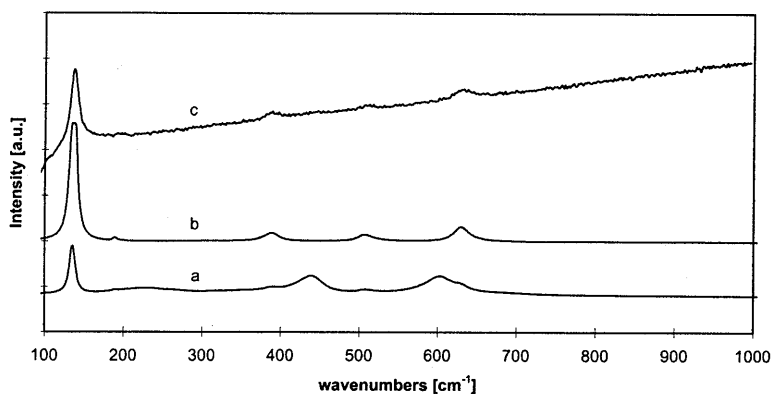


*Figure 3.12  Raman spectra of [a] $TiO_2$ (predominantly) rutile, [b] $TiO_2$ anatase, [c] Ti19Mor/I-150.*

*Table 3.4  Elemental and spectroscopic analysis of fluid bed titanated Beta.*

| sample[a] | Ti/uc | Al/uc removed | O1s (TiO$_2$) / O1s (SiO$_2$) | Ti 2p$_{3/2}$ BE [eV] | Ti 2p / Ti 3p | Raman spectrum |
|---|---|---|---|---|---|---|
| Ti56Bea-450 | 1.12 | 1.52 | 0 | 458.9 | 1.9 | free of TiO$_2$ |
| Ti43Bea-160 | 1.44 | 1.26 | 0 | 459.1 | 1.8 | free of TiO$_2$ |
| Ti32Bea-267 | 1.93 | 1.42 | 0.03 | 458.5 | 1.3 | TiO$_2$ present |
| Ti30Bea-321 | 2.08 | 1.46 | 0.01 | 458.6 | 1.7 | TiO$_2$ present |
| Ti27Bea-72 | 2.33 | 0.79 | 0.02 | 458.7 | 1.2 | TiO$_2$ present |
| Ti21Bea-170 | 2.90 | 1.29 | 0.03 | 458.8 | 1.4 | * |

*[a] Sample names consist of the Si/Ti ratio, followed by type of zeolite, and the Si/Al ratio (see also Section 3.6). * : too much fluorescence made it impossible to analyze the Raman spectrum.*

When we take into account the amount of aluminum removed compared to the amount of titanium introduced for titanium Beta, a good correlation can be seen from table 3.4 regarding the TiO$_2$ formation. In this table the formation of TiO$_2$ can be seen from the O 1s band ascribed to TiO$_2$ (which intensity is given relative to the O 1s band for SiO$_2$) and Raman spectroscopy. Both confirm the formation of TiO$_2$ when the amount of titanium introduced is higher than the amount of aluminum removed. This dependency is visualized in figure 3.13 in which the difference of the Ti per unit cell and the removed Al per unit cell is plotted *versus* the Ti/uc. When this difference crosses zero, the formation of TiO$_2$ species starts to occur.
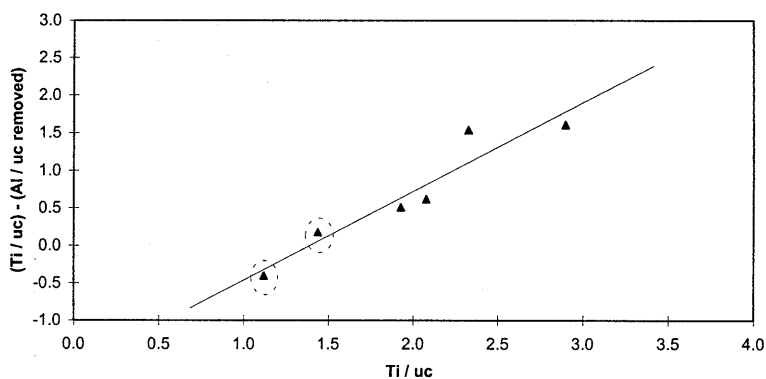


*Figure 3.13  Number of titanium atoms per unit cell (Ti/uc) minus number of aluminum atoms removed per unit cell (Al/uc removed) plotted versus Ti/uc for the titanium Beta samples as summarized in table 3.4. Dotted circles represent the TiO$_2$ free samples.*

A typical spectrum of a titanium oxide containing zeolite together with a TiO$_2$ free sample is shown in Figure 3.14. Obviously, the strong anatase bands can be recognized in the TiO$_2$ containing sample. The traces of titanium oxide species, which were detected by Raman spectroscopy on certain titanium zeolites, exhibited in all cases the anatase structure.
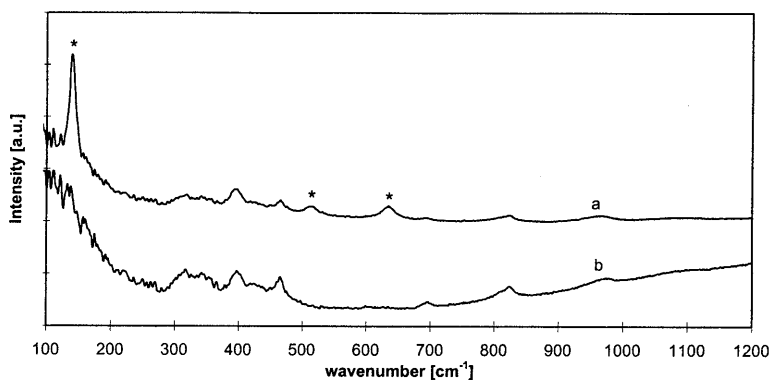
*Figure 3.14  Raman spectra of [a] an anatase containing titanium Beta, Ti32Bea-267, [b] an $TiO_2$ free titanium Beta, Ti56Bea-450. Spectral bands marked with an asterisk are typical for the anatase structure.*

Regarding the titanium Mordenites series II, already at very low titanium contents the formation of $TiO_2$ can be observed (see table 3.5). For sample Ti226Mor/II-116 this amount of titanium oxide was impossible to detect using the O 1s band assigned to $TiO_2$. In this case, only Raman spectroscopy could be used to detect the very low titanium oxide content of this sample. The amount of aluminum removed for all these samples after the second acid leach treatment is equal to 1.0 aluminum atom per unit cell. In this way, the calcination step in between is considered as totally destructive for all hydroxyl nests, and only the aluminum removed thereafter is taken into account. For all titanium Mordenites (Mor/II-116 series) this amount of removed aluminum is higher or close to the amount of titanium incorporated. Therefore, the formation of $TiO_2$ species in the case of titanated Mordenites is not (only) related to the defect site concentration.

*Table 3.5  Elemental and spectroscopic analysis of titanated Mordenite.*

| sample[a] | O1s ($TiO_2$) O1s ($SiO_2$) | Ti $2p_{3/2}$ BE [eV] | Ti 2p Ti 3p | Raman spectrum |
|---|---|---|---|---|
| Ti226Mor/II-116 | 0 | 458.3 | 3.3 | $TiO_2$ present |
| Ti75Mor/II-116 | 0.02 | 458.3 | 1.8 | * |
| Ti65Mor/II-116 | 0.03 | 458.1 | 1.5 | $TiO_2$ present |
| Ti58Mor/II-116 | 0.04 | 458.2 | 1.4 | * |
| Ti33Mor/II-6.1 | 0.19 | 458.6 | 1.1 | $TiO_2$ present |
| Ti51Mor/II-116 | 0.17 | 458.3 | 0.9 | * |
| Ti43Mor/II-116 | 0.08 | 458.5 | 1.1 | $TiO_2$ present |

*[a] Fixed bed (upper 4 samples) and fluid bed (lower 3 samples) titanated Mordenite. Sample names consist of the Si/Ti ratio, followed by type of zeolite, and the Si/Al ratio (see also Section 3.6).*
*\* : too much fluorescence made it impossible to analyze the Raman spectrum.*

Another parameter from XPS analysis that should be affected by the formation of $TiO_2$ is the Ti2p/Ti3p ratio. This ratio gives information about the distribution of the titanium atoms, which are visible for XPS. Since the photoelectrons exited from the Ti 2p level have a higher binding energy, BE (Ti $2p_{3/2}$ BE around 459 eV) than the Ti 3p level (Ti 3p BE around 38 eV) their corresponding kinetic energies are *lower* than for the Ti 3p (see also table 3.6). This, according to the formula of the photoelectric effect[33], equation 3.1:

$$E_k = h\nu - E_b - \varphi \qquad (3.1)$$

In this equation $E_k$ is the kinetic energy with which the photoelectron is rejected, $h\nu$ is the adsorbed energy, $E_b$ is the binding energy (BE) of the core or valence electron and $\varphi$ is the work function of the spectrometer. The lower kinetic energy results in a lower probability for the photoelectrons exited from the Ti $2p_{3/2}$ level to leave the sample. In other words, the mean free path of the exited photoelectrons is lower for the Ti $2p_{3/2}$ level than for photoelectrons from the Ti 3p level. This mean free path can be expressed as the, so-called, attenuation length. The for this study relevant estimations of the attenuation lengths for the various electron levels are given in table 3.6. Especially for titanium and oxygen, the influence of the binding energy on the resulting attenuation length is evident from these data.

When relatively many titanium atoms are situated on the outer surface, a higher Ti2p/Ti3p ratio is expected. This, since the Ti 2p signal is the most sensitive for deeply located titanium sites, having the lowest mean free path. The lower this ratio gets, the better the distribution of titanium over the zeolite crystal *or* the larger the titanium oxide particles present outside the zeolite crystals. To rule out other possible factors that could have an effect on this elemental ratio, the elemental ratios for silicon (Si2p/Si2s) and oxygen (O1s/O2s) were also measured. Especially for oxygen, the difference between the O 1s and O 2s binding energy has the same order of magnitude as for titanium, as can be derived from table 3.6.

*Table 3.6   The approximate binding energies (BE) and estimated attenuation lengths for the corresponding electron levels of titanium, silicon and oxygen.*

| element | Ti | | Si | | O | |
|---|---|---|---|---|---|---|
| electron level | $2p_{3/2}$ | 3p | 2p | 2s | 1s | 2s |
| BE [eV] | 459 | 38 | 103 | 154 | 532 | 25 |
| attenuation length [nm][a] | 2.3 | 3.3 | 3.1 | 3.2 | 2.2 | 3.4 |

*[a] Calculated for a $SiO_2$ matrix with an average density of 1.6 ml/g, using a Mg source and a pass energy of 20 eV.*

The ratios for silicon and oxygen as a function of Si/Ti XPS ratio are plotted in figure 3.15. Obviously, a constant and non correlated behavior for both elemental ratios as a function of Si/Ti XPS ratio can be seen. This should be expected, since both silicon and oxygen are assumed to be distributed perfectly over the zeolite crystals. The  O1s and O2s have a

relatively high difference in their mean free paths. The fact that this O1s/O2s ratio is unaffected, indicates the potential of the derived information from the variation in Ti2p/Ti3p ratio.
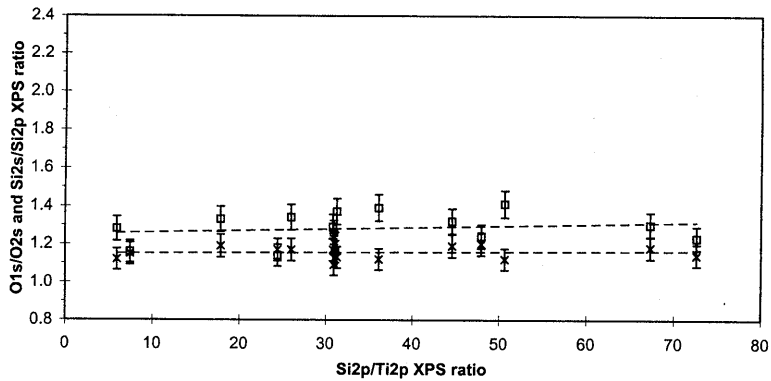


*Figure 3.15 XPS ratios for silicon, Si2p/Si2s(×) and oxygen, O1s/O2s (□) as a function of Si2p/Ti2p XPS ratio.*

When the Ti2p/Ti3p ratio is plotted against the Si/Ti XPS ratio a positive trend can be observed: with lower Si/Ti ratios lower Ti2p/Ti3p ratios are obtained (see figure 3.16). In the case of titanated Beta already an almost perfect titanium distribution was established (see figure 3.8), which excludes the influence of the titanium distribution on the Ti2p/Ti3p ratio. Therefore, we must conclude that the fast decrease of this ratio with lower Si/Ti ratios is indicative for the formation of $TiO_2$. This titanated Beta series displays a nice correlation of this ratio with the formation of $TiO_2$: only samples which a high Ti2p/Ti3p ratio are free from $TiO_2$ (see also table 3.4).



*Figure 3.16 XPS ratio for titanium (Ti2p/Ti3p) as a function of Si2p/Ti2p XPS ratio. An dotted arrow indicates the presence of $TiO_2$ and a dotted circle represents a $TiO_2$ free sample.*

The blank experiment resulting in Ti33Mor/II-6.1, a reference material which was not dealuminated at all before titanation, showed unmistakably the formation of titanium oxide (see O1s($TiO_2$)/O1s($SiO_2$) ratio and Raman analysis in table 3.5) and its Ti2p/Ti3p ratio is about the lowest of all titanated zeolites.
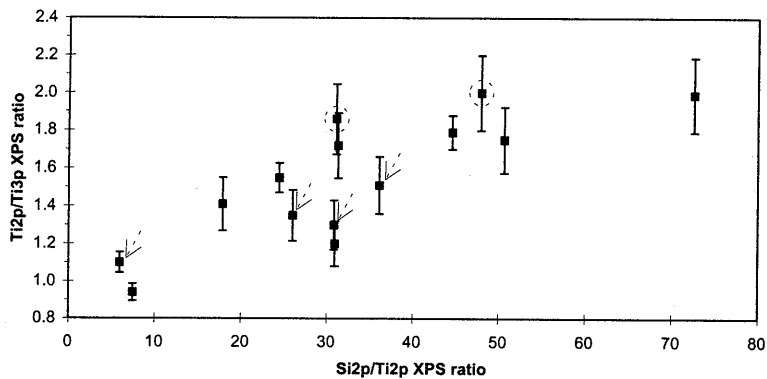
Finally, regarding the Ti $2p_{3/2}$ binding energy, the low binding energies found for $TiO_2$ (around 458 eV) are in line with our results: all $TiO_2$ containing samples have their Ti $2p_{2/3}$ maximum between 458.1 and 458.7 eV. For the $TiO_2$ free samples higher binding energies were obtained, although, still relatively low: around 459 eV instead of the reported values of the Ti $2p_{2/3}$ band around 460 eV for TS-1 or TS-2. This can be due to the different titanium environment in a titanium Mordenite or Beta compared to the environment inside a silicalite framework. The angles and distances of the T-atoms with its surrounding oxygen atoms differ for those large pore zeolites in comparison with the medium pore silicalite structures. Moreover, in titanium incorporated silicalite almost perfect crystals can be considered, whereas in the case of titanium Mordenite or Beta we are dealing with zeolites with a relatively high defect site concentration and that also contain traces of aluminum. It is reported that the Madelung potential, which can be affected by those parameters, causes significant shifts in binding energies[34]. We would expect, in this case, for the other elements as silicon and oxygen to shift also. The binding energy for O 1s, however, is extremely stable on 352.5 eV ± 0.1 eV (normalized on Si 2p at 103.3 eV). These observations suggest that the shift in the Ti 2p band probably is caused by a more local charge effect.
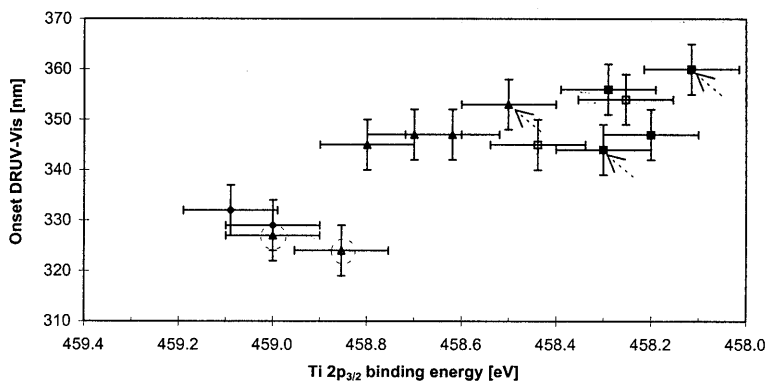


*Figure 3.17 The onset of the diffuse reflectance UV-Vis spectra versus the XPS Ti $2p_{3/2}$ binding energy for the titanium Mordenites/I (◇), the titanated Mordenites/II fluid bed (□), and fixed bed (■) and titanium Beta (▲). A dotted arrow indicates the presence of $TiO_2$ and a circle represents a $TiO_2$ free sample.*

The Ti $2p_{2/3}$ binding energy is compared with the diffuse reflectance UV-Vis spectra. Since the last spectra consist of very broad bands, an accurate parameter to derive from these plots is the onset: the intersection of the slope of the right side of the curve with the x-axis. In a plot

in which the Ti $2p_{3/2}$ binding energy is plotted against the onset of the DRUV-Vis spectra, an apparent positive slope can be recognized (figure 3.17). As expected, a higher onset results in a higher binding energy, finally resulting in bulk $TiO_2$ with a binding energy of 460 eV and an onset of about 370 nm.

## 3.5  Discussion and conclusions

Obviously, the crystal size of a zeolite will have its influence on the probed area measured with XPS. An XPS analysis on the large crystals of the Mor/II series, implies that only information is obtained about the elements present in the outer regions or shells of the particles and that the majority of the sample volume inside cannot be 'seen'. The formation of titanium oxide was confirmed in all cases having Mor/II-116 as the parent Mordenite. This, however, does not rule out the existence of isolated, tetrahedral titanium sites, probably located inside the Mordenite micropores. The very low Si/Ti XPS ratios obtained compared with the bulk Si/Ti ratios are caused by the relatively high titanium content of the outer regions. This relatively high titanium content is present in only a few percent of the sample volume (which is what is visible for XPS). Furthermore, the low binding energies found for Ti $2p_{3/2}$ imply that the majority of these visible titanium species are present as titanium oxide particles.

The Mor/I series, on the contrary, involve smaller crystals and have Si/Ti ratios obtained with XPS that are comparable to the bulk Si/Ti ratios. Also their Ti $2p_{3/2}$ binding energies as well as their DRUV-Vis onset indicate the absence of $TiO_2$ species. The 10 - 20 times larger crystals of the Mor/II series can explain the diffusion limitations of the $TiCl_4$ precursor during titanation. This results in an enrichment of titanium in the outer shells of the zeolite crystal and therefore the formation of $TiO_2$ tents to start there with a lower titanium content compared to the titanated Mor/I series. Already at very low titanium contents, the preferential titanation of the outer regions is obviously.

The Beta series have perfect matching Si/Ti XPS and bulk ratios while the difference with the Mor/I series indicates that even with their same very small crystal sizes not all material is visible for XPS under the conditions used. Nicely, the amount of $TiO_2$ formed decreases with the decreasing amount of titanium introduced up to a minimum at which we succeeded in preparing $TiO_2$ free titanium substituted zeolites. This minimum was shown to match to the amount of aluminum removed by the dealumination procedure. This implies that the defect sites created upon acid dealumination are relatively stable until they reacted with $TiCl_4$ during titanation. With the combination of the three dimensional Beta pore structure and its small crystal size, no symptoms of diffusion limitations can be found and the highest distribution of titanium over the zeolite crystals is obtained. This perfect spreading of the titanium over the zeolite sample, causes the low probability for titanium oxide species to form and agrees well with the assumption that almost all defect sites are filled with titanium.

In conclusion, the O 1s band at 530 eV, the Ti2p/Ti3p ratio below 1.7 and the Ti $2p_{3/2}$ binding energy below 458.8 eV, all derived from the XPS analysis, are good indicators when the formation of $TiO_2$ is studied. Also the DRUV-Vis onset correlates well with these parameters, concerning the presence of titanium oxide (onset above 340 nm). For very low titanium oxide contents, however, Raman spectroscopy is the decisive tool to determine the presence of $TiO_2$ in a zeolite sample.

## 3.6 Experimental

The dealuminated Mordenite and Beta zeolites used for titanation are extensively described in Chapter 2. Sample names for the different titanated zeolites begin with 'Ti', followed by the Si/Ti ratio, than their zeolite structure (Mor or Bea), the different parent batches in the case of Mordenite (I or II) followed by the Si/Al bulk ratio of that sample. In the case of two dealuminated samples with the same Si/Al ratio, they are numbered a, b, c, etc. (for example: Ti19Mor/I-150: zeolite Mordenite, batch I, Si/Ti = 19, Si/Al = 150). The TS-1 sample used as reference material is the well known EUROTS-1, as described by Martens *et al.* (reference [35]). The $TiO_2$ used as reference material are anatase (Aldrich, $TiO_2$ 99.9+ %) and rutile (Aldrich, $TiO_2$ 99.9+ %, predominantly rutile).

In a CVD fluid bed titanation experiment an optimum amount of dried zeolite sample for fluidization (typically 2.5 gram for Mor/I and Beta and 5 gram for Mor/II) was loaded in the CVD reactor (see figure 3.17). For fixed bed titanation a desired amount of zeolite was used. The sample was dried in a nitrogen stream of typically 177l/h (by-pass flow in figure 3.17) at 120°C for 1 hour. Then the temperature was raised to the desired titanation temperature (400 - 500°C) and a second flow (saturator flow in figure 3.17, typically 3 or 6 l/h) was introduced, saturated with $TiCl_4$ (ACROS, 99.9%; 11.3 mBar partial pressure of $TiCl_4$ at 19°C). After the desired time of reaction, the sample was purged with nitrogen for 1.5 h at the same temperature used for titanation to free the zeolite sample of all the unreacted titanium chloride species. Finally, the sample was calcined in air at 550°C for 4 hours.
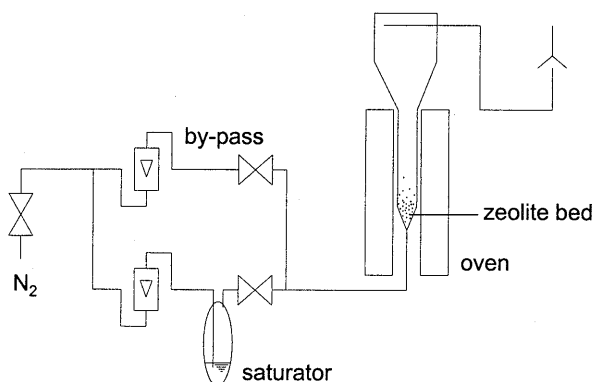


*Figure 3.17 Experimental set-up for titanation experiments.*

In an aqueous phase titanation experiment 70 ml of 0.05 M ammonium fluorotitanate (Aldrich, 99.99%) solution was slowly added (approximately 10 - 20 ml/h) to a slurry of 4 g dealuminated zeolite in a buffered solution of 12.4 g ammonium acetate in 120 ml distilled water. The very low concentration of ammonium fluorotitanate used together with the buffered solution provided a reliable control of the pH during reaction between 6.7 and 5.9. The titanium fluoride species were allowed to react for 24 h with the zeolite at RT. Afterwards, the titanium zeolite was washed thoroughly with an excess of distilled water at 100°C for three times and dried at 80°C overnight. Finally, the sample was calcined in air at 550°C for 4 hours.

Diffuse Reflectance UV-Vis (DRUV-Vis) spectra were recorded on a Hitachi 150-20 Spectrometer with a DIA Integration Sphere Accessory between 500 and 200 nm using a scan speed of 2 nm/min. Samples were measured in a cell of non-adsorbing suprasil quartz glass (with dimensions of 13x13x1 mm) using a reference sample of grinded $Ca(OH)_2$. All spectra were converted to Kubelka-Munk intensities.

X-ray Photoelectron Spectroscopy (XPS) measurements were performed on zeolite samples pressed on indium stubs using a VG ESCALAB 200 Spectrometer equipped with a standard X-ray source (Mg Kα) and a hemispherical analyzer. Measurements were done at 20 eV pass energy and charging was corrected using the Si 2p signal at 103.3 eV. Spectra were fitted for determining surface areas and peak maxima using the VGS program fit routine, with a Shirley background subtraction and Gauss-Lorentz curves. Elemental ratios were calculated with the correction for their cross-sections (reference [36]). For reasons of clarity the XP spectra plotted were normalized on the highest peak.

Raman spectra were recorded with a Labram spectrometer from Dilor S.A. (France). A Spectra Physics Millenium II Nd:YVO$_4$ laser at 532 nm was used as an excitation source. The initial laser power was 0.20 W. Spectra were taken from zeolites samples under ambient conditions. Laser light was focused on the sample using a slit width of 0.1 mm and a 10× microscope objective. The 180° back scattered radiation from the sample was dispersed with a 1800 mm$^{-1}$ grating onto a CCD detector.

The weight percentages of titanium were determined by atomic absorption spectrometry (AAS) using a Perkin Elmer 3030 Atomic Absorption Spectrophotometer. For this purpose the samples were wetted with a few drops distilled water and sulfuric acid (Merck, p.a.) and then dissolved in concentrated hydrofluoric acid. The volatile silicon fluoride formed, was evaporated and to the residue 1 g $K_2S_2O_7$ (Merck, p.a.) was added and melted. The cooled melt was dissolved in 2.5 molar sulfuric acid. The standard addition method was used to determine the titanium concentration.

Water contents of the zeolite samples, were determined with a Shimadzu TGA-50 thermogravimetric analyzer. About 10-15 mg of sample was heated under static conditions in air to 700°C with a rate of 5°C per minute.

Micro pore volumes were determined by adsorption of n-butane from a dry helium flow at room temperature. Before this, samples were dehydrated at 350°C for 15 minutes. The relative increase of mass due to the adsorbed n-butane was measured using a Cahn 2000 electrobalance. The pore volume was calculated using the density of liquid n-butane at 20°C relative to water at 4°C.

Fourier Transformed Infrared (FT-IR) spectra were taken at room temperature on a Bruker IFS 113V spectrophotometer equipped with a vacuum cell. Before this, the samples were pressed into self-supporting wafers of 10 mg and dried at 450°C for 1 hour in vacuum. The obtained spectra were baseline corrected linearly from 3000 cm$^{-1}$ to 4000 cm$^{-1}$.

X-Ray Diffraction (XRD) data were obtained with a Philips PW 7200 X-ray powder diffractometer, using Cu-Kα radiation. Diffractograms were taken between 5° and 50° 2θ, using a scan speed of 1° per minute. The obtained diffraction patterns were corrected for baseline, background, and Kα2 elimination.

# References

1. B. Kraushaar, J.H.C. van Hooff, *Catal. Lett, 1*, (**1988**), p. 81.
2. C. Ferrini, H.W. Kouwenhoven, *Stud. Surf. Sci. Catal., 55*, (**1990**), p. 53.
3. P.J. Kooyman, P. van der Waal, P.A.J. Verdaasdonk, K.C. Jansen, H. van Bekkum, *Catal. Lett., 13*, (**1992**), p. 229.
4. P. Wu, T. Komatsu, T. Yashima, *J. Phys. Chem., 100*, (**1996**), p. 10316.
5. J.P. Blitz, *Colloid. Surface, 63*, (**1992**), p. 11.
6. E.F. Vansant, P. van der Voort, K.C. Vranken, *Stud. Surf. Sci. Catal., 93*, (**1995**), p. 357.
7. J.S. Reddy, A. Sayari, *J. Chem. Soc. Chem. Commun.*, (**1995**), p. 23.
8. J.S. Reddy, A. Sayari, *Stud. Surf. Sci. Catal., 94*, (**1995**), p. 309.
9. T. Ito, H. Kanai, T. Nakai, S. Imamura, *React. Kinet, Catal. Lett., 52*, (**1994**), p. 421.
10. G. W. Skeels, E.M. Flanigen, *A.C.S. Symp. Ser., 398*, (**1988**), p. 420.
11. G.P. Schindler, P. Bartl, W.F. Hölderich, *Appl. Catal. A., 166*, (**1998**), p. 267.
12. J. Livage, *Stud. Surf. Sci. Catal., 85*, (**1994**), p. 1.
13. R. Szostak, *Stud. Surf. Sci. Catal., 58*, (**1991**), p. 153.
14. D. Geldart, *Types of Gas Fluidization*, Powder Technology, 7, (**1973**), p. 285.
15. M. Pell, *in: Handbook of Powder Technology* (Ed. J.C. Williams, T. Allen), Elsevier Amsterdam (**1990**).
16. For a review concerning the XPS on zeolites: M. Stöcker, *Microporous Materials, 6*, (**1996**), p. 235.
17. For a review concerning different characterization techniques on titanium silicates: G.N. Vayssilov, *Catal. Rev.-Sci. Eng., 39*(3), (**1997**), p. 209.
18. F. Geobaldo, S. Bordiga, A. Zecchina, E. Giamello, G. Leofanti, G. Petrini, *Catal. Lett., 16*, (**1992**), p. 109.
19. E. Astorino, J.B. Peri, R.J. Willey, G. Busca, *J. Catal., 157*, (**1995**), p. 482.
20. A. Zecchina, *et al., Catal. Today, 32*, (**1996**), p. 97.
21. M. Anpo, *et al., J. Phys. Chem., 89*, (**1985**), p. 5017.
22. R.J. Davis, *Chem. Mater., 4*, (**1992**), p. 1410.
23. Y.-L. Kim, R.L. Riley, M.J. Huq, S. Salim, A.N. Le, T.E. Mallouk, *Mat. Res. Soc. Symp. Proc.* (Ed. R.L. Bedard *et al.*) *233*, Pittsburgh, Pennsylvania, (**1991**).
24. J.S. Reddy, A. Dicko, A. Sayari, *in: Synthesis of microporous Materials: Zeolites, Clays and Nanostructures*, (Ed. M. Occelli, H. Kessler), New York, (**1997**), p. 405.
25. D. Trong On, L. Bonneviot, A. Bittar, A. Sayari, S. Kaliaguine, *J. Mol. Catal., 74*, (**1992**), p. 233.
26. T. Blasco, M.A. Camblor, J.L.G. Fierro, J. Perez-Pariente, *J. Am. Chem. Soc., 115*, (**1993**), p. 11806.
27. M. Montes, F.P. Getton, M.S.W. Vong, P.A. Sermon, *J. Sol-Gel. Sci. Tech., 8*, (**1997**), p. 131.
28. Keshavaraja, V. Ramaswamy, H.S. Soni, A.V. Ramaswamy, P. Ratnasamy, *J. Catal., 157*, (**1995**), p. 501.
29. E. Benazzi, J. Slva, M. Ribeiro, F. Ribeiro, M. Guisnet, *Zeolites, 16*, (**1995**), p. 393.
30. J. Silva, M. Ribeiro, F. Ribeiro, E. Benazzi, N. Gnep, M. Guisnet, *Zeolites, 16*, (**1995**), p. 275.
31. G. Deo, A.M. Tukey, I.E. Wachs, D. R.C. Huybrechts, P.A. Jacobs, *Zeolites, 13*, (**1993**), p. 365.
32. W. Pilz, Ch. Peuker, V.A. Tuan, R. Fricke, H. Kosslick, *Ber. Bunsen-Ges. Phys. Chem., 97*, (**1993**), p. 1037.
33. J. W. Niemantsverdriet, *Spectroscopy in Catalysis*, VCH, Weinheim, (**1995**).
34. S. Kaliaguine, *Stud. Surf. Sci. Catal. 102*, (**1996**), p. 191.
35. J.A. Martens *et al., Appl. Catal. A. Gen., 99*, (**1993**), p. 71.
36. J.H. Scofield, *J. Electron Spectrosc. Rel. Phenom., 8*, (**1976**), p. 129.

# 4

# Epoxidation catalysis by titanium zeolites

The titanium zeolites, prepared *via* a post-synthesis modification in Chapter 2 and 3, are applied as catalysts for the selective epoxidation of alkenes. In liquid phase catalysis using peroxides, these titanium zeolites were proven to be truly heterogeneous epoxidation catalysts. Our results once more indicate that a titanium zeolite will be an active and selective epoxidation catalyst only when the zeolite consists of very small crystallites with a hydrophobic framework. From epoxidation catalysis of a substrate which can impossibly enter the micropores of Beta or Mordenite, we conclude that with both Ti-Mor and Ti-Beta catalysts a minor external surface activity is present. Interestingly, the post-synthesis prepared very active Ti-Beta catalyst showed a catalytic performance in the epoxidation of 1-octene using $H_2O_2$, which is at least comparable to the activity of TS-1 under the same reaction conditions.

## 4.1 Introduction

Titanium substituted zeolites are well known oxidation catalysts[1]. As described in Chapter 1 they catalyze a variety of oxidation reactions, such as; olefin epoxidation, oxidation of primary alcohols to aldehydes, aromatic hydroxylation and ammoxidation of cyclohexanone to cylcohexanone oxim[2]. Among these various types of oxidation reactions, epoxidation of olefins, schematically depicted in figure 4.1, plays an important role. The formed epoxides are intermediates that can be converted to a variety of products, especially interesting in the field of the fine chemical industry.
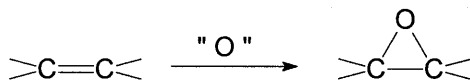
*Figure 4.1 Schematic representation of the epoxidation of an alkene substrate.*

A non catalytic route for the synthesis of epoxides involves peracids, using a stoichiometric amount of peracid per mole of product. There are, however, examples in which this peracid is catalytically synthesized, for instance by redox molecular sieves[3]. Recently, the use of transition metal complexes to catalyze epoxidation reactions, has received increased attention[4]. Applying catalytic reaction path ways, would enable the use of cheaper and environmentally more friendly oxygen donors like $O_2$, $H_2O_2$ or TBHP (*tert.*-butyl hydroperoxide).

Titanium catalysts have already proven themselves as active and selective epoxidation catalysts using peroxides as oxygen donor. Titanium deposited on amorphous silica, Ti(IV)/SiO$_2$, is patented by Shell as an active epoxidation catalyst using TBHP[5]. The high activity of this catalyst, also referred to as the Shell catalyst, is ascribed to *isolated* titanium sites, anchored to its SiO$_2$ host by siloxy units. Later, such isolated titanium sites were generated in crystalline, microporous structures, as zeolites. Titanium silicalite 1, abbreviated as TS-1, is the most well known example of such a titanium substituted zeolite[2,6,7]. This catalyst shows markedly distinct reactivities and selectivities in comparison with other titanium based catalysts[1,8]. Its catalytic performance is based on the use of hydrogen peroxide as the oxidizing agent. As depicted in figure 4.2, cycle I, the coordination of hydrogen peroxide involves the hydrolysis of a Ti-O-Si bond *via* coordination of $H_2O_2$, resulting in an active titanium hydroperoxo (Ti-OOH) species.



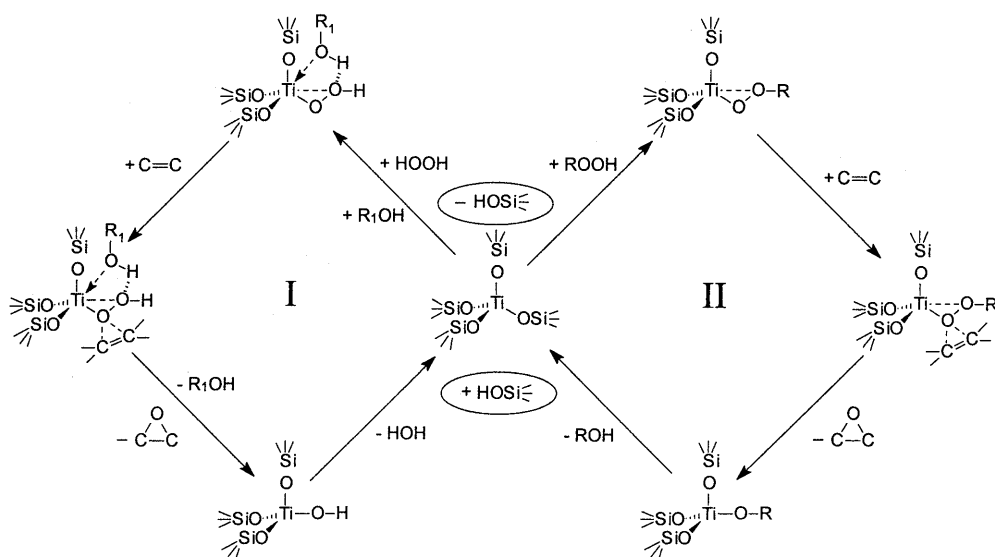*Figure 4.2  Possible catalytic cycles of a titanium catalyzed epoxidation reaction: cycle I in the presence of a protic solvent (R₁OH) and hydrogen peroxide (HOOH), cycle II in the presence of an aprotic solvent and TBHP (ROOH). For reasons of clarity the encircled Si-OH unit resulting from the hydrolysis of a Si-O-Ti bond is omitted in the activated clusters.*

In cycle II, the same type of catalysis is shown, however in the absence of a protic solvent and with an organic peroxide (ROOH) as the oxidizing agent. According to Clerici *et al.*, a promotion effect of the protic solvent can be rationalized by the formation of a five-membered ring, as can be seen in cycle I, resulting in an increased electrophilicity of the hydroperoxo species[9]. Reported by the same authors is the assumption that the second oxygen atom is transferred to the epoxide (counting from the metal center: Ti-$O^1$-$O^2$-H), on the basis of steric arguments. Very recent calculations, however, predict that the *first* oxygen attacks the alkene. This prediction is founded on a significant energy difference of the two different transition states, each with an alkene coordination either to $O^1$ or $O^2$ [10]. Yet, this hypothesis is not confirming earlier results, concerning the diastereoselective epoxidation catalysis with different titanium zeolites, in which a preference for the second oxygen is reported[11]. To our knowledge, no definite proof has been given so far concerning which of the two oxygen atoms is reacted with the alkene to an epoxide. Nevertheless, because of the latest published results, we suppose a transition of the first oxygen to the alkene, as depicted in figure 4.2. Moreover, the steric arguments used by Clerici *et al.* can as well apply for the second oxygen atom, when attached to a *tert.*-butyl group, favoring the hypothesis of a reaction of the *first* oxygen atom with the alkene[9].

The interesting contrast between the Shell catalyst, Ti/$SiO_2$, which is mainly active with TBHP, and TS-1, which is only active using $H_2O_2$ can be explained by the dominant influence the molecular sieve framework has on the catalytic performance of the incorporated metal. The titanium alkylperoxo complex formed by hydrolysis of the Ti-O-Si band is much more bulky than the hydroperoxide analogue. It is, however, shown that TBHP can enter the micropore system of the MFI structure and, therefore, it is postulated that the alkyl peroxo complex can be formed inside the TS-1 micropore[12]. Hence, it is concluded that the inactivity of TS-1 towards oxidation catalysis using TBHP is due to the steric hindrance of the bulky alkyl groups, preventing the reactants to approach the active site. Using hydrogen peroxide as oxidizing agent, the hydroperoxo titanium complex should be small enough to allow coordination of an alkene substrate. At the same time, the hydrophobic all silica zeolite framework, prevents the strong adsorption of water or other polar reactants or solvents used. In this way, the micropore structure will not be blocked by the adsorption of these polar molecules and the titanium site is effectively screened from bulk water. This in contrast to the relatively hydrophilic Ti/$SiO_2$ catalyst, in which the preferential adsorption of water, when using aqueous hydrogen peroxide as oxidizing agent, will deactivate the titanium site. This effect favors the application of the Ti/$SiO_2$ catalyst in an absolutely water-free environment. Noteworthy, the same counts for the highly active Sharpless asymmetric epoxidation catalysts (see also section 1.2).

From an industrial point of view, the usage of $H_2O_2$ as oxidizing agent is preferred over TBHP because it is cheaper, has a much higher atom utilization and produces only water as a by-product. The usage of this oxidant, however, results in the highest activities in the presence of a protic solvent, as described above and depicted in figure 4.2, cycle I [13]. This is

not favorable when the zeolite has still a relatively hydrophilic framework. The hydrophobicity of the zeolite is a dominant factor in the success of a titanium zeolite using $H_2O_2$ as oxidant in liquid phase oxidation catalysis[14]. Thus, a titanium zeolite, arising from a post-synthesis procedure, should have an aluminum content which is as low as possible, resulting in a minimum amount of cations present and, therefore, a low hydrophilicity. Besides this, such cations can be acid sites and, as such can catalyze possible unwanted side reactions, such as the hydrolysis or solvolysis of the epoxide ring resulting in the formation of diols[15].

The heterogeneity of the obtained titanium zeolites is of major importance. This term refers to the heterogeneous behavior of the titanium zeolite as a catalyst in liquid phase applications. Note here, that this is in contrast to a possible heterogeneous *distribution* of titanium over the zeolite crystal, which is described in Chapter 3. Heterogeneity in this catalytic context means that the solid catalyst is stable and does not lose metal species which can cause homogeneous reactions. There are, however, different ways to examine if a catalyst is truly heterogeneous. For instance, one can examine the stability of the catalyst by a regeneration test. A few reports are dealing with the catalytic activity of a repeatedly recycled catalyst[15-17]. From an industrial point of view, however, a lab scale recycling is hardly comparable with a continuous catalytic process. For instance, the reported leaching of the Shell catalyst during the first few hours time-on-stream[18]. Moreover, no information is given about a homogeneous contribution to the measured activity. In line with this technique, one can investigate the metal content of the heterogeneous catalyst after it has been used as an oxidation catalyst[19,20]. Since only very small amounts of metal ions or -complexes in solution can be responsible for a significant part of the measured activity, we doubt that this is the right way to test the catalyst's heterogeneity. Another way to cope with this problem, is by an elemental analysis of the reaction mixture to trace homogeneous metal ions. This procedure, however, requires very sensitive analysis techniques, since the amount of leached metal can be already active at a ppb level. Moreover, it gives no information about the activity of the leached metal particles and, in general, will be a rather laborious procedure. To our opinion, the most elegant and easy way to test the heterogeneity of the catalyst is by a filtration of the reaction mixture during catalysis[21]. First, the heterogeneous catalyst is treated under reaction conditions to allow the (possible loosely bound) metal species to leach out the zeolite framework. Then, in general after a few hours, the catalyst is filtered off and the activity of the clear filtrate is investigated, treated at reaction temperature. Important to mention is that this filtration is carried out under reaction temperature. This, because a cooling period in between can cause the leached metal species to precipitate on the solid particles. The catalytic 'performance' of the clear solution must be compared to the activity of the unfiltered reaction mixture, to get information about the contribution of a possible homogeneous activity to the measured activity. In Chapter 5 a further introduction is given concerning the heterogeneity of (industrial) oxidation catalysts.

## 4.2 Epoxidation activity of titanium substituted zeolites

In table 4.1 the performance of the titanium Mordenite series I in the epoxidation of cyclohexene, using different solvents are summarized. The post-synthesis prepared titanium substituted Mordenites are active and selective epoxidation catalysts. In general, when using acetonitrile as solvent increased conversions are obtained, in agreement with solvent effect studies on Ti-Beta[14], whereas with toluene the selectivity is somewhat higher. The latter observation can be explained by the influence of the polarity of the solvents used: the more polar character of acetonitrile will cause a strong interaction with the hydrophilic Mordenite framework. The resulting diffusion limitations for both substrate and oxidant increase their residence time in the titanium zeolite, which allows possible further reactions. This will reduce the selectivity towards the epoxide, as is the case using acetonitrile as solvent.

*Table 4.1  Catalytic performance of titanium substituted Mordenite/I catalysts in the epoxidation of cyclohexene at 50°C using TBHP as oxidant and acetonitrile or toluene as solvent[a].*

| catalyst | acetonitrile as solvent | | | toluene as solvent | | |
|---|---|---|---|---|---|---|
| | conv. [%] | sel. [%] | TOF [mol mol$^{-1}$h$^{-1}$] | conv. [%] | sel. [%] | TOF [mol mol$^{-1}$h$^{-1}$] |
| Ti63Mor/I-39 | 29 | 43 | 2.3 | 30 | 42 | 2.6 |
| Ti51Mor/I-39 | 50 | 45 | 5.1 | 36 | 74 | 2.2 |
| Ti44Mor/I-39 | 46 | 33 | 3.2 | 37 | 60 | 3.2 |
| Ti51Mor/I-79 | 43 | 36 | 1.5 | 31 | 56 | 4.6 |
| Ti19Mor/I-150 | 46 | 36 | 1.2 | 16 | <5 | 0.5 |

*[a] Conversion of cyclohexene (conv.) and selectivity to epoxide (sel.) measured after 5 hours, TOF measured after 2 hours and corrected for the blank reaction.*

Higher activities in terms of TOF's for the samples titanated to a higher titanium content with the same parent dealuminated Mordenite, can be explained with a lower hydrophobicity of the resulting titanium Mordenite (Ti51Mor/I-39 versus Ti63Mor/I-39). The possible lower hydrophobicity can result from a lower concentration of hydroxyl groups due to a higher titanium concentration. Again, this is an indication for the actual reaction of TiCl$_4$ with the hydroxyl nests of the zeolite. A liquid phase titanated Mordenite, Ti19Mor/I-150 resulting from the deposition of aqueous (NH$_4$)$_2$TiF$_6$, displays much lower activities in terms of turn over frequencies than the other titanium Mordenites. Obviously, this is due to the large content of TiO$_2$ this sample has (showed in Chapter 3), which significantly decreases the activity based on amount of titanium. None of these titanium Mordenites were active using H$_2$O$_2$ as oxidizing agent. Presumably, these samples still have a relatively too hydrophilic framework, resulting from a too high aluminum content.

Regarding the Ti-Beta catalysts, prepared *via* the same post-synthesis treatment, significant higher activities can be obtained in the epoxidation catalysis of cyclohexene. In table 4.2 the catalytic performance of various titanated Beta catalysts are summarized.

A comparison of the catalytic results with the XPS and Raman characterization, previously reported in Chapter 3, leads to the following considerations: First, the influence of the presence of $TiO_2$ in the titanated catalyst is visualized by its effect on the catalyst selectivity towards the epoxide. The catalysts containing titanium oxide species, as was proven by Raman spectroscopy, display the less selectivity to the epoxide. The influence, however, of the presence of $TiO_2$ on the initial activity (TOF) is less pronounced. Yet, the catalysts with the highest turn-over-frequencies have almost the highest titanium content (Ti27Bea-72) or show the most pronounced preferential titanium siting on the outer surface (Ti56Bea-450). This, since its Ti2p/Ti3p ratio is very high while no traces of $TiO_2$ could be detected by Raman spectroscopy (see also Chapter 3).

*Table 4.2   Catalytic performance of titanium substituted Beta catalysts in the epoxidation of cyclohexene at 50°C using TBHP as oxidant and acetonitrile as solvent[a].*

| sample | wt% Ti obtained | Ti 2p Ti 3p | Raman spectrum | conv. [%] | sel. [%] | TOF [mol mol$^{-1}$h$^{-1}$] |
|---|---|---|---|---|---|---|
| Ti56Bea-450 | 1.4 | 1.9 | free of $TiO_2$ | 50 | 30 | 11.5 |
| Ti43Bea-160 | 1.8 | 1.8 | free of $TiO_2$ | 52 | 35 | 8.0 |
| Ti32Bea-267 | 2.4 | 1.3 | $TiO_2$ present | 52 | 22 | 9.2 |
| Ti30Bea-321 | 2.6 | 1.7 | $TiO_2$ present | 45 | 27 | 3.3 |
| Ti27Bea-72 | 2.9 | 1.2 | $TiO_2$ present | 67 | 32 | 11.9 |
| Ti21Bea-170 | 3.6 | 1.4 | * | 56 | 43 | 6.1 |

*[a] Conversion of cyclohexene (conv.) and selectivity to epoxide (sel.) measured after 5 hours, TOF measured after 1 hour and corrected for the blank reaction. * : too much fluorescence made it impossible to analyze the Raman spectrum.*

This indicates the influence the heterogeneous titanium distribution can have on the initial activity, which is understandable when we take into account the catalysts nature of being a microporous zeolite. When the negative influence of the framework hydrophilicity is ruled out (*vide infra*), still the reactants have to diffuse through these micropores. These results indicate that even with a large pore, three dimensional zeolite, with a very small crystal size, the effect of diffusion of reactants through the catalyst micropores still can have a significant influence on the measured activity. This is in agreement with studies on the outer surface activity of zeolite Beta[22]. More about the outer surface activity of these titanium zeolites is discussed in section 4.3.

No influence of the aluminum content of these Ti-Beta catalysts on their oxidation activity can be recognized from these data. Apparently, the reached degrees of dealumination for all these samples are high enough to lose the influence the hydrophilicity of the zeolite framework can have on the catalyst performance. This result opens the possibility to use $H_2O_2$ as the oxidizing agent for these titanium Beta catalysts. This oxidizing agent is preferred over organic peroxides because of economic and environmental reasons (see section 4.1).

All the epoxidation reactions with cyclohexene show rather moderate selectivities. Important to mention is that *no* by-products at all could be detected by GC analysis. This leads to the conclusion that other side produces, possibly oligomeric species which are too large to detect by GC analysis, are formed. This probably relates to the relatively high activity of both the cyclohexene as its epoxide as well as to the presence of some traces of aluminum sites, which are Brønsted or Lewis acid sites, capable of catalyzing unwanted side reactions. In this respect, also the epoxidation reaction of cyclooctene is investigated, which causes less side reactions. In table 4.4 the epoxidation of cyclooctene is reported, using both TBHP and $H_2O_2$ using two titanium Beta catalyst which are free from $TiO_2$ compared to a $TiO_2$ containing Beta catalyst.

*Table 4.3    Catalytic performance of titanium substituted Beta catalysts in the epoxidation of cyclooctene at 50°C using TBHP or $H_2O_2$ as oxidant and acetonitrile as solvent[a].*

| catalyst | oxidant used | conv. [%] | sel. [%] | yield [%] | TOF [mol mol$^{-1}$h$^{-1}$] |
|---|---|---|---|---|---|
| Ti56Bea-450 (TiO$_2$ free) | TBHP | 47 | 71 | 33 | 17 |
|  | $H_2O_2$ | 79 | 78 | 62 | 35 |
| Ti43Bea-160 (TiO$_2$ free) | TBHP | 58 | 70 | 40 | 17 |
|  | $H_2O_2$ | 88 | 74 | 65 | 35 |
| Ti30Bea-321 (TiO$_2$ present) | TBHP | 53 | 76 | 41 | 12 |
|  | $H_2O_2$ | 69 | 75 | 52 | 18 |

[a] Conversion of cyclooctene (conv.), selectivity to epoxide (sel.) and yield of epoxide measured after 5 hours, TOF measured after 1 hour and corrected for the blank reaction.

These results clearly show the same catalytic performance for the two $TiO_2$ free samples, when the initial activity per titanium site is regarded: Using either $H_2O_2$ or TBHP similar TOF's are found for these two catalysts. The measured selectivities towards the epoxide are for all titanium Beta catalysts approximately the same, whereas the initial activities as well as the final yields after 5 hours are considerably higher when using $H_2O_2$ as oxidizing agent. This is explained by the higher intrinsic activity of the formed titanium peroxo complex, as depicted in figure 4.3, cycle I. In the case of $H_2O_2$, the water that is also present can act as the protic ligand. This is in good agreement with the results of Corma et al.[14]. The influence of the presence of traces $TiO_2$ in Ti-Beta (Ti30Bea-321) is reflected in a lower TOF using either $H_2O_2$ or TBHP. In the case of $H_2O_2$, however, the decrease in TOF is more pronounced. This can be explained by an additional effect of the $TiO_2$ species, which are notorious for their capability of the unselective $H_2O_2$ decomposition into oxygen and water. Evidently, using only $TiO_2$ (or the non titanated zeolites) as 'catalyst', no epoxide formation at all could be measured above detection limits. Considering the titanated Mordenite series II (see also section 3.3), all containing traces of $TiO_2$, a good correlation can be observed in the catalytic activity versus the results of the XPS analysis (see table 4.4).

Clearly, the increasing conversion and selectivity as a function of titanium content can be recognized. Normalized on the titanium content, however, the initial activity (TOF) decreases as a function of titanium content, especially for the fixed bed titanated Mordenites. This can be explained with the formation of $TiO_2$ species which increases with a higher titanium content, in agreement with the results of the XPS analysis. The $O1s(TiO_2)/O1s(SiO_2)$ ratio clearly demonstrates a higher titanium oxide content for the catalysts with a higher loading of titanium. The fluid bed titanated samples, display somewhat dissimilar activities and selectivities in the epoxidation of cyclooctene. Fluid bed titanation results in a higher initial activity for epoxidation compared to fixed bed titanation, although the titanium oxide content also tends to increase. Apparently, the incorporated, catalytically active titanium sites are better distributed over the zeolite sample, as can be expected from fluidized bed conditions in comparison with a fixed bed experiment. This is in accordance with the XPS analysis, reported in Chapter 3. But also the formation of $TiO_2$ increased when using fluid bed conditions in the titanation reaction. Therefore, we have to conclude that the formation of $TiO_2$ has a minor effect on the catalyst activity in terms of TOF. Noteworthy, this finding counts for the titanated Mordenites as well as the titanated Betas when using TBHP as oxidizing agent.

*Table 4.4  Catalytic performance of titanium substituted Mordenite/II catalysts in the epoxidation of cyclooctene at 50°C using TBHP as oxidant and acetonitrile as solvent.[a]*

| sample[b] | wt% Ti | $\dfrac{O1s\,(TiO_2)}{O1s\,(SiO_2)}$ | conv. [%] | sel. [%] | TOF [mol mol$^{-1}$h$^{-1}$] |
|---|---|---|---|---|---|
| Ti226Mor/II-116 | 0.35 | 0 | 16 | 23 | 3.7 |
| Ti75Mor/II-116 | 1.04 | 0.02 | 22 | 43 | 1.4 |
| Ti65Mor/II-116 | 1.19 | 0.03 | 26 | 43 | 1.0 |
| Ti58Mor/II-116 | 1.33 | 0.04 | 28 | 53 | 0.5 |
| Ti51Mor/II-116 | 1.52 | 0.17 | 45 | 49 | 2.9 |
| Ti43Mor/II-116 | 1.76 | 0.08 | 56 | 85 | 2.4 |

*[a] Conversion of cyclooctene (conv.), selectivity to epoxide (sel.) measured after 5 hours, TOF measured after 1 hour and corrected for the blank reaction. [b] Upper four fixed bed titanation, lower two fluid bed titanation.*

A remarkable difference can be noticed considering the activities in cyclooctene epoxidation using THBP by titanium Mordenite or titanium Beta. From table 4.2 and 4.4 we have to conclude that Ti-Beta is a more active and selective catalyst in this respect. As clarified above, this difference can hardly be explained by the presence of traces titanium oxide present in the majority of the titanated Mordenites. More likely is the influence the crystal size has on the catalytic performance. The titanated Beta samples have crystal sizes of about 20 times smaller than the titanated Mordenite II series. Moreover, the three dimensionality of the Beta framework facilitates also the diffusion through the zeolite micropores. As was already concluded from the titanation results, reported in Chapter 3, this lead also to the highest distribution of titanium over the zeolite crystal. We proved by adsorption experiments

that the uptake of cyclooctene occurs about 10 times faster in zeolite Beta than in the Mordenite/II (see section 4.3, figure 4.3). This is consistent with our explanation with regard to the crystal size and dimensionality facilitation diffusion through the zeolite pores. Furthermore, using titanium silicalite 1 (TS-1) as oxidation catalyst a strong dependency of the catalyst activity on the crystal size is reported[23]. From these results it is concluded that only really small crystal sizes (crystal diameter < 0.3 μm) can result in highly active TS-1 catalysts.

## 4.3 Outer surface activity and comparison with TS-1

XPS analysis showed that, especially for the titanated Mordenites, the zeolite crystals exhibit a significant surface enrichment of titanium. Also it is suggested that a part of these titanium species seems to be anatase like structures, following from the combined XPS, Raman and DRUV-Vis analysis. At this point, it should be interesting to know if there is any catalytic activity of titanium sites present on the external surface. To test this, we have performed epoxidation catalysis with cyclododecene, a substrate which can impossibly enter the Mordenite or Beta 12-ring pores. First, it was demonstrated by adsorption experiments that cyclododecene cannot be adsorbed in these zeolites. In figure 4.3 the adsorption behavior for cyclohexene, cyclooctene and cyclododecene are compared for a dealuminated Beta and Mordenite. In the case of zeolite Beta, all substrates diffuse easier in the zeolite micropores. This is explained by its smaller crystal size but also its higher dimensionality will have a positive effect on the diffusion of molecules through the zeolite micropores.
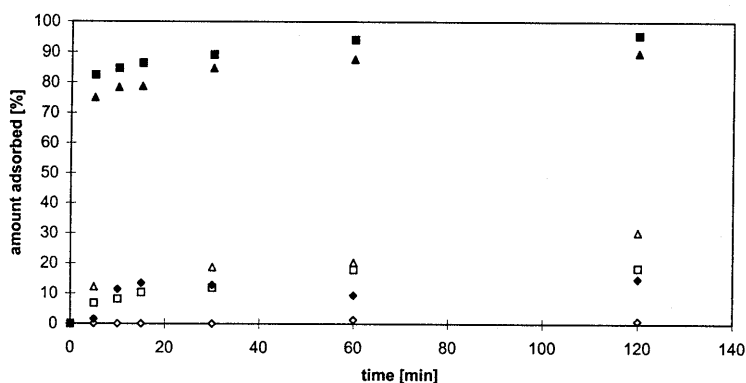


*Figure 4.3  Adsorption behavior of cyclohexene (△,▲), cyclooctene (□,■) and cyclo-dodecene (◇,♦) in dealuminated Beta (closed symbols) and Mordenite/II (open symbols).*

Regarding the Mordenite as adsorbent, it appeared to be impossible for cyclododecene to enter the Mordenite micropores. Dealuminated Beta, on the other hand, shows a slight uptake of cyclododecene to a maximum of about 10 %. Since the pore diameter of Beta is almost

equal to that of Mordenite, we doubt that this adsorption takes place inside the micropores of Beta. Moreover, in such a case a positive trend would be expected due to the (slow) filling of the micropores with cyclododecene. Instead an abrupt maximum is reached within several minutes. This can be indicative for adsorption on the external surface of the zeolite crystal, possibly at pore entrances or in cavities at surface defects. This explanation is in line with the results of Corma *et al.*, who stated that it is impossible for cyclododecene to penetrate the channels of zeolite Beta and proposed an adsorption of cyclododecene in the pockets at the external surface[24]. Furthermore, for zeolite Beta a relatively high external surface area together with a very irregular external surface are reported to result from a dealumination treatment[22]. In line with these results, we propose the cyclododecene to be adsorbed on the external surface only.

Interestingly, in a epoxidation of cyclododecene, using a titanium Mordenite as well as a titanium Beta, both catalysts succeed in converting only very small amounts (< 5%) of cyclododecene to its epoxide (see table 4.5). Since the heterogeneity of these titanium zeolites is ensured (see section 4.4), the measured activity is described to titanium species present on the outer surface. Obviously, the traces of bulk titanium oxide species are unable to catalyze selectively the epoxidation of an alkene. Therefore, the measured activity must be due to isolated titanium species present on the external surface of the zeolite. Cyclododecene is reported to have a comparable activity towards epoxidation as cyclooctene or cyclohexene in peracid type epoxidations[3]. In catalysis by metal activated hydroperoxo complexes only slightly lower activities are measured[25]. As a first estimation, therefore, the measured activity for cyclododecene in relation to the measured activity for cyclooctene can be roughly correlated with the amount of active titanium species on the external surface. Conclusively, a very small but not totally negligible amount of active titanium species is situated on the external surface of the post-synthesis prepared titanium zeolites.

*Table 4.5 Catalytic performance of titanium Mordenite and titanium Beta catalysts in the epoxidation of cyclododecene at 50°C using TBHP as oxidant and acetonitrile as solvent.[a]*

| catalyst | sample | conversion [%] | selectivity [%] | yield [%] |
|---|---|---|---|---|
| Ti-Mordenite | Ti43Mor/II-116 | 5 - 10 | ~20 | <5 |
| Ti-Beta | Ti27Bea-72 | 10 - 20 | ~15 | <5 |

*[a] Conversion of cyclododecene, selectivity to epoxide and yield of epoxide measured after 28 hours.*

A final challenge for the titanium zeolites prepared *via* post-synthesis modification is the comparison of their catalytic activity with the activity of a directly synthesized titanium zeolite, such as TS-1. In this respect, we studied the 1-octene epoxidation using $H_2O_2$ over the best performing titanium Mordenite and titanium Beta and compared these with the activity of TS-1, using EUROTS-1 as a reference material[26]. In table 4.6 the catalytic results are summarized for these three catalysts. Clearly, only the Ti-Beta can compete with the activity of TS-1 in 1-octene epoxidation. We found even a somewhat higher selectivity and yield

towards the epoxide when using Ti-Beta, despite its significant lower titanium content (1.41 wt % titanium in Ti-Beta, 2.3 wt % titanium in TS-1). Initially, their turn-over-numbers are roughly comparable and are in good agreement with the catalytic data reported for the epoxidation of 1-octene in acetonitrile using Ti-Beta[27], and are somewhat lower in comparison with data reported on the epoxidation of 1-hexene using TS-1 or Ti-Beta[24,28]. Surprisingly, the activity of the Ti-Mordenite towards 1-octene epoxidation is almost reaching zero. When compared to the Ti-Beta, however, this difference in activity was already visible from the cyclooctene epoxidation (number between brackets in table 4.6). From the activities of Ti-Mordenite and Ti-Beta for 1-octene and cyclooctene epoxidation, roughly the same trend can be recognized, in which the activation of 1-octene appeared to be significantly more difficult. The difference between Beta and Mordenite can be explained once more with the important effect the crystal size can have on the oxidation activity of a titanium zeolite catalyst[23], respectively 0.01 - 0.1 μm for Beta and 0.1 - 2 μm for Mordenite. This besides a possible small influence of traces of $TiO_2$ present and a slightly less hydrophobic framework of the titanium Mordenite. Adsorption experiments obviously show the diffusion limited adsorption of substrates in larger Mordenite crystals. Consequently, in our opinion the crystal size plays a dominant role in the measured activities. The small difference between Ti-Beta and TS-1 can possibly also be explained in terms of crystal size (TS-1 crystallites ~ 0.15 μm[26]). The findings of Van Der Pol, however, imply that the influence of the crystal size on the catalyst activity starts above crystal sizes of about 0.3 μm, which is much higher than both Ti-Beta and TS-1 crystallites[23]. A more likely reason, therefore, in terms of diffusivity, can be the significant larger micropore diameter of the Beta structure (see figure 1.3, main channels: BEA 0.64 x 0.76 nm *versus* MFI 0.53 x 0.56 nm). This, together with its three dimensional pore structure, will facilitate the diffusion of substrates through the zeolite micropores. These results are in good agreement with the results obtained by Wu *et al.* with their large pore titanium zeolites[29].

*Table 4.6 Catalytic performance of titanium Mordenite, titanium Beta and titanium silicalite catalysts in the epoxidation of 1-octene at 50°C using $H_2O_2$ as oxidant and acetonitrile as solvent[a].*

| sample | catalyst | conversion [%] | selectivity [%] | yield [%] | TOF [mol mol$^{-1}$h$^{-1}$] |
|---|---|---|---|---|---|
| Ti43Mor/II-116 | Ti-Mor | 12 (29) | <5 (38) | <5 (11) | <0.1 (3.6) |
| Ti56Bea-450 | Ti-Beta | 50 (79) | 68 (78) | 34 (62) | 2.7 (35) |
| EUROTS-1 | TS-1 | 56 | 45 | 28 | 4.0 |

*[a] Numbers between brackets refer to the activities in the epoxidation of cyclooctene, under exactly the same conditions. Conversion, selectivity to epoxide and yield measured after 5 hours, TOF measured after 1 hour and corrected for the blank reaction.*

## 4.4  Catalyst heterogeneity

The obtained titanium zeolites, active and selective in epoxidation catalysis, were examined with respect to their heterogeneity. As described in section 4.1, a removal of the heterogeneous catalyst material from the reaction mixture by filtration is the most efficient way to investigate a possible homogeneous contribution to the measured catalytic activity. Since such homogeneous contribution will have to be attributed to leached metal ions or metal complexes in solution, this test will give information about the catalyst stability. Various titanium Mordenites and Betas were investigated by a filtration during reaction conditions. All catalysts tested, showed in the filtrate solution no formation of epoxide at all within detection limits for several hours of reaction after filtration. Two typical examples are given for the epoxidation of cyclooctene using TBHP as well as $H_2O_2$ with the Ti-Mordenite exhibiting the highest activity under the used reaction conditions. In figure 4.4 the unfiltered and filtered epoxidation activity are shown.

The typical curve of the product formation versus time in a batch reactor can be recognized for the unfiltered reaction. The separation of catalyst by a hot filtration was performed after 3 hours. Clearly, the absolutely unchanged level of epoxide can be seen from these figures, indicating the absence of active titanium species in the homogeneous solution. Therefore we conclude that, although the presence of some active, outer surface titanium species is confirmed, titanium zeolites prepared *via* post-synthesis modification are truly heterogeneous epoxidation catalysts using TBHP as well as $H_2O_2$.
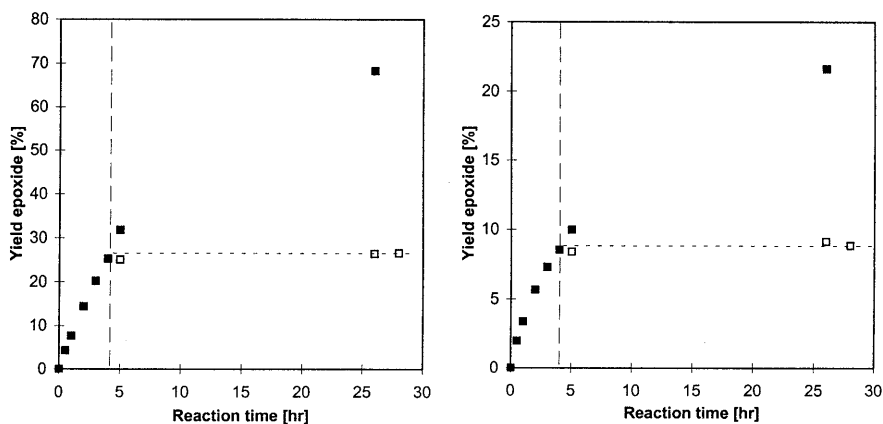


*Figure 4.4   Catalytic performance of the titanium Mordenite Ti43Mor/II-116 versus time in the epoxidation of cyclooctene using TBHP (left) or $H_2O_2$ (right) in acetonitrile at 50°C. Filled symbols represent catalytic data from heterogeneous catalysis (■), whereas open symbols represent catalytic data from the clear filtrate solution  (□), filtration performed after 4 hours reaction.*

## 4.5 Conclusions

In summary, the post-synthesis prepared Ti-Mor and Ti-Beta, are active and selective epoxidation catalysts using TBHP as well as $H_2O_2$. The large crystals of the titanium substituted Mordenite result in a lower activity in epoxidation catalysis, while the Ti-Beta, consisting of relatively small crystals, can easily compete with the activity of TS-1. The hydrophobicity and the presence of traces of $TiO_2$ on the outer surface can explain some slight differences in the performance of the various catalysts, within the Ti-Mordenite series or the Ti-Beta series. The large difference in catalytic activity between Ti-Mor and Ti-Beta can be only explained by the influence of the crystal size, which translates into diffusion problems within the zeolite micropores. This is in agreement with the small difference in activity of Ti-Beta and TS-1, in which the former consists of significantly larger micropores. Although a small contribution of the external surface to the catalytic activity was found, we proved that all titanium zeolites, prepared *via* post-synthesis modification, are truly heterogeneous epoxidation catalysts using TBHP as well as $H_2O_2$ under used the reaction conditions. In summary, the post-synthesis route, which is likely to be applicable for a variety of zeolite structures, is proven to be capable of synthesizing titanium zeolites with catalytic activities which can easily compete with the performance of the direct synthesized TS-1.

## 4.6 Experimental

The titanium Mordenite and Beta zeolites used are extensively described in Chapter 3. The TS-1 sample used is the well known EUROTS-1, as described by Martens *et al.* (reference [26]). The $TiO_2$ used as reference material has the anatase structure (Aldrich, $TiO_2$ 99.9+ %).

Epoxidation catalysis was carried out at 50°C in 5 ml stirred reactor vessels using 50 mg titanium zeolite (dried overnight at 300°C). Typically, 100 µl substrate (~1 mmol cyclohexene, (99 %, Aldrich) or ~0.8 mmol cyclooctene (95 %, Acros)) was added to 4 ml solvent (toluene (p.a., Merck) or acetonitrile (p.a. Merck)) and 1.00 ml of a 1.8 M solution of dry TBHP (originally 70% in $H_2O$, Acros) in the same solvent or to 200 µl $H_2O_2$ solution (35 wt % in $H_2O$, Merck), ca. 2 mmol peroxide. In all cases in a substrate to oxidant ratio between 0.5 and 1 was reached. This slight excess of oxidant ensures reaching theoretical conversions of substrate of 100 %. Samples taken from the reaction mixture were filtered and analyzed by GC analysis using Carlo Erba GC6000 Vega Series equipped with a capillary DB-1 column and a FID. For this purpose all samples contain 25 µl 1,3,5-trimethyl benzene (>98%, Merck) as GC internal standard.

Adsorption experiments were carried out at 50°C in 5 ml stirred reaction vessels using titanium free zeolites. Typically, 25 µl substrate was used in 4 ml 1,3,5-tri-*iso*-propyl benzene (97%, Acros) as solvent and 25 µg 1,3,5-tri-*tert*-butyl benzene (97%, Aldrich) as GC internal standard. The amount of zeolite used was dependent on its micropore volume: a slight excess of total micropore volume over substrate volume was used, resulting typically in 200 µg dealuminated titanium free Beta and 350 µg dealuminated titanium free Mordenite, which were, prior to adsorption, dried overnight at 300°C.

# References

1.   R.A. Sheldon, J. Dakka, Catal. *Today, 19*, (**1994**), p. 215.

2.   U. Romano, A. Esposito, F. Maspero, C. Neri, M.G. Clerici, *Stud. Surf. Sci. Catal., 55*, (**1990**), p. 33.

3.   H.F.W.J. van Breukelen, M.E. Gerritsen, V.M. Ummels, J.S. Broens, J.H.C. van Hooff, *Stud. Surf. Sci. Catal. 105*, (**1997**), p. 1029.

4.   K.A. Jørgensen, *Chem. Rev., 89*, (**1989**), p. 431.

5.   Shell Oil, British Patent 1 249 079, (**1971**).

6.   M. Taramasso, G. Perego, B. Notari, US Pat., 4 410 501, (**1983**).

7.   G. Bellussi, M.S. Rigutto, *Stud. Surf. Sci. Catal., 85*, (**1994**), p. 177.

8.   D.R.C. Huybrechts, P.L. Buskens, P.A. Jacobs, *J. Mol. Catal., 71*, (**1992**), p. 129.

9.   M.G. Clerici, P. Ingallina, *J. Catal., 140*, (**1993**), p. 71.

10.  D. Tantanak, M.A. Vincent, I.A. Hillier, *Chem. Commun.*, (**1998**), p. 1031.

11.  W. Adam, A. Corma, A. Martínez, C.M. Mitchell, T.I. Reddy, M. Renz, A.K. Smerz, *J. Mol. Catal. A., 117*, (**1997**), p. 357.

12.  C.B. Khouw, C.B. Dartt, J.A. Labinger, M.E. Davis, *J. Catal., 149*, (**1994**), p. 195.

13.  M.G. Clerici, *Appl. Catal., 68*, (**1991**), p. 249.

14.  A. Corma, P. Esteve, A. Martínez, *J. Catal., 161*, (**1996**), p. 11.

15.  H.E.B. Lempers, R.A. Sheldon, *Stud. Surf. Sci. Catal., 105*, (**1997**), p. 1061.

16.  F.J. Luna, S.E. Ukawa, M. Wallau, U. Schuchardt, *J. Mol. Catal. A, 117*, (**1997**), p. 405.

17.  R.F. Parton, I.F.J. Vankelecom, D. Tas, K.M.B. Janssen, P.-P. Knops-Gerrits, P.A. Jacobs, *J. Mol. Catal. A., 113*, (**1996**), p. 283.

18.  R.A. Sheldon, *J. Mol. Catal., 7*, (**1980**), p. 107.

19.  P.E.F. Neys, I.F.J. Vankelecom, R.F. Parton, W. Dehaen, G.L.'Abbé, P.A. Jacobs, *J. Mol. Catal. A., 126*, (**1997**), p. L9.

20.  B. Krauhaar-Czarnetzki, W.G.M. Hoogervorst, W.H.J. Stork, *Stud. Surf. Sci. Catal., 84*, (**1994**), p. 1869.

21.  M.J. Haanepen, A.M. Elemans-Mehring, J.H.C. van Hooff, *Appl. Catal. A., 152*, (**1997**), p. 203.

22.  G. Harvey, G. Binder, R, Prins, *Stud. Surf. Sci. Catal. 94*, (**1995**), p. 397.

23.  A.J.H.P. van der Pol, A.J. Verduyn, J.H.C. van Hooff, *Appl. Catal., 92*, (**1992**), p. 111.

24.  A. Corma, M.A. Camblor, P. Esteve, A. Martínez, J. Pérez-Pariente, *J. Catal., 145*, (**1994**), p. 151.

25.  J. Itakura, H. Tanalka, H. Ito, *Bull. Chem. Soc. Japan, 42*, (**1962**), p. 1604.

26.  J.A. Martens *et al.*, *Appl. Catal. A. Gen., 99*, (**1993**), p. 71.

27.  J.C. van der Waal, H. van Bekkum, *J. Mol. Cat. A., 124*, (**1997**), p. 137.

28.  T. Blasco, M.A. Camblor, A. Corma, P. Esteve, J.M. Guil, A. Martínez, J.A. Perdigón-Melón, S. Valencia, *J. Phys. Chem. B., 102*, (**1998**), p. 75.

29.  P. Wu, T. Komatsu, T. Yashima, *Stud. Surf. Sci. Catal. 105*, (**1997**), p. 663.

# 5

## Homogeneous titanium silsesquioxane catalysts§

Using silsesquioxane complexes as model compounds for silica surfaces, this Chapter describes titanium silsesquioxanes as active and selective catalysts in epoxidation reactions. When the titanium siloxy units (Ti-O-Si) result from functionalization of *isolated* silanol groups, the silsesquioxane acts as monodentate ligand. The resulting titanium derivatives effectively catalyze the epoxidation of alkenes with TBHP under mild conditions. The active catalyst, however, is a soluble titanium species that no longer contains siloxy functions. Alternatively, a related homogeneous titanium complex, that contains a *terdentate* silsesquioxane ligand, also effectively catalyzes the same epoxidation reactions. In this case, the catalysis occurs exclusively through titanium siloxy complexes. As such, liquid phase, silica supported titanium epoxidation catalysts are predicted to be accessible and active in many cases but will be truly heterogeneous when stringent conditions are met. Furthermore, with these silsesquioxane complexes, additional evidence is given for the cleavage of a titanium siloxy unit by the peroxide as being essential in the mechanism of titanium epoxidation catalysis.

## 5.1 Introduction

In the current search for non-leaching heterogeneous liquid-phase oxidation catalysts detailed studies of how the catalytically active metal species are bonded to the support are rare. Often, more attention is paid to the performance of the catalyst, rather than to the fundamental question whether the catalyst is truly heterogeneous or not. Forzatti *et al.* showed, for instance, that $MoO_3$ on silica is an effective catalyst for the epoxidation of 1-octene with TBHP but that the activity was due to rapid leaching of the molybdenum from the silica support to give a soluble molybdenum catalyst[1]. Similarly, many other oxides as $WO_3$ and $V_2O_5$ supported on silica or other inert carriers owe their activity to rapid leaching of the metal from the surface to form homogeneous catalysts[2].

---

§ Part of this chapter has already been published in reference [33].

The highly active Shell Ti(IV)/SiO$_2$ epoxidation catalyst[3,4,5], consisting of titanium grafted on a silica support, becomes only truly heterogeneous after a certain time on stream[5]. This partial leaching seems to indicate that the titanium/silica system contains several differently anchored titanium sites. Similar catalysts, therefore, that are currently being reported as the result of grafting silica[6] or MCM-41 mesoporous silica with titanium derivatives[7], or even novel titanosilicates[8], might be only partially heterogeneous when applied in liquid-phase oxidation reactions. As such we have studied epoxidations reactions using titanium silsesquioxanes as model catalysts. In these silsesquioxanes the titanium is incorporated *via* spatially oriented siloxy bonds (Ti-O-Si) which structurally resemble surface sites that have been purportedly identified on silica surfaces.

Silsesquioxane metal complexes are considered as the best chemical models for a variety of silica supported metal catalysts. In addition, porous materials have recently been synthesized from silsesquioxane cage precursors, as well as metal containing polymeric derivatives. In this study silsesquioxanes are used as building blocks for the construction of titanium catalysts that are structurally defined at an molecular level[9]. Currently, several groups are working on titanium silsesquioxanes, partly in order to provide models for titanium substituted zeolites as TS-1[10,11,12], or titanium grafted silica[7]. We provide here the first results of how these model compounds actually perform in oxidation catalysis.

## 5.2 Silsesquioxanes as model compounds

Silsesquioxane (or silasesquioxane) is the general name for a family of molecular spherosilicates with the formula [RSiO$_{3/2}$]$_n$, where R is an inorganic or organic group and n can be between 4 and about 30, but typically 6, 8, 10 or 12. These polyhedral oligosilsesquioxanes (also referred to as POSS) are usually formed by hydrolytic multiple condensation of RSiY$_3$, where Y is a highly reactive substituent such as Cl or an alkoxyde, in an acetone/water mixture to form dimers, quadrimers, etc. The informal names of these molecules consist of the number of RSiO$_{3/2}$-units (referred to as 'T-atoms')[16], followed by the number of hydroxyl groups in the case of incompletely condensed materials or followed by an incorporated metal§. Examples of incompletely condensed materials are shown in figure 5.1, from left to right a hexamer, T$_6$(OH)$_4$, a heptamer, T$_7$(OH)$_3$, and an octamer, T$_8$(OH)$_2$.

Silsesquioxanes were first discovered by Scott in 1946[13], but he was unable to characterize these structures completely, although his assumption for the molecule formula, [CH$_3$SiO$_{3/2}$]$_n$, was correct. Later, Brown and co-workers isolated, beside dimeric and trimeric siloxanes, a tetrameric and hexameric silsesquioxane together with some incompletely condensed silsesquioxanes, as the T$_7$(OH)$_3$ [14].

---

§ The systematic name of, for instance, T$_7$(OH)$_3$ with cyclohexyl groups at the corners is: 1,3,5,7,9,11,14-Hepta-cyclohexyltricyclo[7.3.1$^{5,11}$]heptasiloxane-*endo*-3,7,14-triol.
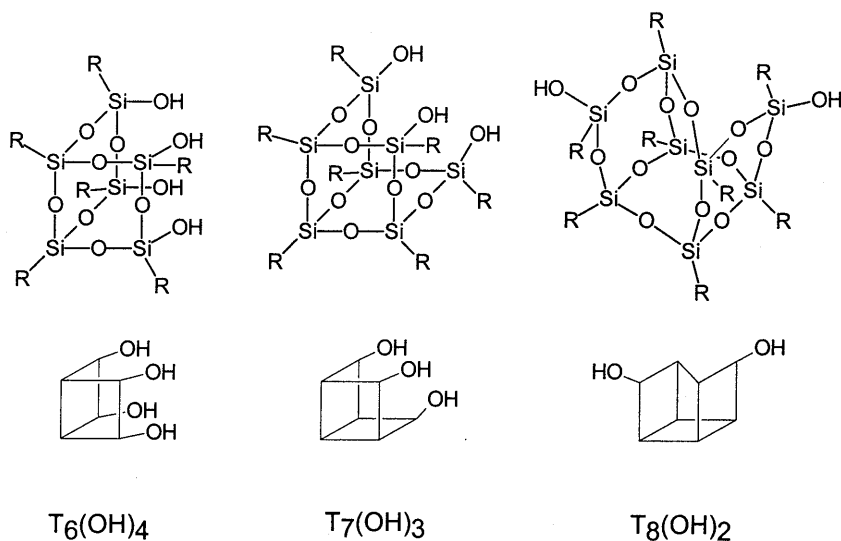
$T_6(OH)_4$ $T_7(OH)_3$ $T_8(OH)_2$

*Figure 5.1 Three examples of incompletely condensed silsesquioxanes, their respective shorthand representations and informal names.*

Silsesquioxanes find their use in various applications[15,16]: for example as precursors for highly defined $SiO_2$ films (used for electrical insulation, anti reflective coatings and optical filters); also in the production of specialized silicon oxy carbide ceramics or in the formation of inorganic/organic hybrid materials. Lately, these structurally well defined materials have been extensively used as model compounds to mimic silica surfaces[17] as well as the grafting properties of such surfaces[18,19] and as ligands for catalytic active metals to model the active sites of heterogeneous catalysts[20,21,22]. The introduction of useful homogeneous models for heterogeneous catalysts offers an opportunity to develop a molecular level understanding of heterogeneous catalysts, which could lead to better strategies for control of catalyst selectivity and stability.

Metal substituted silsesquioxanes result from the reaction of an incompletely condensed silsesquioxane with a metal precursor. An example of such a reaction is the, so-called, corner capping reaction of a silsesquioxane trisilanol with a trifunctional metal reagent (see figure 5.2). The obtained material can be regarded as a mimic for known metal species grafted on silica surfaces[7].

Recently, various titanium silsesquioxane complexes are reported as model compounds for heterogeneous titanium catalysts[20,32]. The application of these soluble, well defined titanium catalysts, gives new insights into the specific factors that determine the activity of known heterogeneous titanium-based oxidation catalysts. In this Chapter, particular interest in the heterogeneity of the titanium catalysts is stressed.
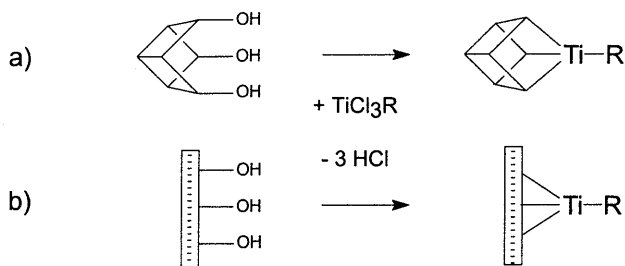
*Figure 5.2 Metal substitution in an incompletely condensed silsesquioxane, $T_7(OH)_3$ (a), as a model for metal grafting on silica surfaces (b). Cycloalkyl groups at the corners of the silsesquioxane complex are omitted for clarity (R = Cp, alkyl, alkoxy).*

## 5.3 Epoxidation catalysis by titanium silsesquioxanes

The silsesquioxane **1** (Figure 5.3) possesses a well-defined structure which includes two reactive, isolated hydroxyl groups that occupy "exo" positions above nearby $Si_4O_4$ rings, that are part of an interdigitated $Si_8O_{11}$ skeleton. Several functionalizations of **1** have already been achieved via clean silanol centered reactions and were in most cases reported to leave the silsesquioxane skeleton intact[23,24,25]. Recently, the construction of a very active, truly heterogeneous catalyst from **1** for Diels-Alder reactions of enones was reported[9].

We found that, in toluene, the silanol groups present in **1** easily react with tetrabenzyltitanium (Figure 5.3, route a), resulting in concomitant formation of toluene and a pale yellow titanium silsesquioxane gel **2a** that occludes the entire volume of the solvent used. When subjected to prolonged centrifugation (20 min. at 900 g), the gel releases toluene till a toluene/silsesquioxane mass ratio of ca. 18 is reached. Upon drying in vacuum, the gel collapses into a powder, yielding **2a** free of solvent in 90% yield. The swelling capacity of the dried titanium silsesquioxane gel **2a** for toluene is reduced to approximately 0.5 ml/g. Related titanium silsesquioxane gels were also prepared from the building block **1** involving reactions with titanium tetrachloride and a base (Figure 5.3, routes b-c). As a result of these synthetic methods, the gels obtained contain enclosed lithium chloride or $[HNEt_3]^+Cl^-$.

The silanol-mediated functionalizations that lead to the formation of the silsesquioxane gels **2** are straightforward and find precedent in the well exploited silanol-centered reactivity of the related silsesquioxane $(C_6H_{11})_7Si_7O_9(OH)_3$[26], abbreviated as $T_7(OH)_3$ in figure 5.1. Powder reflection UV-Vis measurements on **2a-c** show the onset of significant UV absorption only below 350 nm, with a maximum at 220-240 nm. This indicates that in **2a-c** the titanium centers exist as four-coordinated titanium(IV) siloxy units (see also Chapter 3).
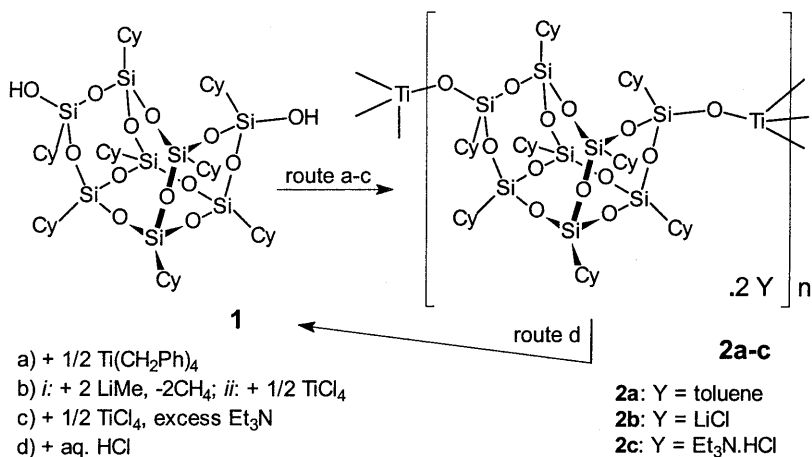
*Figure 5.3 Synthetic routes to the titanium silsesquioxane gels 2a-c (Cy = cyclohexyl).*

Analysis of the titanium silsesquioxane gels **2** by single pulse 79.5 MHz $^{29}$Si MAS NMR provides a method to establish the degree of silanol functionalization during their formation. Upon substitution, the originally lower field resonance of the silanol silicon atoms at δ -58.9 ppm shifts towards the higher field part of the spectrum where the other silsesquioxane silicon resonances are already found (δ -65 to -75 ppm). Comparison of the integrals over the two distinct parts of the spectra indicate that the fraction of remaining silanol units in the titanium gels **2a-c** are, typically, 0.05 (c.f. 0.25 in the silsesquioxane **1**), i.e. ~80% of the silanol units of the starting material **1** have been functionalized in the gel forming process.

Interestingly, when any of the gels **2**, is subjected to acid hydrolysis followed by organic work-up, the silsesquioxane **1** can be recovered in near to quantitative yield (Figure 5.3, route d). From this observation, it can be concluded that the silanol deprotonations involved in the formation of the gels **2** do not induce any change in the silsesquioxane framework.

The titanium silsesquioxane gels **2** efficiently catalyze the epoxidation of alkenes under mild conditions (See Table 5.1). In a typical reaction equimolar amounts of alkene and *tert.*-butyl hydroperoxide (TBHP) were reacted over the catalyst (~ 1 mol% Ti with respect to the substrates) in hexane at 50 °C. Though for the reactions studied, the silsesquioxane gels **2** were reasonable to good catalysts, attempts to filter the catalyst off during epoxidation, and thus to stop the reaction (as reported in section 4.4 for heterogeneous titanium catalysts), met with complications which were indicative of severe leaching of catalytically active species from the titanium gels. Interestingly, NMR studies showed that during epoxidation, rapid hydrolysis of the gel by TBHP occurs resulting in the quantitative reformation of the silsesquioxane **1** and concomitant formation of non-siloxy titanium species that are catalytically active.

*Table 5.1   Epoxidation of alkenes with TBHP catalyzed by titanium silsesquioxanes in hexane as solvent at 50°C with a substrate to epoxide ratio of 1.*

| catalyst | alkene | t (h) | conversion of substrate [%] | selectivity in alkene [%] |
|---|---|---|---|---|
| **2a** | 1-octene | 24 | 15 | 60 |
| **2b** | 1-octene | 24 | 25 | 60 |
| **3** | 1-octene | 24 | 80 | 80 |
| **2a** | cyclooctene | 4 | 50 | >95 |
| **2b** | cyclooctene | 4 | 90 | >95 |
| **3** | cyclooctene | 3 | 90 | >95 |
| **2a** | norbornylene | 4 | 60 | >95 |
| **2b** | norbornylene | 3.5 | 90 | >95 |
| **3** | norbornylene | 3 | 90 | >95 |

An essential feature of several of the proposed mechanisms of alkene epoxidation by titanium silicalites involves hydrolysis of a titanium siloxy function in a tetra-coordinated active site[5,10,27,28]. In figure 5.4, this is schematically presented. For the titanium gel **2**, such a hydrolysis step would lead to rapid degeneration of the material since the titanium siloxy units (Ti-O-Si) result here from functionalization of isolated silanol groups, the silsesquioxane being a bifunctional monodentate ligand (Figure 5.4, route i). This would therefore imply that silsesquioxane titanium species where the silsesquioxane can bind to titanium as a multidentate ligand are more robust epoxidation catalysts (Figure 5.4, route ii).

In order to verify this hypothesis, we have tested the activity of the known silsesquioxane complex **3**, also referred to as $T_7O_3TiCp$, that has a terdentate silsesquioxane ligand[24,29], for similar alkene epoxidations (Table 5.1). A schematic formation of this complex is depicted in figure 5.2a, with R = Cp. Interestingly, complex **3** turned out to be an epoxidation catalyst that is effective at a low concentration and which selectively produces alkene oxides in high yield with good peroxide economy (typical turn-over-frequencies reached are 280 mole cyclooctene converted per mole titanium per hour, see also Chapter 6). Especially, the somewhat difficult epoxidation of 1-octene is catalyzed more effectively by **3**. The same catalytic performance was found for **3** that was repeatedly recrystallized from toluene/acetonitrile, which excludes the possibility that undetected trace impurities in **3** are responsible for the observed catalytic activity. It is likely that due to multidentate silsesquioxane coordination, **3** does not hydrolyze irreversible during epoxidation reactions (Figure 5.4, route ii); in fact, the complex is even stable in 1 M aq. HCl! Under catalytic conditions, complex **3** can be easily monitored by $^1$H and $^{13}$C NMR, it's cyclopentadienyl unit providing a convenient and sensitive NMR probe. From these NMR experiments could be concluded that after ~100 turnovers, complex **3** is still the only observable silsesquioxane species present and that it does not lose the cyclopentadienyl ligand during epoxidation catalysis. These findings are consistent with a mechanism for alkene epoxidation in which

reversible hydrolysis of a titanium siloxy function occurs (see figure 4.2 and 5.4). In our opinion, these observations support the mechanism of heterogeneous alkene epoxidation by titanium silicalites proposed by Clerici and Sheldon[5,10,27,28].
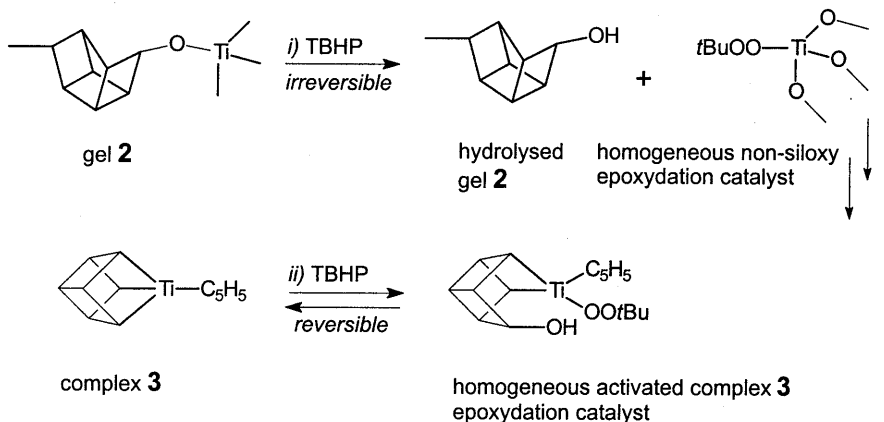


Figure 5.4. Schematic representation of the reaction of titanium silsesquioxane complexes with TBHP, rendering species capable of alkene epoxidation: i) the irreversible hydrolysis of the silsesquioxane as a bifunctional monodentate ligand in gel 2 and ii) the reversible hydrolysis of the terdentate silsesquioxane complex 3. The lines in the cube-type ligands represent Si-O-Si, the cyclohexyl units at the corners are omitted for clarity.

Monitoring the conversion of the homogeneous catalyst for several hours reveals again the outstanding stability of the homogeneous titanium silsesquioxane complex 3. A plot of 1/[alkene] - 1/[alkene]$_{t=0}$ versus time, assuming a simplified second order kinetics, shows a perfect straight line (see figure 5.5).
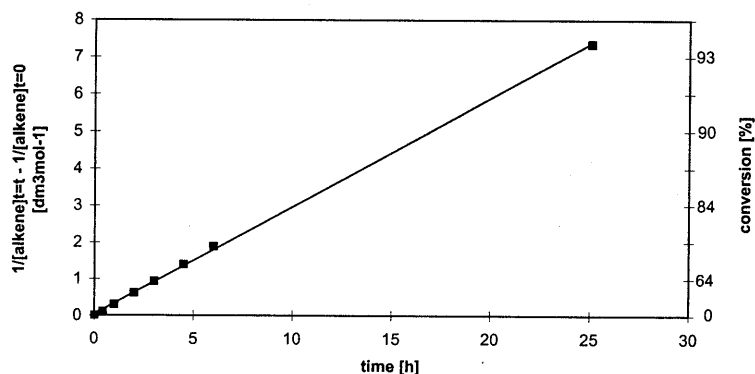


Figure 5.5 Conversion and 1/[alkene]$_{t=t}$ - 1/[alkene]$_{t=0}$ versus time of the $T_7O_3TiCp$ (complex 3) catalyzed epoxidation of cyclooctene with TBHP as oxidant in hexane at 50°C.

## 5.4 Conclusions

In conclusion, new titanium-containing silsesquioxane gels effectively catalyze the epoxidation of alkenes using TBHP under mild conditions. The active catalyst, however, is a soluble, non-siloxy titanium species. Alternatively, the titanium complex **3**, that contains a *terdentate* silsesquioxane ligand, has a high performance in the same epoxidation reactions, in which selectivities over 95 % are obtained with conversions to 90 % within a few hours at 50°C. Moreover, this homogeneous titanium catalyst exhibits an excellent stability during epoxidation catalysis. This stability clearly demonstrates the reversibility of the cleavage of the titanium siloxy bond upon coordination of the peroxide. In this case, the catalysis occurs exclusively through titanium siloxy complexes. As such, liquid phase, silica-supported titanium epoxidation catalysts are predicted to be accessible and active in many cases but will be truly heterogeneous only when stringent conditions are met.

## 5.5 Experimental

Unless otherwise stated, all reactions were performed under an atmosphere of dry Argon using standard Schlenk techniques, reference [30]. Solvents were stored over sodium benzophenone ketyl and distilled prior to use. $^1$H NMR and $^{13}$C NMR spectra were recorded in CDCl$_3$ on a Varian Gemini (300 MHz) and a Bruker AM 400 (400 MHz) with 16 scans for $^1$H NMR and at least 256 scans for $^{13}$C NMR. Spectra were baseline corrected and manually reintegrated. $^{29}$Si MAS NMR spectra were recorded on a Bruker MSL 400 NMR spectrometer (79.5 MHz), operating at a field of 9.4 T. The powder samples were placed in a 7 mm probe and the magic angle spinning rate was 3.5 kHz. Spectra were obtained using 5.5 μs pulses with a delay of 10 s. The chemical shifts were measured with tetrametylsilane as external reference.

The preparation of titanium silsesquioxane gels was performed using three different routes:
*a)* Reaction with tetrabenzyltitanium. To a solution of silsesquioxane **1** (2.87 g, 2.61 mmol) in 150 ml of toluene was added tetrabenzyltitanium (0.58 g, 1.41 mmol) in 50 ml toluene in 5 minutes. Upon addition, the red color of the titanium reagent disappeared and a pale yellow gel resulted. After standing over night, the gel was centrifuged (20 min. at 900 g) and the separated toluene decanted. Five more cycles were carried out involving mixing of the gel with warm (ca. 40°C) toluene (30 ml), centrifugation and decantation, leaving 52.63 g of swollen gel. Subsequent removal of the solvent in *vacuo*, left 2.63 g (90 %) dry **2** as a pale yellow powder.
*b)* Reaction with methyl lithium followed by transmetallation with titanium tetrachloride. To a solution of silsesquioxane **1** (1.26 g, 1.15 mmol) in 100 ml of toluene was added methyl lithium [1.5 ml of a 1.6 M solution in Et$_2$O (2.4 mmol)]. Within a few minutes, the initially vigorous, gas evolution ceased and a colorless gel resulted to with TiCl$_4$ [2.3 ml of a freshly prepared 0.26 M solution in toluene (0.60 mmol)] was subsequently added. The resulting thick, colorless gel was stirred over night followed by removal of the solvent in *vacuo*, leaving **2**, together with occluded LiCl, in quantitative yield, as a white powder.
*c)* Direct reaction with titanium tetrachloride. To a solution of silsesquioxane **1** (0.51 g, 0.46 mmol) in 100 ml of toluene, was added TiCl$_4$ [0.90 ml of a freshly prepared 0.26 M solution in toluene (0.23 mmol)]. To the resulting pale yellow, turbid solution was added 0.5 ml (3.6 mmol) of NEt$_3$, causing the formation of a colorless gel that was stirred over night. Removal of the solvent in *vacuo*, gave **2**, together with occluded [HNEt$_3$]$^+$Cl$^-$, as a white powder in quantitative yield.

The acid hydrolysis of the titanium silsesquioxane gels was performed with a dried sample of **2** (1.2 g) which was added to 100 ml of an aqueous HCl solution (~2 M), stirred for 15 min and subsequently extracted with 3 times 100 ml $Et_2O$. The combined $Et_2O$ extracts were dried over $MgSO_4 \cdot H_2O$, followed by removal of the solvent in *vacuo*, leaving 1.1 g (90 %) of **1** that was pure by $^1H$ and $^{13}C$ NMR.

Epoxidation catalysis was performed using equimolar amounts (1.6 mmol) of alkene and dried *tert.*-butyl hydrogen peroxide  (originally 70 % in $H_2O$, Acros) in 1.0 ml hexane (p.a., Merck). Reactions were performed at 50°C in sealed vials that were magnetically stirred using 25 mg of catalyst. Conversions and yields were determined by $^1H$ NMR using an internal standard (*tert.*-butylbenzene). For determining the kinetic plot in figure 5.5, the reaction was performed using equimolar amounts (7.2 mmol) of substrate and dried TBHP in 4.0 ml hexane (substrate to titanium ratio of 1096) in sealed vials that were magnetically stirred at 50°C.

# References

1.  P. Forzatti, F. Trifiro, React. *Kinet. Catal. Lett., 1,* **(1974)**, p. 367.
2.  F. Mashio, S. Kato, *Mem. Fac. Ind. Arts, Kyoto Tech. Univ., Sci. Technol., 16,* **(1967)**, p. 79, [Chem. Abstr., 69 : 68762e].
3.  H. P. Wulff, US Pat. 3 923 843, **(1975)** [Chem. Abstr., 84 : 89977d].
4.  H. P. Wulff and F. Wattimena, US Pat. 4 021 454, **(1977)** [Chem. Abstr., 87 : 22393d].
5.  R. A. Sheldon, *J. Mol. Catal., 7,* **(1980)**, p. 107
6.  R. Hutter, D. C. M. Dutoit, T. Mallat, M. Schneider and A. Baiker, *J. Chem. Soc., Chem. Commun.,* **(1995)**, p. 163.
7.  T. Maschmeyer, F. Rey, G. Sankar and J. M. Thomas, *Nature, 378,* **(1995)**, p. 159.
8.  M. A. Roberts, G. Sankar, J. M. Thomas, R. H. Jones, H. Du, J. Chen, W. Pang and R. Xu, *Nature, 381,* **(1996)**, p. 401.
9.  H. C. L. Abbenhuis, H. W. G. Van Herwijnen and R. A. Van Santen, *Chem. Commun.,* **(1996)**, p. 1941.
10. M. G. Clerici and P. Ingallina, J. Catal., 140, **(1993)**, p. 71.
11. A. Corma, M.A. Camblor, P. Esteve, A. Martínez, J. Pérez-Pariente, *J. Catal., 145,* **(1994)**, p. 151.
12. O. Franke, J. Rathousky, G. Schultz-Ekloff, J. Stárek, A. Zukal, *Stud. Surf. Sci. Catal., 84,* **(1994)**, p. 77.
13. D.W. Scott, *J. Am. Chem. Soc., 68,* **(1946)**, p. 356.
14. J.F. Brown jr., L.H. Vogt jr, *J. Am. Chem. Soc., 87,* **(1965)**, p. 4313.
15. P.G. Harrison, *J. Org. Met. Chem., 542,* **(1997)**, p. 141.
16. R.H. Baney, M. Itoh, A. Sakakibara, T. Suzuki, *Chem. Rev., 95,* **(1995)**, p. 1409.
17. F.J. Feher, D.A. Newman, J.F. Walzer, *J. Am. Chem. Soc., 111,* **(1989)**, p. 1741.
18. F.J. Feher, T.A. Budzichowski, *Polyhedron, 14,* **(1995)**, p. 3239.
19. I.E. Buys, T.W. Hambley, D.J. Houlton, T. Maschmeyer, A.F. Masters, A.K. Smith, *J. Mol. Catal., 86,* **(1994)**, p. 309.
20. T. Maschmeyer, M.C. Klunduk, C.M. Martin, D.S. Shephard, J.M. Thomas, B.F.G. Johnson, *Chem. Commun.,* **(1997)**, p. 1874.
21. K. Wada, M. Nakashita, A. Yamamoto, T. Mitsudo, *Chem. Commun.,* **(1998)**, p. 133.
22. J.-C. Liu, *Chem. Commun.,* (1996), p. 1109.
23. J. F. Walzer, D. A. Newman and F. J. Feher, *J. Am. Chem. Soc., 111,* **(1989)**, p. 1741.
24. F. J. Feher, T. A. Budzichowski, K. Rahimian and J. W. Ziller, *J. Am. Chem. Soc., 114,* **(1992)**, p. 3859.
25. T. S. Haddad and J. D. Lichtenhan, *J. Inorg. Organomet. Polymers, 5,* **(1995)**, p. 237.
26. F. J. Feher, and T. A. Budzichowski, *Polyhedron, 14,* **(1995)**, p. 3239.
27. M. G. Clerici, *Appl. Catal., 68,* **(1991)**, p. 249.
28. R. A. Sheldon and J. A. Van Doorn, *J. Catal., 31,* **(1973)**, p. 427.
29. I. E. Buys, T. W. Hambley, D. J. Houlton, T. Maschmeyer, A. F. Masters and A. K. Smith, *J. Mol. Catal.,* 86, (1994), p. 309.
30. D.F. Schriver, M.A. Drezdzon, The Manipulation of Air-Sensitive Compounds, 2$^{nd}$ edition, Wiley-Interscience, New York, **(1986)**.
32. M. Crocker, R.H.M. Herold, A.G. Orpen, *Chem. Commun.,* **(1997)**, p. 2411.
33. H.C.L. Abbenhuis, S. Krijnen, R.A. van Santen, *Chem.Commun.,* **(1997)**, p. 331.

# 6

# Heterogeneous titanium silsesquioxane catalysts[§]

The active and robust homogeneous titanium silsesquioxane catalyst, as reported in the previous Chapter, has been successfully heterogenized in MCM-41 mesoporous materials *via* straightforward adsorption. The resulting self assembled materials provide active, truly heterogeneous and recyclable catalysts for liquid phase alkene epoxidation. Tailoring the polarity of the solid catalyst with a silylation procedure, results in heterogeneous catalysts independent on the nature of the MCM-41 host. The remarkable strong but unaltered adsorption of the silsesquioxane complex inside the MCM-41 channel is demonstrated by Raman spectroscopy. These results indicate a specific orientation of the complex in its MCM-41 host, in which the active titanium site is guaranteed to remain accessible for substrate and oxidant in heterogeneous oxidation catalysis, in agreement with the high catalytic activity of the heterogenized complex.

## 6.1 Introduction

The heterogenization of homogeneous catalysts is an important topic in liquid phase oxidation catalysis[1]. Various different ways to heterogenize metal catalysts have been reviewed briefly in section 1.6. Clearly, a distinction can be made between the heterogenization of a single metal center (like in the case of isomorphous substitution) and the heterogenization of a complete homogeneous metal complex. The advantage of the latter over isomorphous substitution of a metal into, for instance, a zeolite host (as reported in Chapter 3), is the aforehand known environment of the metal center. When dealing with stable ligands around the metal center, which are unaffected by the heterogenization procedure, the heterogenized catalyst is unchanged at an molecular level. As such, a well defined and highly active homogeneous complex can be transferred successfully into a heterogeneous support.

---

[§] Part of this Chapter has already been published in reference [14].

The use of the titanium(IV) silsesquioxane complex **3**, $[(c\text{-}C_6H_{11})_7Si_7O_{12}]Ti(\eta^5\text{-}C_5H_5)$ (see figure 6.1),[2] is described in chapter 5 as an active and robust homogeneous catalyst for alkene epoxidation.[3] Under the catalytic conditions employed, **3** is stable and consequently does not leach titanium which makes it an attractive candidate for heterogenization. In this chapter the successful immobilization of **3** in an MCM-41 molecular sieve[4] is reported, for which we especially exploit its strong adsorption in the MCM-41 channel.
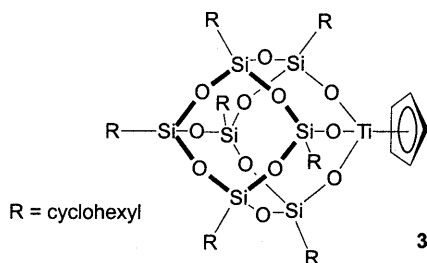


*Figure 6.1 The titanium(IV) silsesquioxane complex **3**, $[(c\text{-}C_6H_{11})_7Si_7O_{12}]Ti(\eta^5\text{-}C_5H_5)$.*

## 6.2 Phase immobilization

The adsorption of the silsesquioxane **3** from hexane into MCM-41 molecular sieves proceeds fast and can be easily followed by solution UV-Vis. As shown in figure 6.2, two typical bands arise from complex **3** in solution: an intense 216 nm band and a broad band around 310 nm. The first band is assigned to tetrahedrally coordinated titanium (as discussed also in section 3.2), whereas the second band corresponds to the cyclopentadienyl chromophore. Both bands rapidly decrease upon adding dry MCM-41 material to a solution of **3**, as can be seen from figure 6.2.
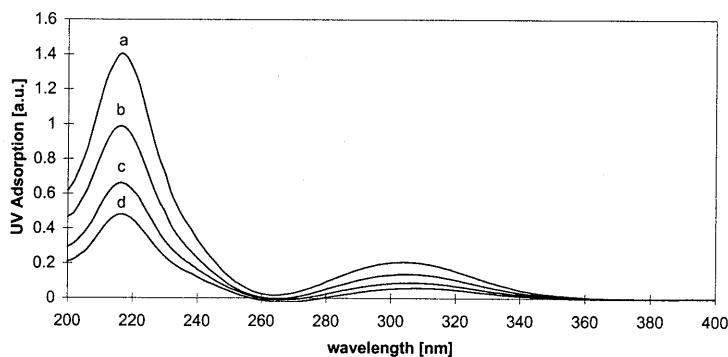


*Figure 6.2 UV-Vis spectroscopy on the impregnation solution of complex **3** during adsorption in an all-silica MCM-41, after 0 (a), 1 (b), 10 (c) and 30 (d) minutes.*

Throughout this work, MCM-41 materials with Si/Al ratios of 42, 125 and ∞ were investigated. Because of the fast and complete adsorption of **3** into the MCM-41 materials, the loading of the catalyst can be tuned easily by varying the total amount of **3** in solution. The maximum loading for the MCM-41 host with a Si/Al ratio of 42 was found to be 97 mg titanium(IV) silsesquioxane / g MCM-41 (i.e. 4.3 mg Ti / g MCM-41). FT-IR (KBr) analysis of MCM-41 materials with a maximum loading of **3** showed, superimposed on the vibration bands characteristic for MCM-41, bands typical for the isolated titanium silsesquioxane **3**: cyclohexyl C-H vibration (2854, 2928 $cm^{-1}$), together with a characteristic H-C-H scissors vibration (1449 $cm^{-1}$).
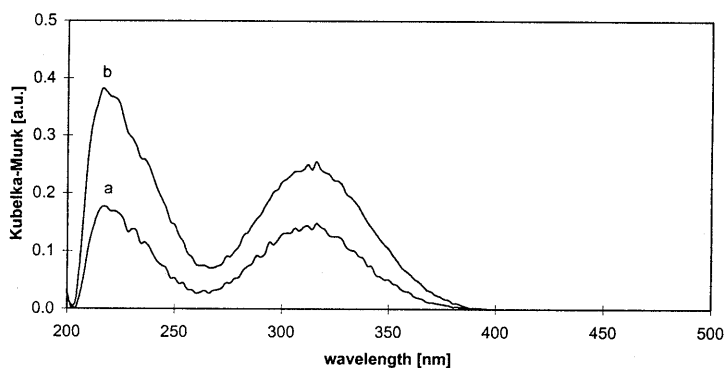


*Figure 6.3  Diffuse Reflectance UV-Vis spectroscopy on complex 3 (a) and on complex 3 immobilized in an all-silica MCM-41 molecular sieve (b).*

After adsorption in the MCM-41 host, diffuse reflectance UV-Vis measurements on the heterogenized complex, still reveals the typical spectrum of the titanium silsesquioxane **3**: a sharp band at 216 nm and a broad band around 310 nm (see figure 6.3). This spectrum is perfectly overlapping with the diffuse reflectance spectrum of the solid complex **3**. Together with the result of the FT-IR measurements, this is the first indication that the complex is adsorbed unaltered inside the MCM-41 host material. A schematic impression of the silsesquioxane complex being adsorbed unaltered in an MCM-41 pore is given in figure 6.4.
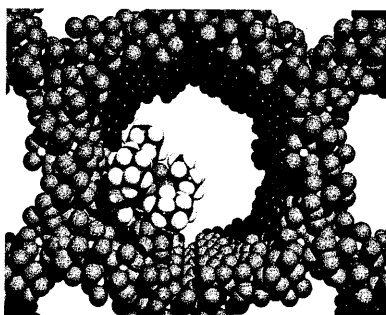


*Figure 6.4  Schematic representation of an immobilized complex 3 inside an MCM-41 molecular sieve (pore diameter ca. 2.9 nm).*

## 6.3 Epoxidation catalysis

The titanium silsesquioxane containing materials efficiently catalyze (*i.e.* > 95 % selectivity) the epoxidation of cyclooctene under mild conditions with *tert.*-butyl hydroperoxide as the oxidant (See Table 6.1 and Figure 6.5). In chapter 5, more data are provided on the scope of **3** in alkene epoxidation. Especially, with the all-silica MCM-41 material, which is essentially free of aluminum, high catalytic activity and heterogeneity was obtained. The catalytic data show that the presence of aluminum in the MCM-41 reduces the activity of the catalyst (Table 6.1, entry 2-7).[6] Moreover, under epoxidizing conditions, the immobilized silsesquioxane **3** quantitatively leaches from its aluminum containing mesoporous host, thus rendering the catalysis *homogeneous*. This result, once more, proves that the complex **3** is adsorbed unaltered inside the channels of the MCM-41 molecular sieve.

*Table 6.1 Activity of [(c-C₆H₁₁)₇Si₇O₁₂]Ti(η⁵-C₅H₅) (3) immobilized in mesoporous MCM-41 or silica for the epoxidation of cyclooctene at 50°C in hexane.*

| Entry | [Ti] Catalyst (Si/Al-ratio)[a] | silylated samples[b] | heterogeneous?[c] | conversion[d] [%] | TOF[e] [mol mol⁻¹h⁻¹] |
|-------|-------------------------------|---------------------|-------------------|-------------------|----------------------|
| 1 | **3** | - | - | 95 | 287 |
| 2 | [Ti] MCM (∞) | - | **yes** | 84 | 202 |
| 3 | [Ti] MCM (∞) | silylated | **yes** | 77 | 184 |
| 4 | [Ti] MCM (125) | - | no | f | - |
| 5 | [Ti] MCM (125) | silylated | **yes** | 65 | 160 |
| 6 | [Ti] MCM (42) | - | no | f | - |
| 7 | [Ti] MCM (42) | silylated | **yes** | 55 | 178 |
| 8 | [Ti] silica | - | no | f | - |
| 9 | [Ti] silica | silylated | no | f | - |
| 10 | MCM (∞) | - | - | 10 | - |
| 11 | MCM (125) | - | - | 21 | - |
| 12 | MCM (42) | - | - | 14 | - |

*[a] Catalysts with the prefix [Ti] contain complex 3 (1.2 mg Ti / g MCM-41), otherwise reference is being made to a blank experiment without 3.*
*[b] Using SiCl₂Ph₂ as the silylating agent.*
*[c] Catalysts are defined as heterogeneous when upon direct filtration, at ca. 30% conversion, no subsequent conversion takes place in the filtrate.*
*[d] Determined after 22 h, all selectivities towards the epoxide > 95 %.*
*[e] Initial turn-over frequency as determined after 2 h.*
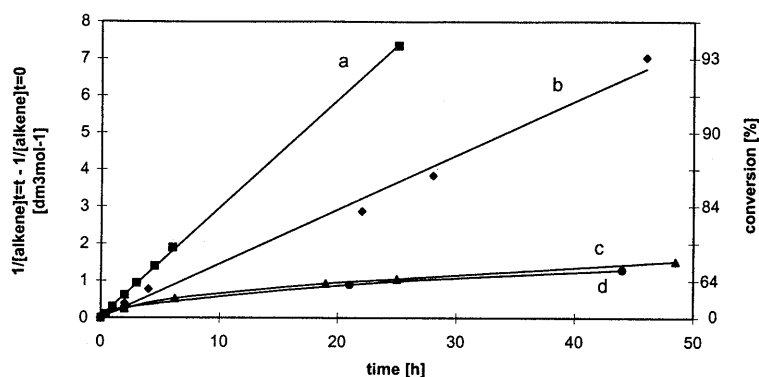*[f] Since the reaction was homogeneous the conversion was not relevant.*

*Figure 6.5 Conversion (right axis) and 1/[alkene]$_{t=t}$ - 1/[alkene]$_{t=0}$ (left axis) versus time for the heterogeneous catalysts: [Ti]MCM($\infty$) (b), [Ti]MCM(42) (c) and [Ti]MCM(125) (d) in comparison with the homogeneous catalyst 3 (a). All reactions were performed using equimolar amounts of alkene and dried tert-butyl hydroperoxide in hexane at 50 °C.*

Fortunately, the undesired leaching of the aluminum containing catalysts can be stopped completely when the MCM-41 molecular sieves are treated with the silylating agent $SiCl_2Ph_2$ prior to catalysis (Table 1, entry 3,5,7).[7] The unresolved phenyl groups of the (-O-)$_2SiPh_2$ functions are found in $^{13}C$ MAS NMR (100 MHz) at $\delta$ 127.3 and 134.3 ppm. BET analysis on an impregnated MCM-41 sample clearly showed a decrease in both pore diameter and mesopore volume upon adsorption of the silsesquioxane 3 as well as an increased surface area due to the additional surface of 3 (See Table 6.2). The effect of the silylation is also expressed in both a reduced pore diameter and a reduced mesopore volume.

The aluminum containing heterogeneous catalysts, obtained by the silylation procedure, were found to deactivate in the course of alkene epoxidation (see figure 6.5). Interestingly, the all-silica based catalyst showed no deactivation at all, in either silylated or non silylated form, as was also found for truly homogeneous reactions using the *free* complex 3 only. The kinetic data obtained for heterogeneous catalysis employing [Ti] MCM-41 ($\infty$) and for homogeneous catalysis by the complex 3, can be described by overall second order rate equations (see figure 6.5). As mentioned above, with the all-silica MCM-41 material, *heterogeneous* catalysis does not require an additional silylation procedure as with the aluminum containing MCM-41 materials. It is noteworthy that a comparison between an all-silica MCM-41 catalyst, and its silylated analogue, showed that the silylation procedure has a negligible influence on the catalytic performance (Table 6.1, entry 2,3). All heterogeneous catalysts can be easily recovered by filtration; the all-silica catalyst can even be re-used for at least three times without an apparent loss of activity.

The effect of silylation was further investigated using a smaller silylation agent. When $SiCl_2(CH_3)_2$ is used, again a heterogeneous, non leaching catalyst is obtained, with a comparable activity to the $SiCl_2Ph_2$ silylated material. This result indicates that the

hydrophobicity of the framework determines whether the catalyst will leach its active complex **3** rather than that **3** is physically trapped by the silylating agent.

*Table 6.2  BET results for the all-silica MCM-41 series employed in catalysis.[1]*

| Entry[a] | Catalyst[b] | surface area[c] [m²g⁻¹] | modus pore diameter[c] [nm] | micropore volume[c] [cm³g⁻¹] | mesopore volume[d] [cm³g⁻¹] |
|---|---|---|---|---|---|
| 10 | MCM (∞) | 552 | 2.9 | 0.20 | 0.15 |
| 2 | [Ti] MCM (∞) | 610 | 2.7 | 0.20 | 0.10 |
| 3 | [Ti] MCM (∞) silylated | 540 | 2.3 | 0.16 | 0.05 |

*[a] Entries as in table 6.1. [b] The [Ti] MCM-41 samples were loaded with 25 mg of **3** / g MCM-41. [c] Data have a maximum error of 5 %. [d] Maximum error is 20 %. The total pore volume of the parent MCM-41 sample (entry **10**) is 0.62 ml/g.*

Clearly, the framework polarity of the MCM-41 will increase significantly when silicon is replaced for aluminum. The influence of the polarity of the framework on the adsorption of substrates was investigated by monitoring the competitive adsorption of 1,2-epoxyoctane and 1-octene. In figure 6.6 the absorption ratio is plotted against time. With the aluminum containing MCM-41 molecular sieves, the 1,2-epoxyoctane/1-octene ratio decreased within a few minutes to 0, whereas when an aluminum free MCM-41 is used, this ratio leveled off around 0.2. This demonstrates that the affinity of the hydrophilic aluminum containing MCM-41 for the more polar epoxide is higher than that of the relatively hydrophobic all-silica MCM-41 framework.
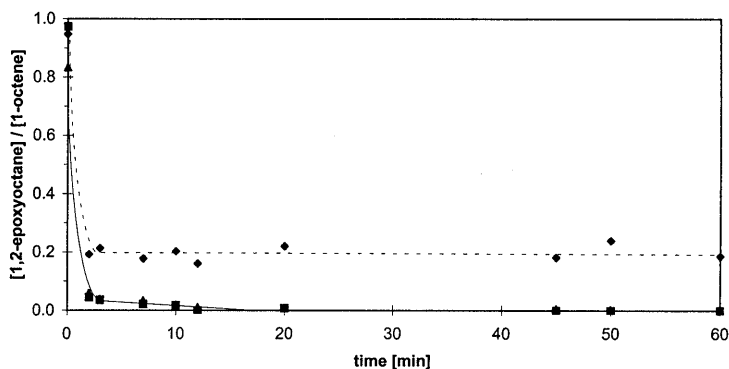


*Figure 6.6  Competitive adsorption of 1,2-epoxyoctane and 1-octene: ratio [1,2-epoxy-octane] / [1-octene] versus time using all-silica MCM-41 (entry 10, ♦), MCM(125) (entry 11, ▲), and MCM(42) (entry 12, ■) as adsorbent, in hexane as solvent at room temperature.*

---

[1] The pore volume and surface area of this MCM-41 sample are somewhat lower than generally reported for MCM-41 materials. The heterogenization of complex **3** is, however, successfully reproduced on several other MCM-41 samples, exhibiting higher surface areas and pore volumes (e.g. respectively 724 m²/g and ca. 1 ml/g).

The more hydrophobic behavior of the all-silica MCM-41 material is supported by thermogravimetric analysis (TGA), which indicates that both the water content and the dehydration temperature for the all-silica MCM-41 are much lower compared to the aluminum containing MCM-41 materials (entry 11-13). In table 6.3 these TGA data are summarized.

*Table 6.3  TGA data for the different MCM-41 host materials (entries as in table 6.1).*

| Entry | parent MCM-41 material | water content[a] | dehydration temperature[b] | amount of non isolated silanols[c] |
|-------|------------------------|------------------|----------------------------|-------------------------------------|
|       |                        | [wt %] | [°C] | [wt %] |
| 10 | MCM ($\infty$) | 1.3 | 49 | 1.0 |
| 11 | MCM (125) | 4.8 | 60 | 1.3 |
| 12 | MCM (42) | 5.5 | 61 | 1.3 |
| 13 | MCM (15) | 4.7 | 68 | 1.2 |

*[a] Defined as the weight loss between 25°C and 150°C.*
*[b] Defined as the maximum in the derivative of the desorption curve.*
*[c] Defined as the weight loss between 150°C and 700°C.*

The higher polarity of the aluminum containing MCM-41 materials is likely to induce leaching.[8] Because of the strong adsorption of the polar organics present during catalysis the apolar silsesquioxane will be desorbed from the relatively hydrophilic aluminum containing MCM-41 hosts. In contrast, the degree of apolarity of an all-silica MCM-41 is ideal for both strong adsorption of the catalyst, leading to a heterogeneous system, and the diffusion of the organics through the MCM-41 channel. In contrast to physically enclosed systems, this will lead to a *self assembled heterogeneous catalyst* that is not prone to neither leaching nor to deactivation.

The use of MCM-41 type materials proved to be essential for successful catalyst immobilization. This notwithstanding the finding that a conventional silica (i.e. Silica Grace SG360, total pore volume ca. 0.9 - 1.0 $cm^3g^{-1}$, surface area about 600 $m^2g^{-1}$) also adsorbs silsesquioxane **3**, as could be confirmed by UV-Vis spectroscopy. During catalytic testing, however, this material undergoes a significant degree of leaching (See table 6.1). From this finding we conclude that a silica with channel type pores such as an MCM-41 material is essential for an irreversible adsorption of the silsesquioxane complex.

## 6.4 Further spectroscopic investigations

Considering the different MCM-41 materials suitable as host for complex **3**, an important difference can be recognized between the all-silica MCM-41 or an aluminum containing MCM-41 as adsorbent. As demonstrated above, applying an aluminum containing MCM-41 material results in an instant leaching of **3** out the molecular sieve when employed in oxidation catalysis (see table 6.1). In addition, the adsorption of the silsesquioxane complex from solution is significantly faster when an aluminum containing MCM-41 host is used (see figure 6.7). Important to mention, in this context, are the comparable crystal size distributions of the three different parent MCM-41 samples used (entry 10,11 and 12).
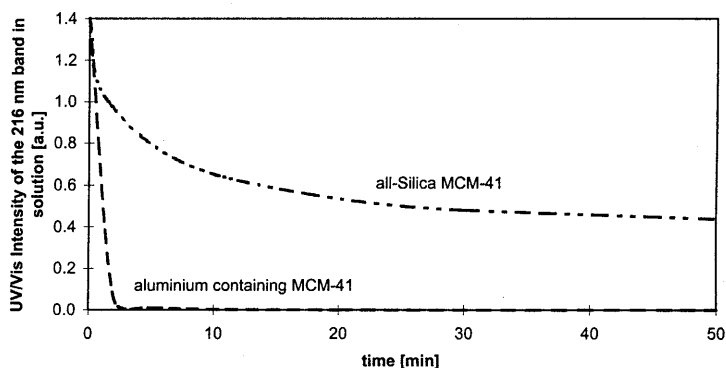


*Figure 6.7  Adsorption behavior of 3 in an all-silica MCM-41 and an aluminum containing MCM-41 host.*

The fact that the minimum diameter of the spherical complex **3** roughly equals half the diameter of the MCM-41 channel, implies that these complexes can hardly pass each other, once being adsorbed inside the MCM-41 channel (see figure 6.5). Although, perhaps somewhat counterintuitive, the slower rate of adsorption of **3** in all-silica MCM-41 material implies a much stronger adsorption of the complex in the hydrophobic, all-silica MCM-41 channels. Furthermore, the difference in adsorption behavior, together with the improbability for the complexes to pass each other, is indicative for single-file-diffusion[5], which demonstrates that the actual adsorption of the complex takes place inside the MCM-41 channels. This is in line with the results obtained by XPS analysis on the heterogeneous catalyst. In figure 6.8 the Si/Ti ratios are plotted for two MCM-41 host materials loaded with different amounts of complex **3.** XPS analysis of a maximum loaded MCM-41 results in the same Si/Ti ratio as expected from the calculated bulk content. A partially loaded MCM-41 host, however, filled with a quarter of the maximum loading, shows a remarkable difference: about twice as much titanium can be observed with XPS as was expected with regarding to the bulk. Conclusively, a preferential adsorption of the silsesquioxane complex in the outer regions of the MCM-41 pores is demonstrated. This confirms the strong interaction of the

complex with the all-silica MCM-41 pore wall, which prevents the complexes to penetrate further than strictly necessary into the mesoporous system. A less than maximum loading, therefore, should result in a relatively higher complex (or titanium) concentration at the outer regions than expected for a homogeneous distribution.
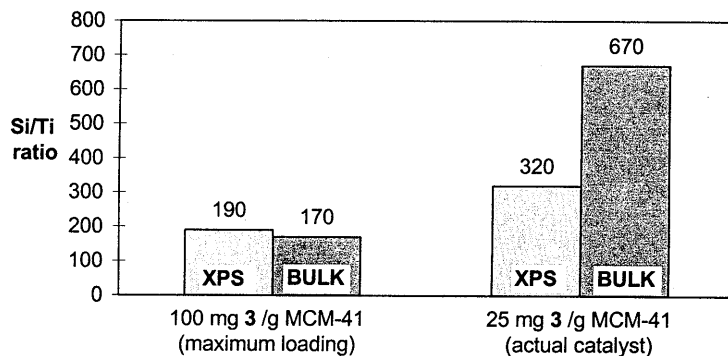


*Figure 6.8 XPS analysis on 3 immobilized in an MCM-41 host with different loadings in comparison with the bulk Si/Ti ratio, which is calculated from the amount of complex adsorbed per gram MCM-41.*

The adsorption characteristics of the silsesquioxane complex **3** have been investigated using Raman spectroscopy. In figure 6.9 the Raman spectra are shown, in the region of 500 - 1500 $cm^{-1}$, of the pure complex **3,** of the pure MCM-41 and of the complex **3** immobilized in the MCM-41 host. This spectral region contains vibration bands typical for the silica skeleton as well as for the cyclohexyl ligands, like the ring breathing vibration at 1125 $cm^{-1}$ and the characteristic H-C-H scissors at 1442 $cm^{-1}$. Unambiguously, in the Raman spectrum of the immobilized complex **3**, the bands typical for **3** can be clearly recognized superimposed on the MCM-41 background signal. The well resolved vibration bands of the immobilized complex **3** are present at unchanged frequencies in comparison with the pure complex **3**. This demonstrates the truly *unaltered* adsorption of the silsesquioxane complex in the MCM-41 molecular sieve.

Interestingly, the high frequency region of the same Raman spectra exhibit a somewhat different behavior. In figure 6.10 these Raman spectra are visualized (2700 - 3200 $cm^{-1}$ region), featuring the C-H stretching vibrations of the ancillary cyclohexyl ligands and cyclopentadienyl ligand of complex **3**. Three important bands to be recognized are: (i) around 2850 $cm^{-1}$, the symmetric $CH_2$ stretching vibration of the cyclohexyl ligands; (ii) around 2930 $cm^{-1}$, the asymmetric $CH_2$ stretching vibration of the cyclohexyl ligands; (iii) around 3120 $cm^{-1}$, the C-H stretching vibration of the cyclopentadienyl group.
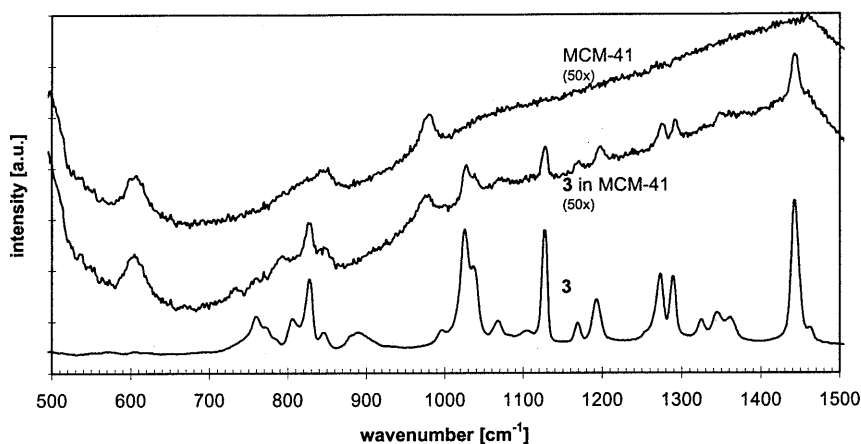
*Figure 6.9   Raman spectroscopy on complex 3, as a free complex and immobilized in all-silica MCM-41 (500 - 1500 cm$^{-1}$).*

While the low frequency region of the Raman spectrum of the adsorbed complex showed no difference from the free complex (*vide supra*), in the C-H stretching region some interesting changes are observed. First, a clear shift can be recognized comparing the spectrum of the free complex **3** and the complex **3** adsorbed in the MCM-41 host. This shift concerns the symmetric CH$_2$ stretching as well as the asymmetric CH$_2$ stretching vibration and equals 10 cm$^{-1}$ to higher frequency. Secondly, a relative change in intensity can be observed of the same two bands upon adsorption of complex **3** in the MCM-41. These observations are indicative for changes in configuration or symmetry of the cyclohexyl ligands. A constrained conformation could result from a reduced freedom of movement due to the strong adsorption of the complex on the MCM-41 pore wall. Concerning the shift of the CH$_2$ vibration bands, other Raman vibrations are unaffected and remain at the same frequency upon adsorption of the complex in the MCM-41 host. The already mentioned typical and very strong H-C-H scissors vibration remains exactly at 1442 cm$^{-1}$. Moreover, no changes in intensities can be observed in this spectral region (see figure 6.9). Noteworthy, the CH$_2$ stretching vibrations of the cyclohexyl ligands of a free silsesquioxane complex **3** measured in a diluted CCl$_4$ solution overlap exactly with the spectrum of the silsesquioxane complex crystals. This implies that the complex in its crystal is as free as in solution. Therefore, the measured shift of the C-H stretching vibrations of the immobilized complex should concern the adsorption of the complex in the MCM-41 pore.

The demonstrated strong adsorption of the silsesquioxane complex in the MCM-41 pore implies an energy minimum of the adsorbed complex. Whereas, the shift of the CH$_2$ stretching vibrations is to a higher frequency, corresponding with a higher energy of these stretching vibrations. The higher energy measured could result from a constrained configuration arising from a reduction in the space available for the CH$_2$ stretching vibration. This can possibly be explained with a reduced space for this stretching vibration as resulting

from the strong adsorption of the silsesquioxane complex on the MCM-41 pore wall. This adsorption is a purely physical phenomenon: no chemical interaction is involved which should weaken the vibration bonds and, therefore, result in a shift towards lower frequency.
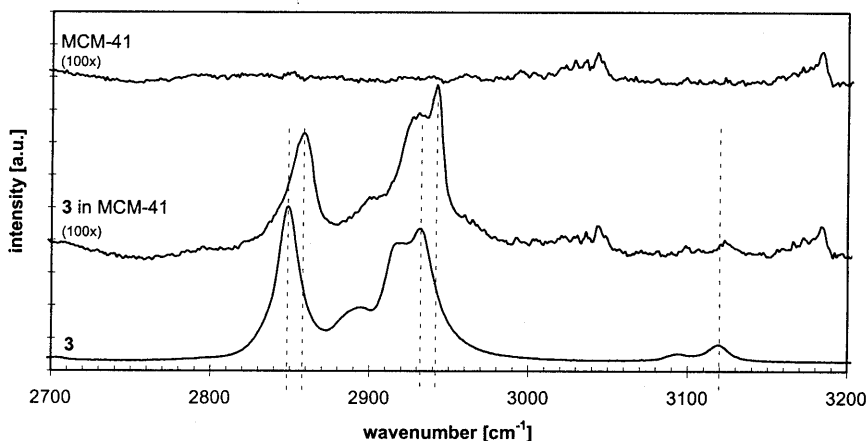


*Figure 6.10   Raman spectroscopy on complex 3, as a free complex and immobilized in all-silica MCM-41 (2700 - 3200 cm⁻¹).*

It can be expected that only the C-H bonds of the cyclohexyl ligands are affected by this adsorption, since these bonds are at the exterior of the silsesquioxane complex. The observed frequency shift upon adsorption for both the asymmetric and symmetric $CH_2$ stretching vibration is not affecting the H-C-H scissors vibration at 1442 cm⁻¹. Apparently, the constrained configuration observed does not influence this scissors vibration. This is still in agreement with the explanation in terms of a reduced space, because this scissors vibration is expected to need hardy any extra space to expand in front of the C-H bond. In summary, the observed shift of the $CH_2$ stretching vibrations as well as the change in their relative intensities can relate to a constrained configuration of the cyclohexyl ligands as a result of the strong adsorption at the MCM-41 pore wall.

The catalytic data of the heterogeneous complex, as reported in section 6.3, show that the performance of the adsorbed complex is hardy changed upon immobilization. This indicates the preserved accessibility of the titanium site when adsorbed in the MCM-41 host. Also we showed in section 5.3 the high stability of the cyclopentadienyl ligand of the titanium site under oxidizing conditions during epoxidation catalysis. Considering the C-H stretch of the cyclopentadienyl ligand (around 3120 cm⁻¹), this vibration seems hardly influenced by the adsorption of the complex (see figure 6.10). A possible slight shift may result from a re-orientation of the cyclohexyl ligands upon adsorption, affecting the C-H groups of the cyclopentadienyl unit. The demonstrated strong adsorption of the cyclohexyl ligands on the MCM-41 pore wall together with the preserved accessibility of the titanium site suggests an oriented adsorption of the complex with the cyclohexyl ligands adsorbed on the MCM-41

pore wall and the titanium site pointing towards the center of the MCM-41 pore. This unique orientation of the complex refines our postulated model of the *self-assembly* properties of the immobilized silsesquioxane complex inside an MCM-41 host.

Generally, evidence can be found for a comparable shift of the C-H stretching vibration upon adsorption of organics in silica-like hosts, as zeolites. In several studies the interaction of a template molecule with the zeolite lattice was investigated using Raman spectroscopy. Nevertheless, little to no attention has been paid to the shift of the C-H stretching vibration upon occlusion in a zeolite pore. From the Raman spectra reported by Brémard *et al.* we could derive a shift of about 12 cm$^{-1}$ upwards of the most resolved peak in the C-H stretching region for the TPA$^+$ occluded in an all-silica MFI framework in comparison with the free TPABr in its crystal[11]. From data reported by Davidson *et al.* we could derive a shift of 8 cm$^{-1}$ upwards for the C-H stretching vibration of pyridine inside all-silica FER in comparison with the free pyridine in solution[12]. Also, we found a shift of 4 and 6 cm$^{-1}$ upwards for the C-H stretching vibration of propylamine inside all-silica FER in comparison with the free propylamine in solution[12]. Important to mention is that also in this adsorption study the above mentioned H-C-H scissors vibration remains perfectly unchanged. Unfortunately, both references do not discuss the feature of the upward shift of the C-H stretching vibration of the different template molecules[11,12]. An explanation considering the reduced space available for these stretching vibrations of the occluded template inside the zeolite pore seems reasonable. Which, however, does not rule out the effect of a possible constrained configuration of the cyclohexyl ligands upon adsorption of the silsesquioxane complex in the MCM-41 pore.

## 6.5 Conclusions

The adsorption of a titanium silsesquioxane complex in an all-silica MCM-41 molecular sieve, results in self-assembled materials, which are active, truly heterogeneous and recyclable catalysts for alkene epoxidation in the liquid phase. Moreover, by tailoring the polarity of the host *via* silylation of the solid catalysts, aluminum containing MCM-41 materials become heterogeneous catalysts. These aluminum containing materials, however, tend to deactivate in the course of reaction. With spectroscopic characterization, evidence is given for the *unaltered* adsorption of the silsesquioxane complexes *inside* the MCM-41 pores. Moreover, the strong adsorption of the silsesquioxane complex is proven by the visualized interaction of the ancillary cyclohexyl ligands of the complex at the MCM-41 pore wall. This result indicates an oriented direction of the complex in the MCM-41 host, in which the titanium site is pointing towards the center of the MCM-41 pore. As such, the accessibility of the titanium site for substrate and oxidant in heterogeneous oxidation catalysis is guaranteed, which is in agreement with the high activity of the heterogenized catalyst.

# 6.6 Experimental

The different MCM-41 samples were prepared following the procedure as used by Beck et al.[9] and adapted by Busio et al.[4] In a typical adsorption experiment 50 ml of a $10^{-3}$ M solution of 3[2b] in hexane (p.a., Acros) was added slowly to a suspension of 2 g of dried MCM-41 in hexane (50 ml) and was stirred for 24 hours. The impregnated MCM-41 was subsequently filtered off, washed with hexane (3 x 20 ml) and dried in air at 80 °C for 24h.

In a typical silylation experiment 0.5 gram of a dried and degassed impregnated MCM-41 sample was stirred in a solution of 70 ml of hexane with 2.5 gram of dichlorodiphenylsilane (96%, Acros). This suspension was refluxed in an inert atmosphere for 72 h. The obtained material was filtered off, washed with hexane (3 x 20 ml) and acetone (p.a., Acros, 3 x 20 ml) and dried in air at 80 °C for 24h.

Epoxidation reactions were carried out at 50°C in small glass reactors (ca. 1.5 ml), in which ca. 62 mg catalyst (1.2 mg Ti/g), ca. 193 mg cyclooctene (1.75 mmol, 95 %, Acros) and 1.00 ml of a 1.8 M TBHP solution (originally 70 % in $H_2O$, Acros) in dry hexane were magnetically stirred. Mesitylene (1,3,5-trimethyl benzene, >98%, Merck) was used as internal standard. The kinetic experiments, as shown in figure 6.4, were performed in 5.0 ml magnetically stirred reactors using equimolar amounts (7.2 mmol) of cyclooctene and dried TBHP in hexane (4.0 ml) at 50°C. Conversions and selectivities were determined by $^1H$ NMR recorded in $CDCl_3$ on a Varian Gemini (300 MHz) with at least 16 scans for $^1H$ NMR.

The competitive adsorption of 1,2-epoxyoctane and 1-octene was performed with 1 g dried MCM-41 material (at least 1 hour in *vacuo*) using 25 µl of each adsorbate in 50.00 ml hexane at room temperature. Concentrations of the adsorbates in solution was followed by GC analysis.

UV-Vis spectra were recorded on a Hitachi 150-20 Spectrometer between 200 and 500 nm using a scan speed of 50 nm/min. Pure hexane was used as reference. Diffuse Reflectance UV-Vis (DRUV-Vis) spectra were recorded on the same apparatus equipped with a DIA Integration Sphere Accessory between 500 and 200 nm using a scan speed of 2 nm/min. Samples were measured in a cell of non-adsorbing suprasil quartz glass (with dimensions of 13x13x1 mm) using a reference sample of grinded $Ca(OH)_2$. All DRUV-Vis spectra were converted to Kubelka-Munk intensities.

Nitrogen adsorption measurements were performed on a Carlo-Erba Sorptomatic 1990. Before analysis, the samples were dried in *vacuo* at 150°C. The surface area was calculated according to the Brunauer-Emmett-and-Teller method (BET).

Water contents of the MCM-41 samples, were determined with a Shimadzu TGA-50 thermogravimetric analyzer. About 10-15 mg of sample was heated under static conditions in air to 700°C with a rate of 5°C per minute.

Fourier Transformed Infrared (FT-IR) spectra were taken at room temperature on a Perkin Elmer FT-IR 1600 series spectrophotometer. Samples were pressed into KBr pellets and measured with at least 1024 scans for the immobilized materials or with 16 scans for the pure compounds.

X-ray Photoelectron Spectroscopy (XPS) measurements were performed on zeolite samples pressed on indium stubs using a VG ESCALAB 200 Spectrometer equipped with a standard X-ray source (Mg Kα) and a hemispherical analyzer. Measurements were done at 20 eV pass energy and charging was corrected using the Si 2p signal at 103.3 eV. Spectra were fitted for determining surface areas and peak maxima using the VGS

program fit routine, with a Shirley background subtraction and Gauss-Lorentz curves. Elemental ratios were calculated with the correction for their cross-sections (reference [13]).

Raman spectra were recorded with a Labram spectrometer from Dilor S.A. (France). A Spectra Physics Millenium II Nd:YVO$_4$ laser at 532 nm was used as an excitation source. The initial laser power was 0.20 W. Spectra were taken from samples under ambient conditions. Laser light was focused on the sample using a slit width of 0.1 mm and a 10× microscope objective. The 180° back scattered radiation from the sample was dispersed with a 1800 mm$^{-1}$ grating onto a CCD detector.

# References

1.  With this aim different procedures have been reported: isomorphous substitution: a) M. Taramasso, G. Perego, B. Notari (Enichem), US Pat. (**1983**), 4 410 501, [*Chem. Abstr.* (**1981**), *95*, 206272k]; for a recent review see: b) I. W. C. E. Arends, R. A. Sheldon, M. Wallau, U. Schuchardt, *Angew. Chem.*, (**1997**), *109*, p. 1190; grafting: c) T. Maschmeyer, F. Rey, G. Sankar, J. M. Thomas, *Nature*, (**1995**), *378*, p. 159; and ship-in-the-bottle catalysts: d) for a review see: D. E. De Vos, F. Thibault-Starzyk, P. P. Knops-Gerrits, R. F. Parton, P. A. Jacobs, *Macromol. Symp.*, (**1994**), *80*, p. 157; for a recent publication: e) K. J. Balkus Jr., A. K. Khanmamedova, K. M. Dixon, F. Bedioui, *Appl. Catal. A*, (**1996**), *143*, p. 159.
2.  a) F. J. Feher, T. A. Budzichowski, K. Rahimian and J. W. Ziller, *J. Am. Chem. Soc.*, (**1992**), *114*, p. 3859; b) I. E. Buys, T. W. Hambley, D. J. Houlton, T. Maschmeyer, A. F. Masters, A. K. Smith,. *Mol. Catal.*, (**1994**), *86*, p. 309.
3.  H. C. L. Abbenhuis, S. Krijnen, R. A. Van Santen, *J. Chem. Soc. Chem. Commun.*, (**1997**), p. 331.
4.  M. Busio, J. Jänchen, J. H. C. Van Hooff, *Microporous Materials*, (**1995**), *5*, p. 211.
5.  J. Kärger, M. Petzold, H. Pfeifer, S. Ernst, J. Weitkamp, *J. Catal.*, (**1992**), *136*, p. 283.
6.  A. Corma, P. Esteve, A. Martínez, *J. Catal.*, (**1996**), *161*, p. 11.
7.  For a related approach involving enzymes in MCM-41 materials: J. F. Díaz, K. J. Balkus Jr., *J. Mol. Catal. B: Enzym.*, (**1996**), *2*, p. 115.
8.  a) J. Jänchen, M. Busio, M. Hintze, H. Stach, J. H. C. Van Hooff, *Stud. Surf. Sci. Catal.*, (**1997**), 105, p. 1731; b) C. Y. Chen, H. X. Li, M. E. Davis, *Microporous Mater.*, (**1993**), *2*, p. 17.
9.  K.T. Wan, M.E. Davis, *Nature, 370*, (**1994**), p. 449.
10. J. S. Beck, J. C. Vartuli, W. J. Roth, M. E. Leonowicz, C. T. Kresge, K. D. Schmitt, C. T-W. Chu, D. H. Olson, E. W. Sheppard, S. B. McCullen, J. B. Higgens, J. L. Schlenker, *J. Am. Chem. Soc.*, (**1992**), *114*, p. 10834.
11. C. Bremard, J. Laureyns, J. Patarin, *J. Raman. Spec.*, 27, (**1996**), p. 439.
12. A. Davidson, S.J. Weigel, L.M. Bull, A.K. Cheetham, *J. Phys. Chem. B.*, 101, (**1997**), p. 3065.
13. J.H. Scofield, J. Electron Spectrosc. Rel. Phenom., 8, (1976), p. 129.
14. S. Krijnen, H.C.L. Abbenhuis, R.W.J.M. Hanssen, J.H.C. van Hooff, R.A. van Santen, *Angew. Chem. Int. Ed. Engl., 37*, (**1997**), p. 356.

# Summary

This thesis involves the synthesis of new, titanium based heterogeneous catalysts and their application in liquid phase epoxidation reactions. Epoxidation reactions are important for the fine chemical industry to prepare oxygenated products. During the past decades there is considerably pressure to replace outdated stoichiometric oxidation methods with cleaner, catalytically technologies. The application of catalytic oxidation reactions can open the possibility to employ environmentally friendly processes, in which oxidants as oxygen and peroxides are used instead of stoichiometric oxidants, which produce large amounts of waste. Furthermore, from an industrial point of view, heterogeneous catalysts are preferred over homogeneous applications because of the advantage of an easy recovery and recyclability of the catalyst. In this perspective, zeolites can be used to act as highly stable ligands for the catalytic site, being a metal center, like titanium. Moreover, these inorganic microporous structures can act as molecular sieves, which enables them to enforce specific selectivities to the catalytic process. Such selectivities in oxidation catalysis can result from sterical constraints provided by the microporous structure or can originate from a preferential adsorption of reactants due to the nature of the supporting material. In this respect, the hydrophobicity of the host material appears to play a dominant role in liquid phase oxidation catalysis.

The first titanium zeolite prepared is titanium silicalite 1 (TS-1), invented by Enichem in Italy. This highly active oxidation catalyst has an important disadvantage with respect to its pore size. The silicalite structure consists of relatively narrow pores, roughly 0.55 nm in diameter, which limits its application when the selective oxidation of large substrates is concerned. The possibility to incorporate titanium centers into large pore zeolitic structures, would widen the application of titanium zeolites in oxidation catalysis. For this purpose, a post-synthesis route is developed to prepare titanium substituted large-pore zeolites (*Chapter 2 and 3*), such as mordenite and beta, with a pore diameter of about 0.7 nm. Such a post-synthesis route consists of a dealumination of an already prepared zeolite, followed in a second step by a titanation of the dealuminated zeolite. This titanation procedure is based on *Chemical Vapor Deposition* (CVD) techniques. The purpose of the first step, the dealumination, is to create vacant sites and to remove as much as aluminum possible, since an aluminum deficient zeolite will have a hydrophobic lattice, which is advantageous in liquid phase oxidation catalysis. The aim of the second step, the titanation, is to incorporate isolated titanium sites at T-atom vacancies in the zeolite lattice. With TS-1 it is proven that those, tetrahedrally, isolated titanium sites are the active catalysts in oxidation reactions with $H_2O_2$.

In the study concerning the dealumination of large pore zeolites, mordenite and beta are dealuminated with various acid and thermal treatments to optimize this dealumination treatment (*Chapter 2*). A maximum of 93 % aluminum removal is reached, applying a combined nitric acid and thermal treatment. In essence, the dealumination behavior of different zeolites upon an nitric acid treatment is demonstrated to involve the possibility of migration of silicon through the zeolite lattice. The obtained aluminum deficient zeolites were subjected to an extensive FT-IR spectroscopic study. The assignment of FT-IR bands resulting from the different vacant sites in FT-IR spectroscopy is clarified by means of density functional calculations on model compounds (*Chapter 5*). This assignment together with the results of the titanation of these zeolites (*Chapter 3*) leads to the important conclusion that the vacancies, which are located in the zeolite micropores, result upon titanation in *isolated* titanium sites. In general, a preferential titanation of the outer regions of the zeolite crystal is found, resulting from the post-synthesis CVD treatment. This titanation mechanism has the consequence that, with high titanium loadings, the formation of $TiO_2$ species starts to occur on the exterior of the zeolite crystals. Raman spectroscopy is proven to be a very powerful technique to search for traces titanium oxide in zeolites, but also XPS (*X-ray Photoelectron Spectroscopy*) and diffuse reflectance UV-Vis spectroscopy give satisfactory evidence. We proved with the fluid-bed CVD titanation using very small crystals of dealuminated zeolite beta, that it was possible to prevent the formation of $TiO_2$ totally. Moreover, the amount of titanium incorporated is in good correlation with the amount of aluminum removed.

The resulting large pore titanium zeolites are demonstrated to be active catalysts in epoxidation reactions of alkenes that are impossible to oxidize with TS-1 (*Chapter 4*). Moreover, the post-synthesis prepared titanium zeolites are truly heterogeneous catalysts in these liquid phase epoxidation reactions, using peroxides. Our results once more prove that titanium zeolites are highly active oxidation catalysts only when they consist of very small crystal sizes (diameter ca. 0.1 μm) with a highly hydrophobic framework. A small contribution of active sites present on the external surface to the measured activity is demonstrated. Interestingly, the post-synthesis prepared titanium zeolites are active and selective catalysts using an organic peroxide (*tert.*-butyl hydroperoxide) as well as hydrogen peroxide ($H_2O_2$) as the oxidizing agent. When using a highly dealuminated zeolite, however, consisting of a very hydrophobic framework, much higher yields of epoxide are obtained when $H_2O_2$ is used as oxidant. This result is in line with the postulated mechanism involving the coordination of a protic ligand to the active titanium site in TS-1. Furthermore, it explains the comparable activity of a post-synthesis prepared titanium beta catalyst with TS-1 in the epoxidation of 1-octene with $H_2O_2$. In summary, the post-synthesis route, which is likely to be applicable for a variety of zeolite structures, is proven to be capable of synthesizing titanium zeolites with catalytic activities which can easily compete with the performance of the direct synthesized TS-1.

The second part of this thesis deals with silsesquioxanes, a family of silica mimic building blocks suitable as well defined ligands for metal centers. These model compounds are used in the stepwise construction of heterogeneous as well as homogeneous catalysts, which are structurally defined at a molecular level (*Chapter 5*). The dentacity of the silsesquioxane ligand of the resulting titanium compounds is proven to be crucial for the heterogeneity of the modeled catalysts. These results demonstrate that a titanium site bounded monodentate to a silica support will result in leaching of the titanium site, due to the irreversible hydrolysis of the titanium siloxy unit, initiated by the coordination of the peroxide. Applying, however, a terdentate coordinated titanium site, results in a truly stable titanium center in its silica host, which still effectively catalysis alkene epoxidation reactions. These results indicate that silica supported titanium epoxidation catalysts will be only truly heterogeneous when stringent conditions are met and are in good agreement with the high stability of the titanium zeolites (*Chapter 4*).

The active and robust terdentate coordinated titanium silsesquioxane catalyst, is subsequently heterogenized in mesoporous host materials, like MCM-41 (*Chapter 6*). Tailoring the polarity of the MCM-41 host, results in *self-assembled* materials that are active, truly heterogeneous and recyclable catalysts for liquid phase alkene epoxidation. In line with the results of the titanium zeolites (*Chapter 4*), the hydrophobicity of the host material plays an decisive role in obtaining active titanium catalysts. Moreover, the titanium silsesquioxane complex displays particularly strong adsorption characteristics when immobilized in an aluminum free MCM-41 host. Raman spectroscopy on the heterogeneous catalyst showed a basically unaltered complex adsorbed inside the MCM-41 pore and simultaneously indicates a preferential orientation of the complex. As such, the accessibility of the titanium site for substrate and oxidant is guaranteed, in agreement with the high activity of the of the heterogeneous catalyst in liquid phase alkene epoxidation.

# Samenvatting

Dit proefschrift beschrijft de synthese van nieuwe, heterogene titaankatalysatoren en hun toepassing in vloeisstoffase epoxidatiereacties. Epoxidatiereacties zijn belangrijk voor de fijnchemische industrie bij de bereiding van gefunctionaliseerde moleculen. De laatste decennia staan verouderde stoichiometrische processen onder zware druk om vervangen te worden door schonere, katalytische technologieën. De toepassing van katalytische oxidatie-reacties opent mogelijkheden voor milieuvriendelijke processen. Deze katalysatoren kunnen gebruik maken van zuurstof of peroxiden als oxidanten in plaats van stoichiometrische oxidanten, die een grote afvalstroom met zich meebrengen. Daarnaast genieten heterogene katalysatoren, vanuit een industrieel oogpunt, de voorkeur boven homogene katalysatoren, omdat deze gemakkelijk zijn af te scheiden en opnieuw te gebruiken. In dit verband kunnen zeolieten gebruikt worden als zeer stabiele liganden voor een actief metaal centrum, zoals titaan(IV). Deze anorganische, microporeuze structuren kunnen bovendien fungeren als moleculaire zeven. Dit maakt het mogelijk om specifieke selectiviteiten op te leggen aan het katalytisch proces. Dit kan bijvoorbeeld zijn het selecteren van reactanten op grond van hun grootte of de preferente adsorptie van reactanten als gevolg van de eigenschappen van het zeoliet. In dit verband blijkt de hydrofobiciteit van de moleculaire zeef een doorslaggevende rol te spelen tijdens vloeistoffase oxidatiekatalyse.

De eerste titaanzeoliet, titaan-silicaliet 1 (TS-1), is ontwikkeld door Enichem in Italië. Deze zeer actieve oxidatiekatalysator heeft als belangrijk nadeel zijn kleine poriediameter (slechts ca. 0.55 nm), die het gebruik van deze katalysator beperkt tot relatief kleine substraten. De mogelijkheid om titaan in te bouwen in zeolieten met grote poriën zal het toepassingsgebied van titaanzeolieten in oxidatiekatalyse sterk vergroten. Met dit doel is een post-synthese route ontwikkeld om titaan in te bouwen in zeolieten met grote poriën (*Hoofdstuk 2 en 3*), zoals Mordeniet en Beta die beide een poriediameter van ca. 0.7 nm hebben. Een dergelijke post-synthese route behelst allereerst een dealuminatie van een reeds gesynthetiseerde zeoliet, waarna als tweede stap een titanatie van het gedealumineerde zeoliet volgt. Deze titanatie procedure is gebaseerd op *Chemical Vapor Deposition* (CVD) technieken. Het doel van de eerste stap, de dealuminatie, is het creëren van vacante posities in het zeolietrooster en om zoveel mogelijk aluminium te verwijderen. Dit laatste is wenselijk omdat een aluminium-arm zeoliet een hydrofoob rooster heeft, wat voordelig is tijdens vloeistoffase oxidatiekatalyse. Het doel van de tweede stap, de titanatie, is het inbouwen van geïsoleerde titaancentra op de vacante posities in het zeolietrooster. Het is aangetoond dat deze tetraedrisch omringde, geïsoleerde titaancentra in TS-1 de katalytische centra zijn in oxidatie reacties met $H_2O_2$.

In het onderzoek naar de dealuminatie van zeolieten, zijn Mordeniet en Beta gedealumineerd met verschillende zure- en thermische behandelingen (*Hoofdstuk 2*). Een gecombineerde toepassing van zowel een salpeterzure- als een thermische behandeling leidt tot een maximale dealuminatiegraad van 93 %. Het is aangetoond dat het dealuminatie-gedrag van de verschillende zeolieten berust op de mogelijkheid van silicium-migratie door het zeolietrooster. De resulterende, aluminium-arme zeolieten zijn uitvoerig geanalyseerd met spectroscopische technieken. De toekenning van de FT-IR banden die behoren tot de hydroxyl groepen in vacante plaatsen in het zeolietrooster, is opgehelderd met behulp van quantum- chemische berekeningen aan model systemen (*Hoofdstuk 5*). Deze toekenning, tezamen met de resultaten van de titanatie procedure (*Hoofdstuk 3*), leidt tot de belangrijke conclusie dat de vacante posities, die zich bevinden in de microporiën van het zeoliet, na titanatie resulteren in tetraedrische titaancentra. In het algemeen wordt, als gevolg van de post-synthese route, een preferente titanering van de buitenste delen van het zeolietkristal gevonden. Dit mechanisme heeft als consequentie dat, bij hoge titaanbeladingen, op de buitenkant van de zeolietkristallen de vorming van titaanoxide plaats vindt. Het is aangetoond dat Raman spectroscopie een zeer krachtige techniek is om sporen titaanoxide in een zeoliet te traceren. Daarnaast kunnen ook XPS (*X-ray Photoelectron Spectroscopy*) en diffuse reflectie UV-Vis spectroscopie de aanwezigheid van titaanoxide op zeolieten doeltreffend aantonen. We hebben bewezen dat het met een gefluïdiseerd CVD bed van zeer kleine zeolietkristallen mogelijk is de vorming van $TiO_2$ te voorkomen. Bovendien is gebleken dat de hoeveelheid titaan die ingebouwd kan worden, in goede overeenstemming is met de hoeveelheid aluminium die verwijderd was.

De titaanzeolieten, met de hierboven beschreven grote poriën, zijn actieve katalysatoren voor de epoxidatie van alkenen die onmogelijk over TS-1 geëpoxideerd kunnen worden. Bovendien zijn deze titaanzeolieten, gemaakt volgens de post-synthese route, stabiele en heterogene katalysatoren in vloeistoffase epoxidatiereacties. Onze resultaten bevestigen dat titaanzeolieten alleen actieve katalysatoren kunnen zijn als zij bestaan uit zeer kleine zeolietkristallen (diameter ca. 0.1μm) èn als zij een hydrofoob rooster hebben. Tevens is een kleine bijdrage van katalytische activiteit aan de buitenkant van het zeolietkristal aangetoond. De post-synthese titaanzeolieten blijken zowel met een organisch peroxide (*tert.-*butylhydroperoxide) als met waterstofperoxide ($H_2O_2$) actieve katalysatoren te zijn. Wanneer echter een hoog gedealumineerde titaanzeoliet wordt gebruikt, derhalve met een zeer hydrofoob rooster, is de behaalde activiteit met $H_2O_2$ veel hoger dan met TBHP. Dit resultaat is in overeenstemming met het voorgestelde mechanisme voor titaanzeolieten, waarbij de coördinatie van een protisch ligand aan het titaancentrum een gunstig effect heeft. Het verklaart bovendien de vergelijkbare activiteit van een post-synthese titaan-Beta katalysator met TS-1 in de epoxidatie van 1-octeen met $H_2O_2$. Samenvattend, we hebben bewezen dat het met de post-synthese route mogelijk is titaanzeolieten te maken die, voor wat betreft hun katalytische activiteit, gemakkelijk kunnen concurreren met de direct gesynthetiseerde TS-1.

Het tweede deel van dit proefschrift beschrijft de katalytische toepassing van silsesquioxanen, een familie van silica-achtige bouwstenen die zeer geschikt zijn om goed gedefinieerde liganden voor metaalcentra te vormen. Deze modelverbindingen zijn gebruikt om zowel heterogene als homogene katalysatoren te ontwikkelen, met een tot op moleculaire schaal goed gedefinieerde structuur (*Hoofdstuk 5*). Onze resultaten hebben bewezen dat de coördinatie van de silsesquioxaan liganden in de analoge titaanverbindingen cruciaal is voor de heterogeniteit van de gemodelleerde katalysatoren. Deze resultaten tonen aan dat een titaancentrum, dat slechts met één binding vast zit aan de silicadrager, ongetwijfeld zal resulteren in het oplossen van het titaancentrum tijdens katalyse. Dit wordt veroorzaakt door de irreversibele hydrolyse van de titaan-siloxy binding door de coördinatie van het peroxide. Wanneer echter een drievoudig (terdentate) gecoördineerd silsesquioxaan ligand wordt toegepast, blijkt het resulterende titaancentrum volledig stabiel en bovendien nog steeds actief in alkeen epoxidatiekatalyse. Deze resultaten impliceren dat silica-gedragen titaankatalysatoren alleen heterogeen zullen zijn wanneer er voldaan wordt aan stringente voorwaarden met betrekking tot de coördinatie van het titaancentrum. Dat blijkt tevens uit de hoge stabiliteit van de titaanzeolieten, waarvan de katalytische eigenschappen berusten op een tetraedrisch titaancentrum (*Hoofdstuk 4*).

De actieve en robuuste, drievoudig gecoördineerde titaan-silsesquioxaan katalysator is geïmmobiliseerd in een mesoporeus dragermateriaal, zoals MCM-41 (*Hoofdstuk 6*). Door het manipuleren van de polariteit van de MCM-41 drager, zijn zelf-organiserende systemen ontwikkeld, die actief, heterogeen en bovendien recyclebaar zijn in vloeistoffase epoxidatie-katalyse. De hydrofobiciteit van het dragermateriaal speelt opnieuw een doorslaggevende rol in het verkrijgen van actieve titaankatalysatoren. Dit is conform de katalytische resultaten van de titaanzeolieten (*Hoofdstuk 4*). Bovendien blijkt dat het titaan-silsesquioxaan complex zeer sterke adsorptie-eigenschappen vertoont wanneer deze geïmmobiliseerd wordt in een aluminium-vrije MCM-41 drager. Met Raman spectroscopie is bewezen dat het complex onveranderd is geadsorbeerd in de MCM-41 porie en tegelijkertijd een preferente oriëntatie vertoont. Door deze oriëntatie is de toegankelijkheid tot het titaancentrum voor substraat en oxidant verzekerd, wat in overeenstemming is met de hoge activiteit van deze heterogene, vloeistoffase epoxidatiekatalysator.

# Publications

**Heterogenization of a novel epoxidation catalyst: Phase immobilization of a titanium silsesquioxane in an MCM-41 molecular sieve**
S. Krijnen, H.C.L. Abbenhuis, R.W.J.M. Hanssen, J.H.C. van Hooff, R.A. van Santen,
*Proceedings of the Material Research Society; accepted, expected December 1998.*

**Solid Phase Immobilization of a New Epoxidation Catalyst**
S. Krijnen, H.C.L. Abbenhuis, R.W.J.M. Hanssen, J.H.C. van Hooff, R.A. van Santen,
*Angewandte Chemie, International Edition in English, 37,* **1998**, p. 356-358.
*Angewandte Chemie, 110,* **1998**, p. 374-376.

**Modelling the active sites of heterogeneous titanium oxidation catalysts using titanium silsesquioxanes: insight into specific factors that determine leaching in liquid-phase processes**
H.C.L. Abbenhuis, S. Krijnen, R.A. Van Santen,
*Journal of the Chemical Society, Chemical Communications,* **1997**, p. 331-332.

**A controlled post-synthesis route to well-defined active titanium Beta epoxidation catalysts**
S. Krijnen, P. Sánchez Paredez, B.T.F. Jakobs, J.H.C. Van Hooff,
*Microporous and Mesoporous Materials, to be submitted.*

**MCM-41 heterogenised titanium silsesquioxane epoxidation catalysts: A spectroscopic investigation to the adsorption characteristics**
S. Krijnen, B.L. Mojet, H.C.L. Abbenhuis, J.H.C. van Hooff, R.A. van Santen,
*Journal of the Chemical Society, Faraday Transactions, to be submitted.*

**Silsesquioxanes as model compounds for zeolite defect sites: new insight in the assignment of FT-IR hydroxyl vibration bands**
S. Krijnen, R.J. Harmsen, J.H.C. van Hooff, R.A. van Santen,
*in preparation.*

**Patent application 197 30 376.5**
**'Verfahren zur Herstellung eines Trägerkatalysators' (Solvay Pharmaceuticals GmbH)**
R.A. van Santen, H.C.L. Abbenhuis, S. Krijnen, R.W.J.M. Hanssen
*filed 16-07-1997.*

# Nawoord

De vier jaar van onderzoek, die de basis waren voor de resultaten zoals beschreven in dit proefschrift, zouden niet zo goed zijn verlopen zonder de hulp en steun van verscheidene personen. Mijn beide promotoren, Jan van Hooff en Rutger van Santen wil ik bijzonder bedanken voor alle ruimte die zij mij hebben gegeven tijdens het onderzoek. Voor vragen of problemen kon ik altijd bij jullie aankloppen en de verscheidene werkbesprekingen zetten mij altijd weer goed op het spoor. Mijn co-promotor Erik Abbenhuis wil bedanken voor de prettige samenwerking tijdens het silsesquioxaan-onderzoek. Erik, met veel enthousiasme heb je mij de beginselen en de praktijk van de organo-metaal chemie bijgebracht. Onze werkbesprekingen waren altijd een bron van nieuwe ideeën op het grensvlak van organische complexen en anorganische structuren. Ik hoop dat ik op mijn beurt wat 'feeling' voor de zeolieten heb kunnen achterlaten. Hierbij wilde ik natuurlijk ook mijn dank uitbrengen aan alle andere leden van de (kern-)commissie, voor hun bereidheid deel te nemen in mijn promotiecommissie.

Het NIOK (Nederlandse Instituut voor Onderzoek in de Katalyse) ben ik zeer erkentelijk voor de financiële steun die mijn onderzoek mogelijk maakte. Mijn dank gaat ook uit naar alle leden in de begeleidingscommissie met wie ik mijn onderzoeksresultaten kon bediscussiëren tijdens onze halfjaarlijkse meetings. Tegelijkertijd was dit onderzoek een samenwerkingsverband met De Technische Universiteit Delft, vakgroep Organische Chemie en Katalyse; Hans Lempers en Roger Sheldon bedank ik hierbij voor de vlotte samenwerking en de nuttige discussies.

Voor het synthetiseren van de titaanzeolieten hebben ik en mijn studenten veelvuldig gebruikgemaakt van de fluidbed CVD-opstelling van Hans Linden, in de groep van Dick Koster, divisie Materialen, TNO-TPD Eindhoven. Bedankt voor alle ruimte die ons werd gegeven. Mijn afstudeerders ben ik veel dank verschuldigd voor het vele werk wat zij verzet hebben. Zonder jullie inzet zou mijn proefschrift er zeker anders hebben uit gezien. Bedankt Niels Hamel, Marcel Demarteau, Rob Hanssen, en Bas Jakobs! Jullie vragen en opmerkingen hielden mij scherp en ik hoop dat jullie mijn soms wat chaotisch voorkomen op z'n waarde hebben kunnen schatten. Ook wil ik bij deze twee stagiaires bedanken: Jeroen Manders (HTS, Eindhoven) en Uwe Couhorn (RTWH, Aachen) bedankt voor jullie hulp. Jullie research was van wezenlijk belang. Natuurlijk ook een woord van dank aan de research-studenten, Marcel Geboers, Job Verpoorte en Joris Vermunt, jullie enthousiasme en inzet heeft zeker bijgedragen aan het onderzoek. Helaas heeft niet al het werk dat jullie allemaal verzet hebben een plaats kunnen vinden in dit proefschrift.

# Curriculum vitae

Simon Krijnen werd geboren op 15 mei 1970 in Son en Breugel. In 1982 begon hij zijn middelbare school opleiding aan de Gemeenschappelijke Scholengemeenschap Woensel in Eindhoven, die hij in juni 1988 afrondde met het VWO diploma, Atheneum B. In augustus 1988 is de auteur begonnen aan de studie Scheikundige Technologie aan de Technische Universiteit Eindhoven. Het propedeutische examen werd afgelegd in augustus 1989. Zijn bedrijfsstage heeft hij uitgevoerd bij Akzo Nobel Central Research waar hij onderzoek heeft gedaan naar een sporenvullende lijm voor de verlijming van composiet-substraten. Het afstudeeronderzoek, uitgevoerd binnen de groep van prof.dr. R.A. van Santen, betrof de ontwikkeling van de experimentele set-up en kinetische metingen aan de hydro-isomerisatie van n-hexaan over platinagedragen zeolietkatalysatoren. Dit leidde tot het behalen van het scheikundig technologisch ingenieursdiploma in juni 1994. Hij startte zijn promotieonderzoek in juli 1994, onder leiding van prof.dr.ir. J.H.C. van Hooff en prof.dr. R.A. van Santen, binnen de vakgroep Katalyse en Anorganische Chemie, welke een onderdeel is van het Schuit Katalyse Instituut. De belangrijkste resultaten van dit onderzoek naar heterogene titaan-katalysatoren, gebaseerd op zeoliet- en silsesquioxaan-systemen, zijn beschreven in dit proefschrift en diverse publicaties en resulteerde in een patent-aanvraag.

*All right,*
*Stay bright !*